STRUCTURAL STUDIES OF FERROELECTRICS OF THE BORACITE AND KH_2PO_4 TYPE

WILLIAM JOHN HAY

DOCTOR OF PHILOSOPHY

UNIVERSITY OF EDINBURGH

1978

The research described in this thesis was the unaided work of the author, unless otherwise indicated. Where the research was done in collaboration with others, there was a significant contribution by the author.

ACKNOWLEDGEMENTS

I would like to express my gratitude to all those who have helped to make this work possible.

In particular my personal thanks go to my supervisor Dr R J Nelmes for his guidance, assistance and encouragement.

I am very grateful to Professors N Feather and W Cochran for extending to me the facilities of the Department of Physics at Edinburgh University; to the Science Research Council for granting me access to the facilities of A.E.R.E., Harwell; to Professor Woolfson for extending to me the facilities of the Department of Physics at York University; and to Dr P Main of York University for his kindness and assistance.

I would like to thank the Atomic Energy Authority for the award of a research studentship.

Finally I would also like to thank the staff of A.E.R.E., Harwell for their kindness and assistance, my friends and colleagues at Edinburgh for their help and encouragement, Mrs P Wood for her patient and painstaking work in preparing this thesis and my wife and family for their unstinted encouragement and support.

A B S T R A C T

This thesis is concerned with structural studies of ferroelectric crystals, in particular the structure of CsD_2AsO_4 in its tetragonal paraelectric phase and orthorhombic ferroelectric phase and the structures of $Co_3B_7O_{13}I$ and $Cu_3B_7O_{13}Br$ in their cubic paraelectric phases.

Both X-ray and neutron single-crystal diffraction techniques were used. The methods of constrained least-squares refinement and significance testing were used to determine the significance of certain structural features of interest.

Details of the development of a technique for the collection of single-crystal data from an unpoled and physically unconstrained crystal in its ferroelectric phase are given.

The structural studies of tetragonal CsD_2AsO_4 revealed that the D ions are disordered in double minimum potential wells. In the orthorhombic phase the D ions order onto one of their two possible sites in the tetragonal phase. The displacements of the Cs, As and O ions are related to the choice of site of the D ion on the O.....O bond. The As ions move away from the O ions which the D ions have moved towards.

The unusual feature of the ferroelectric transition in $Cs(D_xH_{1-x})_2AsO_4$ suggests an inhomogeneous mixing of the hydrogen and deuterium concentration.

The studies of $Co_3B_7O_{13}I$ and $Cu_3B_7O_{13}Br$ show that it is not necessary to postulate disorder to explain the crystal structures of these boracites in their cubic phase.

Table of Contents

CHAPTER 1

INTRODUCTION

CHAPTER 1

INTRODUCTION

1.1 Objectives

The object of this work is to contribute to the understanding of the mechanisms of structural phase transitions in ferroelectric crystals by the application of the methods of crystal structure analysis.

In particular this work is concerned with the determination of the crystal structures of ferroelectrics of the KH_2PO_4 and boracite (i.e. $Mg_3B_7O_{13}Cl$) type using the techniques of X-ray and neutron diffraction. Included in this work is the development of a technique for collecting single-crystal data from an unpoled and physically unconstrained crystal in the ferroelectric phase where poling and physically constraining the crystal would normally be considered necessary. The unusual nature of the low-temperature phase transition in the material $Cs(D_xH_{1-x})_2AsO_4$ is also investigated.

1.2 Ferroelectricity and Ferroelectric Phase Transitions

A ferroelectric crystal is one that possesses a spontaneous dielectric polarization which can be switched by an externally applied electric field. The existence of a spontaneous polarization requires that a ferroelectric crystal belongs to one of the ten crystallographic polar classes. A ferroelectric crystal is thus a pyroelectric crystal with switchable polarization.

Most ferroelectrics possess a spontaneous dipole moment only in a certain temperature range. At the boundary of this range the crystal undergoes a phase transition to a non-ferroelectric phase. The phases with and without a spontaneous polarization are referred to as ferroelectric and paraelectric respectively. The crystal symmetry is generally lowered on passing into the ferroelectric phase. The temperature, T_c, at which the transition to the ferroelectric phase occurs is known as the Curie temperature, or Curie point. Known Curie temperatures range from $7^{o}K$ for potassium lithium tantalate ($K_3Li_2Ta_5O_{15}$) to $1483^{o}K$ for lithium niobate ($LiNbO_3$).

A ferroelectric crystal may have transitions between two or more ferroelectric phases, e.g. barium titanate ($BaTiO_3$) and sodium nitrite ($NaNO_2$) have several phases between their lowest-symmetry and highest-symmetry forms. A ferroelectric crystal may also have none, one or more than one paraelectric phase, e.g. barium magnesium fluoride ($BaMgF_4$) does not have a paraelectric phase (below its melting point at 1 bar) and Rochelle salt ($NaKC_4H_6.4H_2O$) has a paraelectric phase above $297^{o}K$ and below $255^{o}K$.

In the region of T_c large anomalies are usually observed in the dielectric and thermodynamic properties of the crystal. In the paraelectric phase most ferroelectrics have a Curie-Weiss type of anomaly in the low frequency dielectric constant, $\varepsilon(0)$, [in the direction(s) in which spontaneous polarization develops].

$$\varepsilon(0) \propto (T-T_o)^{-1}$$

where T_o is the Curie-Weiss temperature. In the case of a second order-phase transition (see below) T_o is the same as the transition temperature T_c, while in the case of a first-order transition, T_o is lower than T_c.

A phase transition can be described as first or second order (Pippard, 1964). A first-order ferroelectric transition has discontinuities in the static susceptibility, spontaneous polarization, unit cell volume, entropy and specific heat at the transition point. A second-order transition has discontinuities in the temperature derivatives of these properties.

The theories of ferroelectricity can be divided into phenomenological theories and model theories.

The development of the phenomenological theories of ferroelectricity is mainly due to Devonshire (1954), who, in a review article, summarized and integrated earlier theories of Mueller (1940) and Devonshire (1949, 1951). These theories consider the crystal from a macroscopic, thermodynamic point of view. The transition is examined by considering the free energy of the crystal as a function of a number of independent variables, usually temperature, stress and polarization. However, since they are independent of any particular microscopic model, phenomenological theories do not establish any relationship between dielectric properties, atomic displacements

and lattice vibrations and so give no direct insight into the phase transition mechanism.

Model theories on the other hand, attempt to derive macroscopic properties of crystals in terms of a microscopic model of their structure and interatomic forces. Early model theories often applied only to one material, e.g. Slater's theory for KH_2PO_4 (1941). Although Slater developed a relatively successful theory of the phase transition and the dielectric constant of KH_2PO_4 it does not explain the large isotope effect (i.e. the large increase in T_c on the substitution of deuterium for hydrogen in KH_2PO_4) or why $NH_4H_2PO_4$ - isomorphous in the paraelectric phase - is not ferroelectric.

The more general approach to the theory of ferroelectric phase transitions in terms of lattice dynamics was proposed by Cochran (1959, 1960). A characteristic of ferroelectrics is that the static dielectric constant, $\varepsilon(0)$, following a Curie-Weiss law, varies as $(T-T_o)^{-1}$ as the transition temperature is approached and diverges at T_o. This feature along with the Lyddane-Sachs-Teller relationship (Lyddane, Sachs, Teller, 1941)

$$\frac{\omega_{LO}^2}{\omega_{TO}^2} = \frac{\varepsilon(0)}{\varepsilon(\infty)}$$

implies an anomaly in the lattice vibrational spectrum of ferroelectric crystals at T_c. (ω_{LO} and ω_{TO} are the frequencies of the longitudinal and transverse optic modes of wave vector q = zero, $\varepsilon(0)$ is the static dielectric constant, and $\varepsilon(\infty)$ is the high-

frequency dielectric constant.) As T_c is approached $\varepsilon(0)$ diverges and so ω_{TO} should tend to zero.

The ferroelectric transition in certain crystals could therefore be regarded as the result of an instability of the paraelectric phase of the crystal against one of the transverse optic normal modes of vibration. The frequency of this so-called 'soft' mode is temperature dependent and decreases to zero on approaching the transition temperature. The change in crystal structure on going from the paraelectric to the ferroelectric phase is thus essentially the 'frozen-in' atomic displacements (eigenvectors) of the soft mode.

Cochran (1960) suggested that this was the case in $BaTiO_3$ - a crystal that has a displacive type of transition from a cubic paraelectric phase to a tetragonal ferroelectric phase - and later extended the theory (Cochran, 1961) to include crystals with order-disorder transitions such as KH_2PO_4.

Experimental evidence in support of Cochran's theory was soon found in strontium titanate, $SrTiO_3$, (Cowley, 1962) where a mode with the characteristics of a 'soft' mode was observed. Kaminow and Damen (1968) observed a heavily damped soft mode in KH_2PO_4 and Skalyo, Frazer and Shirane (1970) identified the ferroelectric soft mode in KD_2PO_4. The coupling of the soft mode to an optic mode of the lattice was demonstrated in crystals isomorphous with KH_2PO_4 by Katiyar, Ryan and Scott (1971).

A more detailed account of the investigation into the 'soft' mode is given in Chapter 5 where the theoretical and experimental work on KH_2PO_4-type materials is reviewed.

The structure of the ferroelectric phase is characteristically pseudosymmetric. The low-temperature phase has an atomic arrangement which approximates closely to the high-temperature phase, as the ferroelectric phase is derived from the paraelectric phase by relative atomic displacements which are generally small compared with the unit cell. As already pointed out, it is not necessarily the case that the transition to the high temperature phase is always reached before decomposition or melting.

That structural phase transitions are describable in terms of an order parameter, η, whose appearance at the Curie point breaks the symmetry of the paraelectric phase, was suggested by Landau (1937). In a 'proper' ferroelectric phase transition, the order parameter of the transition (the primary order parameter) is the spontaneous polarization. 'Improper' ferroelectrics are crystals for which the spontaneous polarization is not the primary order parameter and the appearance of the polarization is due to the coupling of the actual primary order parameter with the polarization. In the case of boracites (for example) the order parameter is the normal coordinate of a mode at the zone boundary of the high-temperature phase so the order parameter and the spontaneous polarization have different symmetry properties. KH_2PO_4 (and perhaps its isomorphs) can also be regarded as an 'improper' ferroelectric in that the primary order

parameter measures the ordering of the protons in the hydrogen bond. However, the primary order parameter and the spontaneous polarization have the same symmetry. In general improper ferroelectrics of this second type behave exactly like proper ferroelectrics as far as static properties are concerned.

Ferroelectric transitions can often be regarded broadly as being of one of two types, either a) order-disorder transitions or b) displacive transitions. In an order-disorder transition, the ferroelectric transition involves the ordering of structure elements that are disordered in the paraelectric phase. Hydrogen-bonded ferroelectrics often display order-disorder transitions. In a displacive transition, the change in structure at the transition involves only small atomic displacements from the configuration of the higher-symmetry phase. The ferroelectric transition in barium titanate and quartz are regarded as displacive transitions.

The distinction between the purely displacive transition and the order-disorder transition becomes uncertain in the limit of the site separation of the relevant disordered atoms being comparable with the mean thermal amplitude of these atoms. The phase transition in some materials can be regarded as involving both types, e.g. in KH_2PO_4 where the ferroelectric transition involves both the ordering of the hydrogens and the relative displacements of the potassium and phosphorus ions.

1.3 Materials Studied and Present Work

This thesis is concerned with structural studies of ferroelectrics of the KH_2PO_4 and boracite type.

KH_2PO_4 was one of the first materials in which ferroelectricity was discovered (Busch and Sherrer, 1935). Because of its relatively simple structure, it has attracted a large amount of theoretical and experimental attention. K, Rb and Cs dihydrogen arsenates, Rb and Cs dihydrogen phosphates and their deuterated counterparts are assumed to be isomorphous with KH_2PO_4. A comprehensive consistent theory of ferroelectric phenomena in this class of compounds should account for the similarities and differences in these materials isomorphous with KH_2PO_4. Important changes of dielectric behaviour, dynamical response and presumably structure are obtained on variation of deuteration level, temperature and pressure. Very little structural work has been done on the isomorphous materials although increasing attention has been paid recently to them, especially in Raman scattering work where some definite differences in dynamical behaviour from KH_2PO_4 have been found (Lowndes, Tornberg and Leung, 1974). Isotopic and isomorphic substitutions lead not only to a considerable change in the ferroelectric transition temperature, Curie constant and saturated spontaneous polarization, but also to a change in the character of the phase transition.

Further interest was stimulated in $Cs(D_xH_{1-x})_2AsO_4$ through the results of Dietrich, Cowley and Shapiro (1974).

They appeared to find evidence for a complex domain structure in the ferroelectric phase but these results have since been shown to be attributable to multiple Bragg scattering (Meyer, Dietrich, Nelmes, Hay and Cowley, 1976).

The shear angle in the orthorhombic phase of $Cs(D_xH_{1-x})_2AsO_4$ is very much larger ($2.0(1)^o$) than that found in KH_2PO_4 (0.45^o) and this allows the possibility of investigating the ferroelectric structure without having to pole and physically constrain the crystal (see Section 4.1).

In view of all this, a detailed structural investigation has been undertaken to contribute to a more overall view of the KH_2PO_4-type compounds in general and to provide structural parameters for the analysis of experiments on $Cs(D_xH_{1-x})_2AsO_4$ in particular.

Boracites have also attracted increasing attention over recent years. The transition in boracites is thought to be an example of a coupled phase transition (a transition involving more than one order parameter). Boracites also exhibit unusual ferroelectric, magnetic, dynamical and structural properties and progress within these areas of interest requires accurate knowledge of the crystal structures involved. There has been a lack of accurate structural information available and uncertainty exists in the interpretation of thermal motion in the cubic phase, and in the structures of the orthorhombic and rhombohedral phases (see Section 7.1).

With this in mind, a programme of structural studies of boracites has been instigated in Edinburgh - of which the work reported here is part.

The interpretation of thermal motion in the cubic phase of boracites is open to some doubt (see Section 7.1), though Nelmes and Thornley (1974, 1976) and Nelmes, Thornley and Kennedy (1976) claim to have removed much of the uncertainty in the cases of chromium chlorine boracite, nickel iodine boracite and copper chlorine boracite respectively. The structural studies of the two boracites (cobalt iodine boracite and copper bromine boracite) reported in this thesis have been carried out to obtain further information about the thermal motion in the cubic phase - particularly of the metal and halogen ions.

Full introductions relating to $Cs(D_xH_{1-x})_2AsO_4$ and the two boracites, $Co_3B_7O_{13}I$ and $Cu_3B_7O_{13}Br$, are given in Chapters 5 and 7 respectively.

Chapter 2 gives details of sample source, preparation and initial testing.

The general methods of study employed in the collecting and analysis of data from the various crystals studied are described in Chapter 3.

In Chapter 4 a specific method for investigating the ferroelectric phase in $Cs(D_xH_{1-x})_2AsO_4$ is described.

As mentioned earlier, this technique is possible because of the relatively large ($2.0(1)^{o}$) shear angle found in this crystal and it avoids the need for poling and physically constraining the crystal.

In Chapter 5 the structure and properties of, and research on, the KH_2PO_4-family are reviewed. The structural studies (using neutrons) of $Cs(D_xH_{1-x})_2AsO_4$ at room temperature, $T_c+5^{o}K$ ($T_c=203^{o}K$) and $77^{o}K$ are described and the results are compared with those for KH_2PO_4 and KD_2PO_4. The validity of various structural models is assessed using constrained-refinement and significance-testing techniques.

Chapter 6 describes some investigations of features of the transition in $Cs(D_xH_{1-x})_2AsO_4$ that have not as yet been observed in other isomorphs. The behaviour of the crystal at the transition suggests an inhomogeneity of the hydrogen - deuterium concentration.

The properties of boracites are reviewed in Chapter 7 and an account is given of the crystal structure determination (using X-rays) of cubic $Co_3B_7O_{13}I$ and $Cu_3B_7O_{13}Br$ at room temperature. As in Chapter 5 constrained-refinement and significance-testing techniques are used to assess various structural models.

C H A P T E R 2

SAMPLE PREPARATION

CHAPTER 2

SAMPLE PREPARATION

This chapter describes the preparation and testing of the crystal samples used for the experiments described in later chapters of this thesis. Section 1 deals with the crystal samples for the various experiments on $Cs(D_xH_{1-x})_2AsO_4$ and Section 2 describes the initial preparation of $Co_3B_7O_{13}I$ and $Cu_3B_7O_{13}Br$. The crystal samples are listed in Table 2.1.

2.1 $Cs(D_xH_{1-x})_2AsO_4$

2.1.1 Crystal samples for neutron structural experiments: The parent crystal (CP) was a 1 cm^3 crystal of $Cs(D_xH_{1-x})_2AsO_4$ (with x nominally 0.95) bought from Quantum Technology Ltd. The required crystals were cut from this main crystal.

$Cs(D_xH_{1-x})_2AsO_4$ is slightly deliquescent and this necessitated extra precautions to be taken during cutting and mounting. Several lamps were lowered over the working area to decrease the relative humidity in the region of the crystal. A drying agent - silica gel - was used to indicate the presence of any appreciable amounts of water vapour around the crystal sample. Gloves were worn at all times.

Three crystal pieces were cut from the same parent sample (CP).

Sample CN1: This crystal was used for room-temperature four-circle data collection. It is a 2 mm cube and because of its deliquescence and to prevent D→H exchange, it was enclosed in a glass bulb. The glass for the bulb was soda glass as 'common' glass contains boron, which has a high absorption cross-section for neutrons.

Samples CN2 and CN3: These two crystals were used for low-temperature neutron data collection and so were sealed in dry helium atmospheres in cryostats, making it unnecessary to enclose them in glass bulbs. CN2 has dimensions 2 x 2 x 4 mm^3 and CN3 has dimensions 1.5 x 1.5 x 4 mm^3.

All the crystals were examined with X-rays before being accepted as suitable specimens for data collection. Oscillation and back-reflection Laue photographs were taken of the samples to orient them and the photographs were examined for any evidence that the crystals were not single. The three specimens were satisfactory.

2.1.2 Crystals for transition investigation: As described in Chapter 6, the transition in crystals cut from CP was found to occur for only part of the crystal at the nominal transition temperature with the remainder transforming over a 60°K temperature range. To investigate this a comparison was made with several samples of $Cs(D_xH_{1-x})_2AsO_4$ kindly supplied by G Loiacono of Philip's Laboratories, USA.

The crystals (see below) were each cut from larger parent crystals in the same manner as has been described previously. They were kept in a sealed jar of silica gel except during the experiment when they were sealed in a dry helium atmosphere in a cryostat. All the crystals were cut to approximately the same size, 1.5 x 1.5 x 4 mm^3.

CN5: The deuteration level corresponded to a transition temperature of 223°K.

CN6: The deuteration level corresponded to a transition temperature of 192°K.

CN7: The deuteration level corresponded to a transition temperature of 183°K.

(Loiacono's figures)

As with previous samples, back-reflection Laue photographs were taken of the crystals to orient them. These photographs were examined for any evidence that the crystals were not single.

2.2 Boracites

The boracite crystals were used for X-ray four-circle diffractometer data collection.

For an X-ray sample - where absorption effects cannot be neglected (see Section 3.2) - it is desirable that the crystal size is small enough for the absorption correction to vary only slowly with θ and large enough to give an adequate intensity.

From these criteria, the optimum size would correspond to a μR value of about 1.0 (Arndt and Willis, 1966, p240) where μ is the linear absorption coefficient and R is a typical dimension - strictly the radius of a spherical specimen. This approximate criterion was applied for both samples.

2.2.1 Co-I boracite ($Co_3B_7O_{13}I$): A crystal of Co-I was kindly supplied by Dr H Schmid of the Battelle Institute, Geneva. For $\mu R \approx 1$ (where $\mu = 96.3$ cm^{-1} for Co-I irradiated with MoK_α radiation), a crystal of linear dimension 0.1 mm is required. A crystal of linear dimension 0.17 mm was cut from the bulk sample using a razor blade and was then glued to the end of a thin glass fibre. X-ray Laue photographs were taken to check that the crystal was single.

2.2.2 Cu-Br boracite ($Cu_3B_7O_{13}Br$): A crystal of Cu-Br was also supplied by Dr H Schmid of the Battelle Institute. The linear absorption coefficient for Cu-Br is 127.4 cm^{-1} for MoK_α radiation, indicating an optimum size of the crystal to be of average dimension 0.08 mm. A crystal of linear dimension 0.15 mm was cut from the parent sample. Because of the hardness of Cu-Br, the crystal sample was chipped rather than cut from the parent crystal, resulting in a badly shaped crystal. This resulted in rather unsatisfactory absorption corrections being made at a later stage (see Section 7.4.1). Laue photographs were used to check that the crystal was single.

Table 2.1

Sample	Name	Experiment		Section
		Phase	Temperature ^{o}K	
$Cs(D_xH_{1-x})_2AsO_4$	CN1	Tetragonal	292	5.3.1
$Cs(D_xH_{1-x})_2AsO_4$	CN2	Tetragonal	208 (T_c+5)	5.3.2
$Cs(D_xH_{1-x})_2AsO_4$	CN3	Orthorhombic	77	5.3.3
$Cs(D_xH_{1-x})_2AsO_4$	CN5	Investigation of the tetragonal→ orthorhombic transition :		Chapter 6
$Cs(D_xH_{1-x})_2AsO_4$	CN6			
$Cs(D_xH_{1-x})_2AsO_4$	CN7			
$Co_3B_7O_{13}I$	Co-I	Cubic	291	7.3
$Cu_3B_7O_{13}Br$	Cu-Br	Cubic	291	7.4

CHAPTER 3

METHODS OF STUDY

CHAPTER 3

METHODS OF STUDY

3.1 Introduction

This chapter describes the general methods used for the collection and analysis of data from the single crystal samples. Both X-ray and neutron techniques were used in the collection of the data sets and relative advantages and disadvantages are pointed out.

In a structural study of an ideal crystal, the beam of X-rays or neutrons is diffracted by planes of atoms in the crystal. The measured integrated intensities of the reflections ideally yield structure amplitudes (see Section 3.5) directly after certain known geometrical factors are taken into account. In a real crystal, random and systematic errors in the measurement of the integrated intensity caused by general background, absorption, simultaneous reflections, extinction and thermal diffuse scattering (T.D.S.) have to be taken into account and, if possible, corrected for. For the work described in this thesis, the crystal structure is known to a good approximation from the outset. The resulting corrected structure amplitudes can then be compared with the structure amplitudes calculated from the approximate structure, whose parameters are adjusted by least-squares refinement to achieve the best fit (see Section 3.6.1). The final parameters are taken as a description of the crystal structure.

3.2 X-Ray and Neutron Diffraction

When investigating the arrangement of atoms in solids, it is necessary that the wavelength of the incident radiation be of the same order as the separation of these atoms.

In the X-ray case, the studies were carried out using the characteristic K_α radiation of molybdenum. Higher-order 'contaminants' and the K_β line were removed by the standard techniques of, respectively, a pulse-height discriminator and a β-filter (Zr). The resultant quasi-monochromatic beam is taken to have a wavelength of 0.7107Å.

The neutron source was the PLUTO research reactor at A.E.R.E., Harwell. In a reactor neutrons in thermal equilibrium with the moderator have a Maxwellian energy spectrum. Using the de Broglie relationship

$$\lambda = h/mv$$

where h is Plank's constant and m and v are the mass and velocity respectively of the neutron, it can be shown that the wavelength corresponding to the root-mean-square velocity of neutrons in equilibrium at a temperature of 100°C is 1.55Å. The range of wavelengths around the peak of the distribution is of the right magnitude for the investigation of atomic arrangements.

A narrow band of neutron wavelengths is selected from the continuous distribution by Bragg reflection off a single-crystal monochromator. The most commonly used crystals are beryllium, copper, graphite and germanium.

The range of wavelengths reflected and the intensity of the reflected beam depend on the degree of perfection of the monochromating crystal. It is usual to work at wavelengths below the peak of the Maxwellian distribution (about 1Å or less) to minimise second and higher order contamination. (The use of silicon or germanium overcomes this difficulty.)

In the determination of the diffracted intensity, both systematic and random errors are introduced by incoherent and non-sample background scattering. Incoherent scattering of X-rays is due to the Compton effect and the photoelectric effect. In neutron diffraction, the main sources of incoherent scattering are isotope incoherence and spin incoherence - the latter being of particular importance in compounds containing hydrogen. Scattering of the radiation may also be caused by materials surrounding the specimen, e.g. a cryostat in low-temperature work. Another cause of general background is the component of 'white' radiation remaining in the X-ray beam. This coherent background is not uniform across the reflection and can lead to errors in the low-angle data : the problem can be reduced in diffractometer data collection by removing the β-filter for the low-θ range (Nelmes, 1975).

In their passage through the crystal, both X-ray and neutron beams are attenuated by true absorption processes - photoelectric absorption for X-rays and nuclear capture for neutrons. However, neutrons in general interact rather weakly with matter and so the neutron absorption coefficients are very much smaller than the corresponding X-ray

absorption coefficients and can often be neglected. The exact reduction of intensity depends on the paths through the crystal and the magnitude of the absorption coefficient, the absorption factor being

$$A^*_{hkl} = V\left[\int \exp\left\{-\mu(p + q)\right\}\, dV\right]^{-1}$$

where μ is the linear absorption coefficient, p and q the pathlengths of the incident and reflected beams in the crystal and V is the crystal volume. A typical value of μ for neutrons is 0.3 cm^{-1} in comparison with values of 10-100 cm^{-1} for X-rays. Notable exceptions to this are boron, cadmium and gadolinium which have a high capture cross-section for neutrons. In the X-ray case, it is usually necessary to calculate the effect of absorption (see Section 3.5).

A reduction in the observed intensity of a given reflection can also result from extinction. This is the attenuation of the radiation by diffraction processes within the crystal and can be divided into two types, primary and secondary.

Primary extinction is the attenuation of the incident and reflected beams by interference effects within each perfect region of the crystal. If the crystal has large perfect regions, the incident beam can only penetrate a short distance before being totally reflected and the inner parts of the crystal do not contribute. However, this effect in general is much reduced as most crystals are made up of rather small 'mosaic blocks' of perfect crystal separated by dislocations, impurities and other imperfections which give rise to small misorientations between the crystal blocks or small variations in lattice constants. On passing from one block to another, the coherence of the incident

and scattered beam is lost, so that the total scattered intensity is the sum of the intensities scattered by each block individually.

Secondary extinction occurs when, in any given orientation of the whole crystal, an appreciable proportion of the mosaic blocks have the same orientation. This results in succeeding blocks receiving an incident beam which is significantly reduced by the intensity scattered by the previous identically oriented block.

Extinction is greatest for the strongest reflections, as these scatter the maximum amount of energy from the incident beam, and in particular, for those strong reflections for which the incident-beam path-length is long. The amount of extinction decreases with wavelength. An extinction factor was applied to the collected data (see Appendix A).

Simultaneous reflections occur when the Bragg reflecting condition is simultaneously satisfied for more than one family of planes, and can give rise to a modification of the observed intensity. This effect can be minimised when using normal-beam geometry on a four-circle diffractometer (see Section 3.4) by avoiding having a symmetry axis parallel to the goniometer head axis (Ø axis).

T.D.S. rises to a maximum at the same position as the Bragg peak and can constitute a substantial portion of the observed intensity. The origin of the T.D.S. peak lies in the $\frac{1}{\omega_j^2(q)}$ dependence of the first-order scattering by lattice vibrations. Neglecting to correct for T.D.S. will give rise to significant errors in the temperature

factors only (Cooper and Rouse, 1968).

X-ray samples have to be quite small to reduce absorption to a level than can be corrected at all accurately. A generally accepted criterion for the optimum size of a crystal is that $\mu R \simeq 1$, where μ is the linear absorption coefficient and R the average crystal radius. This leads to the requirement that X-ray samples have linear dimensions of approximately 0.1 mm. However, due to the relatively low scattering cross-section for neutrons (and the much lower flux of a neutron source in comparison to an X-ray source), neutron samples are generally of the order of a few millimetres across. However, this leads, on the whole, to higher secondary extinction in neutron diffraction data.

The scattering of X-rays from crystals varies with Bragg angle and atomic number. As the scattering angle is increased the scattering amplitude is reduced by interference. The scattering increases with increasing atomic number. Anomalous scattering of X-rays, which occurs when the frequency of the incident radiation is close to any natural absorption frequency of the scattering atom, requires the treatment of the atomic scattering factor as a complex number.

On the other hand, the scattering length for neutrons is essentially isotropic and independent of atomic number. This offers the advantage of increased resolution in direct space because Bragg reflections at higher θ values can be measured more readily than in the X-ray case. It also allows the accurate location of light atoms in the neighbourhood of heavy ones - in particular the difficulty of locating

hydrogen atoms with X-rays is overcome. This has direct relevance to the study of $Cs(D_xH_{1-x})_2AsO_4$. One of the main objects of the investigation was to determine whether the deuteriums in the paraelectric phase of $Cs(D_xH_{1-x})_2AsO_4$ were disordered in a double minimum well or were ordered at the centre of the O-H.....O bond. This could not be determined using X-rays and hence the major portion of the work on $Cs(D_xH_{1-x})_2AsO_4$ was carried out using neutron diffraction.

The boracites are studied using X-rays. If neutrons had been used, the experiments would have required the crystals to be enriched with the B^{11} isotope to minimise absorption.

3.3 X-Ray and Neutron Structure Factors

The structure factor, a Fourier component of the scattering density, depends on the atomic scattering factors (or scattering lengths) of the various types of atoms present and the relative positions of such atoms in the unit cell. In its simplest form (for the static structure - ignoring all thermal motion), it is given as

$$F(\underline{h}) = \sum_{i=1}^{n} l_i \exp(2\pi i \, \underline{H} \cdot \underline{X}_i)$$

where $\underline{h}$ = (h, k, l) the Bragg indices, $\underline{H} = (\underline{a}^* h + \underline{b}^* k + \underline{c}^* l)$ a reciprocal lattice vector, $\underline{X}_i = (X_i, Y_i, Z_i)$ the co-ordinates of the i^{th} atom with respect to some origin and l_i represents the scattering length (for the neutron case) or the atomic scattering factor (for the X-ray case) of the i^{th} atom. The sum is taken over all n atoms in one unit cell. The structure amplitude (Section 3.1) is the modulus of the structure factor.

When account is taken of the effect of thermal motion of the atoms about their mean position, a so-called temperature factor must be determined for each atom. In the general case of anisotropic vibration, the displacements due to the thermal motion are described in terms of a symmetric tensor

$$\beta = \begin{pmatrix} \beta_{11}, & \beta_{12}, & \beta_{13} \\ \beta_{12}, & \beta_{22}, & \beta_{23} \\ \beta_{13}, & \beta_{23}, & \beta_{33} \end{pmatrix}$$

where the temperature factors β_{11}, β_{12}, etc. for each atom define the principal axes and direction cosines of the thermal vibration ellipsoid. The temperature factor (T.F.) in the structure factor equation

$$F(\underline{h}) = \sum_{i=1}^{n} l_i \exp(2\pi i \, \underline{H}. \, \underline{X}_i)(T.F.)_i$$

takes the form

$$T.F. = \exp - (\beta_{11} h^2 + \beta_{22} k^2 + \beta_{33} l^2 + \beta_{12} hk + \beta_{13} hl + \beta_{23} kl)$$

(The temperature factors are treated as adjustable parameters in the least-squares refinement.) The above only applies in the 'harmonic approximation' where the expansion of the crystal potential is terminated at second order terms.

In the case of anharmonic effects, when departures from harmonic thermal motion are taken into account, third and higher order contributions must be included. Third and forth cumulants will be considered in the structure refinement of the two boracites (see Section 7.2).

3.4 Instruments and Data Collection

The X-ray and neutron intensity data were collected using single-crystal diffractometers. The X-ray experiments were carried out on a Hilger and Watts four-circle automatic diffractometer in the Department of Physics, York University. The neutron data were collected using the diffractometers at the PLUTO reactor, A.E.R.E., Harwell. As the X-ray and neutron diffractometers were essentially similar (the main difference being that the neutron machines tend to be bulkier because of the necessary heavy radiation shielding), only a general description of a diffractometer is given.

In all experiments at room temperature, full three-dimensional data were collected using a four-circle diffractometer in normal-beam equatorial geometry (see Figure 3.1, a reproduction of Figure 3 of Arndt and Willis, 1966). The crystal sample is located at the diffractometer centre - defined as the point of intersection of all the axes of rotation - and any vector within the crystal can be aligned with any direction specified (in the laboratory frame) by rotation of the ϕ, χ and ω shafts.

For the collection of intensity data below room temperature, a cryostat was used to cool the crystal. The cryostat used is large and bulky and the ϕ and χ circles have to be removed. The resultant two-circle diffractometer can still be used to collect three-dimensional data. The usual method is to mount the sample with a principal axis vertical and to collect the data in layers

Figure 3.1 Normal-beam equatorial geometry. The crystal is mounted on a goniometer-head attached to the ϕ axis; the ϕ circle moves around the vertical χ-circle, and the ϕ-χ assembly rotates as a whole about the vertical ω-axis. The detector moves in the horizontal, equatorial plane and the incident beam is normal to the crystal oscillation axis ω. The detector moves about the 2θ-axis, which is parallel to and independent of the ω-axis.

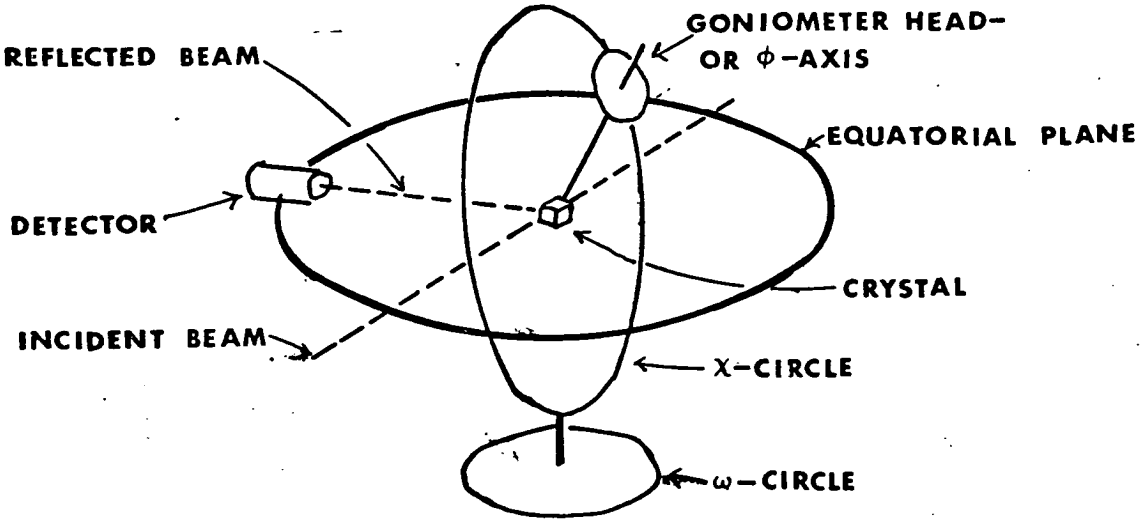
REFLECTED BEAM
GONIOMETER HEAD-
OR φ-AXIS
EQUATORIAL PLANE
DETECTOR
CRYSTAL
INCIDENT BEAM
χ-CIRCLE
ω-CIRCLE

using a tilting counter and normal beam inclination geometry (see Figure 3.2). The main limitation of a two-circle diffractometer with tilting counter is that it is only possible to collect a few layers in any one mounting of the crystal - the number of layers is dependent on the wavelength and cell dimensions because of limited tilt angle, ν. The maximum tilt angle attainable on the machine used was 38^{o} : above that the counter is restricted by the cryostat assembly. Another small limitation arises because in this geometry it is impossible to collect data from the centre of higher layers. There is also the probability of higher layers suffering from a greater absorption of the diffracted beam due to the diffracted beam passing through thicker portions of the cryostat and also having longer path lengths through the cryostat. Some careful measurements are required to determine how significant an effect this is.

The cryostat used for the low temperature work was a Cryogenics Associates CT14 cryostat with a Thor temperature controller (see Figure 3.3). The inner flask can be filled with either liquid nitrogen or liquid helium giving a range of temperatures from $4.2^{o}K$ to room temperature. The temperature was measured by a sensor placed just above the sample; a controller linked to a heater in the cryostat regulated the temperature at the required value with an expected stability of $\pm$ $0.25^{o}K$.

The diffractometers were controlled directly by a PDP8 computer. This allowed the machine to be run automatically with little

Figure 3.2 Normal-beam inclination geometry. The crystal is mounted on a goniometer head attached to the ϕ-axis. The detector moves around the 2θ-axis with a variable tilt angle ν.

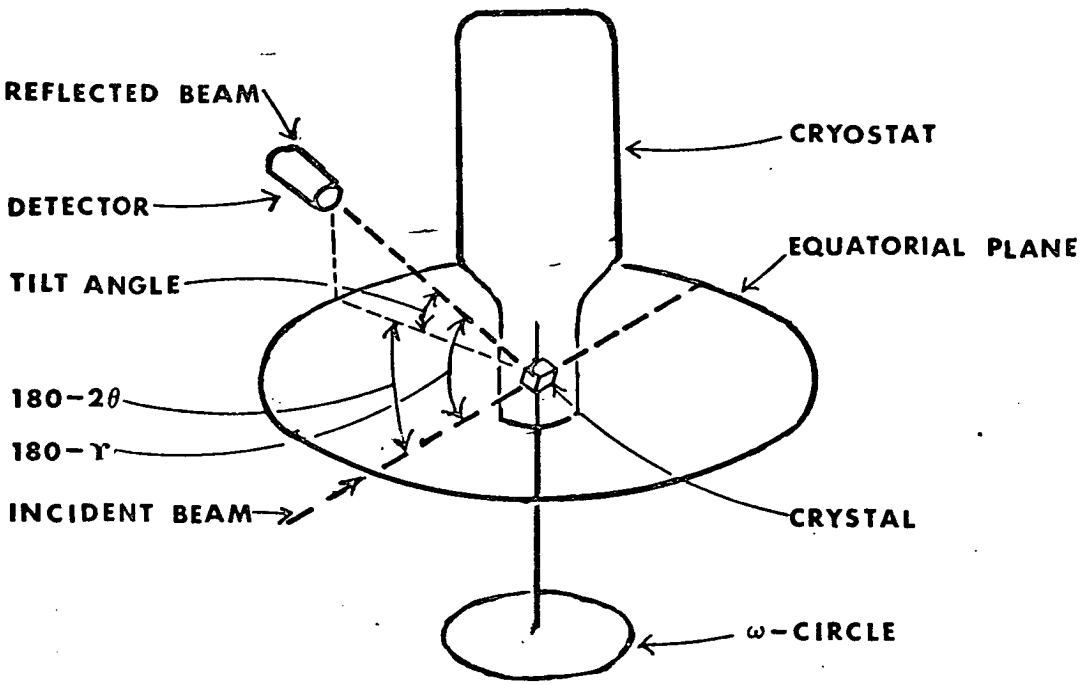
REFLECTED BEAM
DETECTOR
TILT ANGLE
180−2θ
180−ϒ
INCIDENT BEAM
CRYOSTAT
EQUATORIAL PLANE
CRYSTAL
ω−CIRCLE

Figure 3.3 A schematic drawing of the cryostat illustrating the practical limitation on ω.

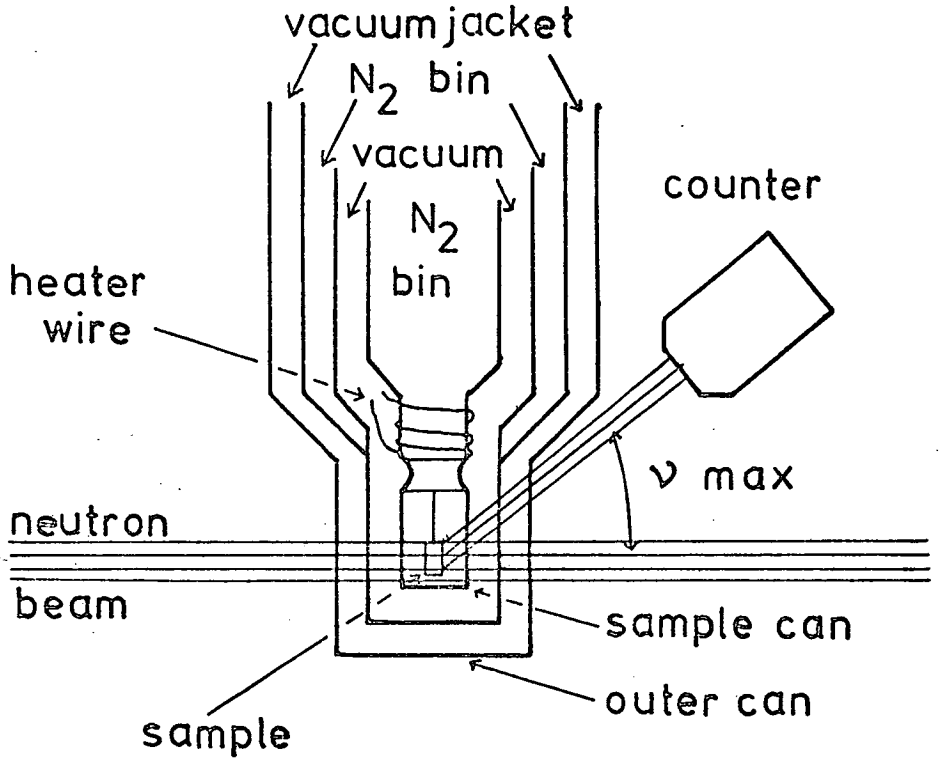
vacuum jacket
N_2 bin
vacuum
N_2 bin
counter
heater wire
ν max
neutron beam
sample can
outer can
sample

operator intervention after the initial setting up. The data were recorded on magnetic or paper tape. The teleprinter output afforded a back-up copy and also a complete sequential record of the experiment.

The type of scan used with the diffractometer was in all cases that of the ω-2θ type, where the 2θ arm (detector) is linked to the ω shaft (crystal) in the ratio 2:1. Each Bragg reflection was measured by making a single stepped scan through the peak, including background level counts on both sides. (When using a cryostat it is preferable to remove the background by repeating the scan with the crystal offset from the peak (by about 2^{o} usually). In this way the background measurement includes any structure in the scattering from the cryostat, and so a more accurate subtraction of the background is achieved. However, at the times of performing the experiments with the cryostat, this type of scan was not available on the machine used.) Scans were always over a range at least twice the expected peak width.

The time set for each scan properly depends on the strength of the reflection and the required accuracy - which in turn depends on the purpose of the experiment. None of the diffractometers used had software of sufficient sophistication to optimise the time spent on each reflection and so an average accuracy had to be the aim. (Reflected intensitites from the boracites fall into two classes, strong and weak, and were collected separately with appropriately different counting times.) Furthermore, all

experiments were done under conditions of limited total time : it was necessary then to balance adequate accuracy with adequate number and resolution (the sin θ/λ limit) of reflections.

For the boracites, previous studies of the cubic phase (see Chapter 7) were taken as a guide to the accuracy and resolution required. In the tetragonal phase of the KH_2PO_4 isomorphs, the main problem is to resolve the disordered hydrogen (or deuterium): in this respect earlier studies of KD_2PO_4 were a useful guide for the $Cs(D_xH_{1-x})_2AsO_4$ experiments.

In the neutron case, because of the random fluctuation of the output from the reactor, a low-efficiency monitor in the incident beam is used to ensure that for each reflection the crystal is exposed to the same amount of radiation. Counts are accumulated at each step of the scan for a set monitor count rather than a set time.

As a check that the crystal orientation and the counter efficiency remained constant, a standard reflection was measured every few hours. In the case of the two-circle data collection, a standard reflection was chosen for each layer. A common standard reflection in the zero layer was measured each time the layer was changed and at the end of the experiment.

Before carrying out a standard check, the machine was required to check the setting position of each shaft by returning each one to the datum position. In this way any accidental mis-setting of the

crystal was detected.

True symmetry-equivalent reflections were measured in all the experiments. The number of equivalents measured depended primarily on the symmetry of the crystal and also on the time available for the experiment. Particularly in the neutron diffraction experiments, shaft-setting takes a significant portion of the time spent on each reflection; the measurement of many equivalents is then inefficient.

3.5 Data Handling Procedures

The scan is divided into steps on the background to the low-angle side of the peak (b_1), steps through the peak (P), and steps on the background to the high-angle side of the peak (b_2). The integrated intensity, I, is then

$$I = \sum P - \left\{ \left\{ \sum b_1 + \sum b_2)/(n_1+n_3) \right\} \times n_2 \right\} \times {}^{m_2}/_{m_1}$$

where P is a peak count, b_1 and b_2 are background counts; n_1, n_2 and n_3 are the number of steps in the low-angle background, the peak, and the high-angle background respectively: m_2 and m_1 are the monitor counts in the neutron case and the time in seconds in the X-ray case for the peak steps and the background steps respectively. (In all experiments $n_3 = n_1$; in the neutron diffraction experiments m_2 was set equal to m_1; for the X-ray diffraction experiments $m_1 = \frac{m_2 \times n_2}{n_1 + n_3}$).

The standard deviation in the intensity, taking account only of counting statistics, is given by -

$$\sigma(I) = \left(\sum P + n_2^2 \frac{(\sum b_1 + \sum b_2)}{(n_1 + n_3)^2} \frac{m_2^2}{m_1^2} \right)^{\frac{1}{2}}$$

At this stage some bad measurements were deleted: reflections at such a low angle that the beam stop obstructed the diffracted beam, reflections at certain high-angle settings in which part of the machine assembly obstructed either the incident beam or the diffracted beam (a software fault made the avoidance of these 'blind' regions under automatic control unreliable), reflections whose scans clearly included some spurious high counts (generally caused by electrical interference), and reflections that were collected in periods when there was a discrepancy in the measurement of the standard reflection or when errors occurred at the following datum check. When wide disagreement was observed between equivalent reflections not clearly attributable to any of these causes the measurements were retained but were noted for re-examination after absorption corrections were carried out.

The integrated intensities and errors are then corrected by the Lorentz-polarisation factor (LP) to take into account geometrical and polarisation factors. For the normal-beam equatorial geometry the Lorentz factor correction is sin 2θ and for the tilting-counter normal-beam geometry it is cos ν sin γ (where ν is the tilt angle and γ the setting angle of the detector). In neutron diffraction P=1 as there is no polarisation effect associated with the nuclear reflections. For X-rays however a correction of the form

$$P = \tfrac{1}{2}(1 + \cos^2 2\theta)$$

has to be applied if, as here, the incident X-rays are unpolarised.

An examination of the equivalent reflections indicated that the effect of absorption in the neutron data sets was small and no corrections have been made for it in this study. For the X-ray data however, absorption corrections were applied using the program ABSCOR of the XRAY system of crystallographic computer programs (Stewart, 1972). This program requires a detailed description of the shape of the crystal, the linear absorption coefficient, μ, and the orientation of the crystal with respect to the diffractometer axes. The program then calculates the path through the crystal for each reflection and yields a correction that is as accurate as the description of the crystal shape and orientation, and the value of μ. Satisfactory results cannot be obtained however in the case of crystal faces having re-entrant angles.

The intensities and errors thus corrected for absorption and the LP-factor are taken as measures of the structure amplitudes (and errors) on a common relative scale.

Each set of symmetry-related observed structure amplitudes are averaged to give one non-equivalent observed structure amplitude, F_{obs}, for the set. The standard deviation, $\sigma(F_{obs})$ is taken to be the larger of a) the counting statistics error, and b) the root-mean-square deviation of the set of equivalent reflections.

If this comparison and averaging of symmetry-related reflections shows up large discrepancies the original data are re-examined thoroughly to check for underestimated errors, or to detect and delete suspect reflections - as described for the individual experiments in Chapters 5 and 7.

3.6 Data Analysis

3.6.1 Crystallographic Least Squares Refinement: The refining of a crystal structure from diffraction measurements, by means of the least-squares method, consists of minimising the function

$$R = \sum W_i \, (F_o - c.E.F_c)_i^2 = \sum W_i \Delta_i^2$$

by varying the positional and thermal parameters of the atoms in the unit cell. The summation is over all the measured Bragg reflections, F_o is the measured structure amplitude, F_c is the calculated structure amplitude, W is the statistical weight assigned to each reflection, c is a scale factor, and E is a correction factor for the effects of extinction. The procedure followed is described by Lipson and Cochran (1966).

When the approximate values of the parameters are known, the approximate corrections to the parameters are found from the normal equations

$$\sum_j \left[\sum_i W_i \frac{\partial Fc}{\partial P_i} \frac{\partial Fc}{\partial P_j} \right] \delta P_j = \sum_i W_i \frac{\partial F_c}{\partial P_i} (F_o - F_c)_i$$

The equations may be written in matrix form as $\underline{M}.\underline{\delta P} = \underline{E}$. The required solution is then $\underline{\delta P} = \underline{N}.\underline{E}$, where $\underline{N} = \underline{M}^{-1}$. As F_c and $\partial F_c / \partial P_j$ are functions of the parameters P_j, this procedure has

to be iterated until convergence is reached - usually when every δP_j is small compared with its standard deviation.

The refinements were all carried out using the full-matrix least-squares program developed from the standard ORFLS program by Dr G S Pawley of this department. The program allows for various weighting schemes (for values of W_i). If only random errors are present the weight assigned to each observation is

$$W_i = \frac{1}{\sigma^2(F_o)_i}$$

The correctness of the weights used in each case was tested by checking that $\overline{W\Delta^2}$ - the mean value of $W_i \Delta_i^2$, taken over successive small ranges of sin θ, F_o and E (extinction) - had no significant dependence on either sin θ, F_o or E. This analysis is provided by the program.

The coherent neutron scattering lengths were taken from Bacon (1972). Neutral-atom form factors were used (Doyle and Turner, 1968) for the X-ray refinements. Real and imaginary parts of the anomalous dispersion were included (Cromer, 1965).

The extinction factor E was approximated in all cases by including in the refinement a parameter describing isotropic secondary extinction (Cooper et al, 1968 - see Appendix A).

3.6.2 Constrained Refinement and Significance Testing: It may be valid to reduce the number of parameters describing a particular model by the introduction of certain constraints. For example, the

thermal motion of an atom may not be significantly anisotropic, in which case it can be constrained to be isotropic; a point at issue in the paraelectric phase of KH_2PO_4-type materials is whether the distribution of the hydrogen (deuterium) can be constrained to the five parameters required to describe a single (ordered) position or requires the nine parameters that describe a disordered distribution over two sites; both $Cs(D_xH_{1-x})_2AsO_4$ and the boracites have tetrahedral structural elements which, whilst not required to by symmetry, are very close to being regular. It may also be valid to increase the number of parameters to describe, for example, anharmonic thermal motion.

It is necessary to test the statistical significance of parameters added to the model - either to allow a constraint to be lifted, or to describe extra features such as anharmonicity. The goodness of fit of any model is characterised by $R_\omega = \sum_i w_i \Delta_i^2$. The ratio

$$\mathcal{R} = \left(\frac{R_\omega \text{ (for model with less parameters)}}{R_\omega \text{ (for model with more parameters)}} \right)^{\frac{1}{2}}$$ is distributed as (Hamilton, 1965)

$$\mathcal{R}_\alpha = \left(\frac{N-n}{M-N} F_\alpha + 1 \right)^{\frac{1}{2}}$$

where M is the number of observations, N is the greater number of parameters, n is the lesser number of parameters, α is the probability level, and F_α is the α point of the F-distribution with N-n and M-N degrees of freedom. Hence the significance of any improvement in fit obtained by increasing the number of parameters in the model from n to N can be tested statistically. The practice adopted here has been to test both constrained models and

models with additional parameters against the common reference of the best fit obtained with the usual (unconstrained) harmonic model (designated Model I).

The techniques of constrained refinement and significance testing (Hamilton, 1965) have been fully reviewed by Pawley (1971). Because of non-linearities inherent in the least-squares procedure, the procedure outlined above is of considerably greater rigour than any depending on a single refinement and its estimated least-squares errors. Nonetheless, there is still not a strict connection between statistical and physical significance, a problem to which Pawley (1971) suggests an empirical approach. An index of scepticism, $\mathcal{S}$, is defined as $(\mathcal{R}-1)/(\mathcal{R}(0.01)-1)$ where $\mathcal{R}(0.01)$ is the 0.01 point of the $\mathcal{R}$-distribution for the appropriate degrees of freedom. Pawley suggests that $\mathcal{S}$ values of 2 to 3 or more are needed to put <u>physical</u> significance beyond reasonable doubt.

CHAPTER 4

A SPECIFIC TECHNIQUE DEVELOPED FOR THE INVESTIGATION OF THE FERROELECTRIC PHASE OF $Cs(D_xH_{1-x})_2AsO_4$

CHAPTER 4

A SPECIFIC TECHNIQUE DEVELOPED FOR THE INVESTIGATION OF THE FERROELECTRIC PHASE OF $Cs(D_xH_{1-x})_2AsO_4$

4.1 Introduction

$Cs(D_xH_{1-x})_2AsO_4$ (hereafter DCsDA) at room temperature is tetragonal in structure. On cooling through its ferroelectric transition, the structure changes to an orthorhombic one. The transition temperature varies with deuteration (Loiacono, Ladell, Osborne and Nicolosi, 1976) - the higher the level of deuteration, the higher the transition temperature. On going from the room-temperature paraelectric phase to the low-temperature ferroelectric phase, the tetragonal cell shears in the ab plane, and the orthorhombic axes are taken along the diagonals of the sheared cell. The shearing of the tetragonal cell can result in four orthorhombic lattices (see Figure 4.1), two with the polarization in the positive C direction and two with the polarization in the negative C direction. The crystal can not now be regarded as consisting of a single domain, with the result that data collection is no longer the straight-forward task it is in the tetragonal phase.

To overcome the problem of the crystal having more than one domain in the ferroelectric phase, a choice of two possible methods of data collection is usually considered: a) the crystal sample is ground into a powder and a powder diffraction experiment is performed, or

Figure 4.1 The shearing of the tetragonal cell in the hk plane, resulting in four ferroelectric domains.

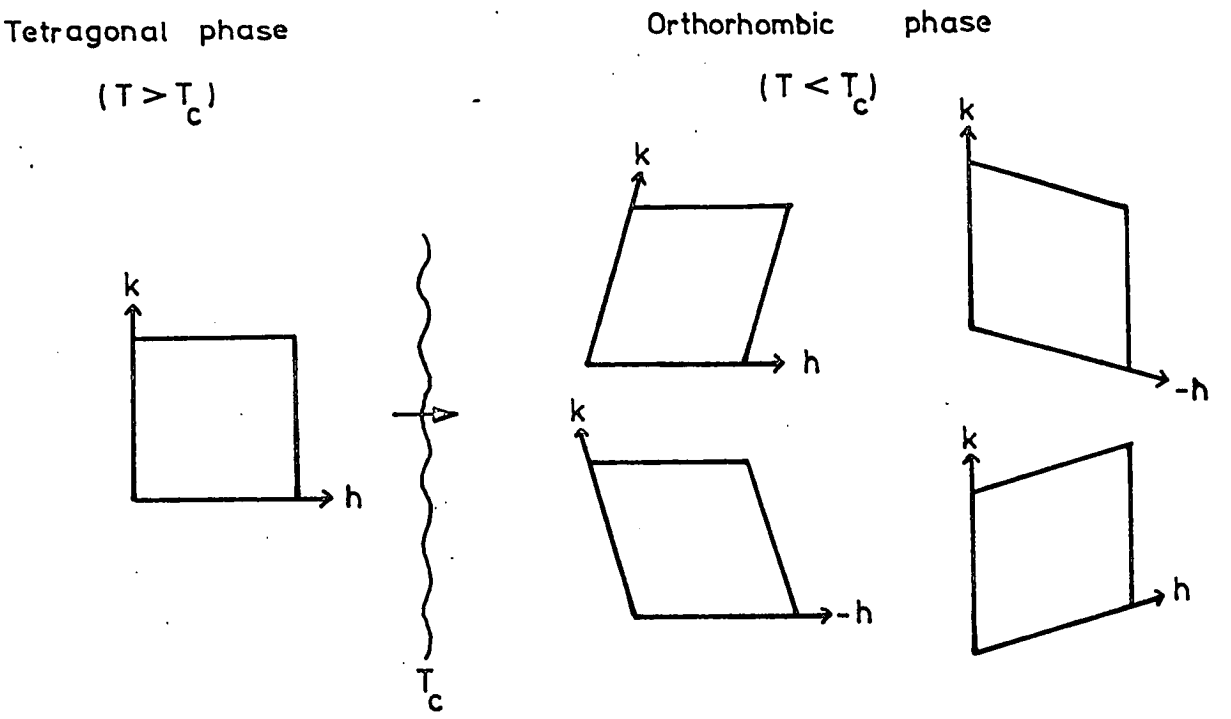
Tetragonal phase
(T > T_c)
k
h
T_c
Orthorhombic phase
(T < T_c)
k
h
k
-h
k
-h
k
h

b) the crystal is poled and physically constrained so that only one ferroelectric lattice exists in the orthorhombic phase - a single-crystal diffraction experiment then being possible. Method a) was not suitable for two reasons: 1) it was desirable to keep the sample intact for future experimental work, and 2) there was not enough sample to make a powder diffraction experiment feasible. Method b) was not considered because, although poling and physically constraining crystals has been carried out successfully in the past, recent attempts by colleagues have been unsuccessful.

The relatively large shear angle ($2.0(1)^{o}$) measured in DCsDA provides a possible way round the above problems. With a shear angle as large as $2.0(1)^{o}$ there are regions in reciprocal space where all four ferroelectric reciprocal lattices are separated enough to allow data collection from only one of them. By collecting data in these regions and in regions in reciprocal space where the overlap from the other lattices is small enough to enable the resolution of individual reflections, from the particular lattice being investigated, by using a curve fitting technique, it proves possible to collect sufficient data to perform a structural investigation.

4.2 Method

In the ferroelectric phase, if we retain the tetragonal indexing, each lattice can be regarded as a monoclinic lattice with C as the unique axis.

The cylindrical polar coordinates, ξ, φ, τ, for a monoclinic lattice are defined as

$$\xi = \left[h^2a^{*2} + k^2b^{*2} + 2hka^*b^* \cos\gamma^*\right]^{\frac{1}{2}}$$

$$\varphi = \ell c^*$$

$$\tau = \tan^{-1}\left[(kb^* \sin\gamma^*)/(ha^* + kb^* \cos\gamma^*)\right]$$

(Arndt and Willis, 1966)

For normal-beam inclination geometry (this setting was used because of the need to cool the sample using a cryostat (see Section 3.4)) the setting angles are given as

$$\theta = 180 - \tau - \cos^{-1}\left[(\xi^2 + \varphi^2)/2\xi\right]$$

$$\nu = \sin^{-1}\varphi$$

$$\Upsilon = \cos^{-1}\left[(2 - \xi^2 - \varphi^2)/2(1 - \varphi^2)^{\frac{1}{2}}\right]$$

where θ is the setting angle of the crystal, ν is the tilt angle of the counter and Υ is the setting angle of the counter.

When a single crystal of DCsDA is cooled through its ferroelectric transition it can, in general, shear four ways. There are thus four ferroelectric domains, distinguished by their mutual orientation. Each tetragonal reflection can be regarded as splitting into four reflections, A, B, C, D. If reflection A has the indices h, k, l then the other three can be related to this. B is equivalent to $\bar{h}kl$, C to $\bar{h}\bar{k}l$ with the h,k axis rotated by 2^o about c and D to $hk\bar{l}$ with the h,k axis rotated by 2^o about c (see Figure 4.2). (This is with the tetragonal indexing retained and the low-temperature structure being regarded as monoclinic.)

Figure 4.2 a) The 'splitting' of tetragonal reflections in (h,k,o) and parallel planes. For h=o or k=o, two superpose so that only three peaks are distinguished. The reflections 'split' only in the hk plane.

b) The four reflections A,B,C and D resulting from the 'splitting' of a tetragonal reflection.

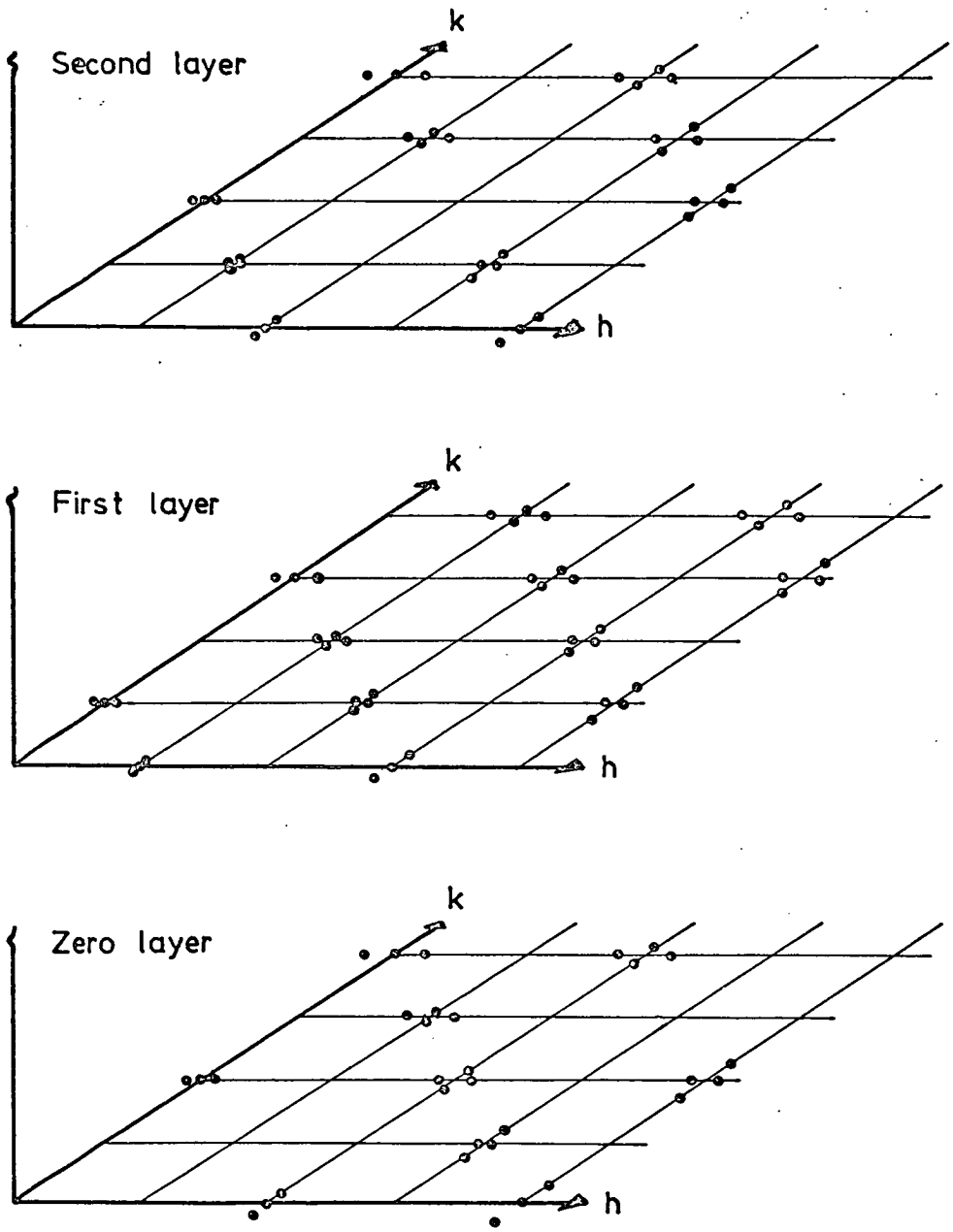

(a)

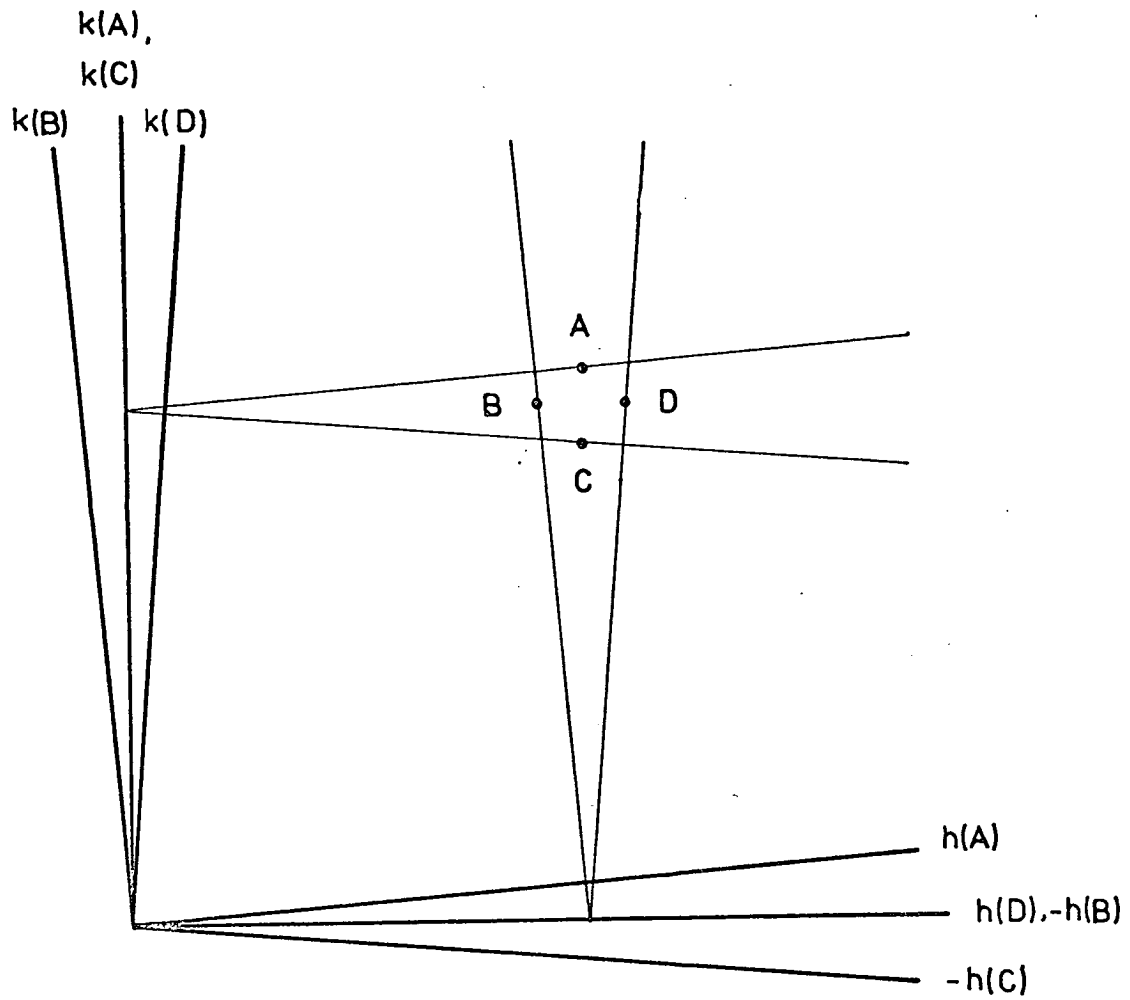

(b)

There are thus two values for the counter setting angle Υ (for each 'split' tegragonal reflection) resulting from the two values of ζ: one for positive h and one for negative h.

Assuming an orientation with C vertical and -h pointing towards the source, the reflection setting angles, ϕ_i then take the values

$$\phi_i = 180 - \Upsilon_i - \cos^{-1}\left(\frac{\zeta^2 + \rho^2}{2\zeta}\right) \qquad i = A, B, C, D$$

where $\Upsilon_D = \Upsilon_A - 2.0^o$

and $\Upsilon_C = \Upsilon_B + 2.0^o$

It is now possible to calculate the counter setting angles, Υ_i, and the crystal setting angles, ϕ_i, for each of the four reflections in the orthorhombic phase that correspond to one reflection in the tetragonal phase, and to tabulate their differences, $\Delta\phi_{(i,j)}$ and $\Delta\Upsilon_{(i,j)}$. ($i = A, B, C, D$; $j = A, B, C, D$; $i \neq j$)

With this information it is possible to collect data principally from only one of the ferroelectric domains. In practice, because the number of reflections from regions where the lattices are totally separated is relatively few, the profiles of the reflections suffering from overlap with the reflections from the other domains are collected as well. Some of these reflections can be resolved using a curve-fitting technique (see Section 4.4).

4.3 Data Collection

On cooling through the ferroelectric phase transition it was found that the proportion of the DCsDA crystal forming each domain can vary, but the process is otherwise reversible. The domain chosen for data collection was the one that contained the highest proportion of the crystal and so gave the largest integrated intensity for each reflection. Having decided upon which particular domain the data were to be collected from, the data collection procedure was essentially that described in Section 3.4 for normal-beam inclination geometry. The scan width was always wide enough to include the principal Bragg peak plus any overlap on both the low-angle and high-angle sides of the reflection. For each reflection the data points were recorded point by point to permit the reconstruction of the profile during the analysis.

4.4 Data Reduction

Using a least-squares fitting method, Gaussian functions can be fitted to each reflection profile to resolve the principal reflection (the reflection from the chosen ferroelectric domain) from reflections arising from the other three domains.

The program used was one adapted from a program developed by Dr J Arthur (then of this Department) for the analysis of Raman spectral data. Up to four Gaussians - the number of peaks in each scan varies from one to four depending on where in reciprocal space the profile data have been collected from - of the form

Figure 4.3 Graphical comparison of observed and calculated profiles for some resolved reflections.

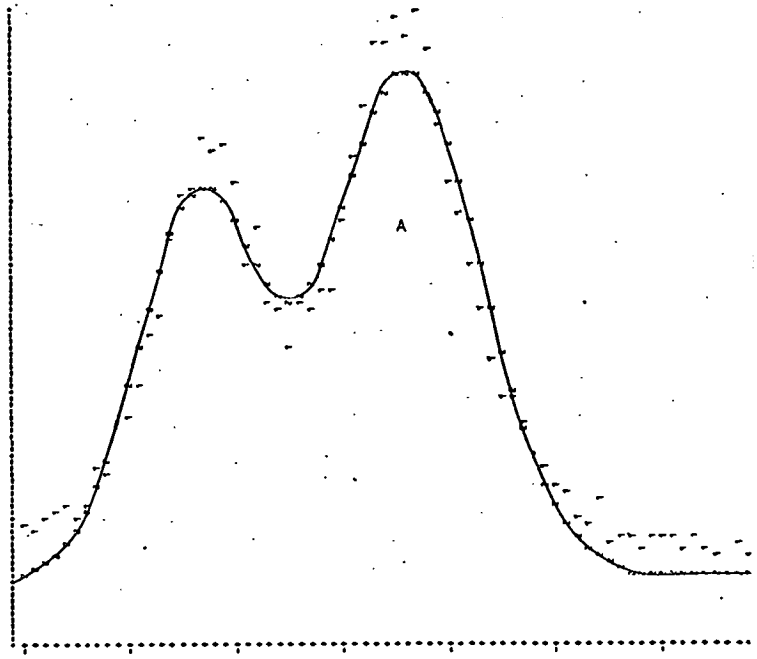

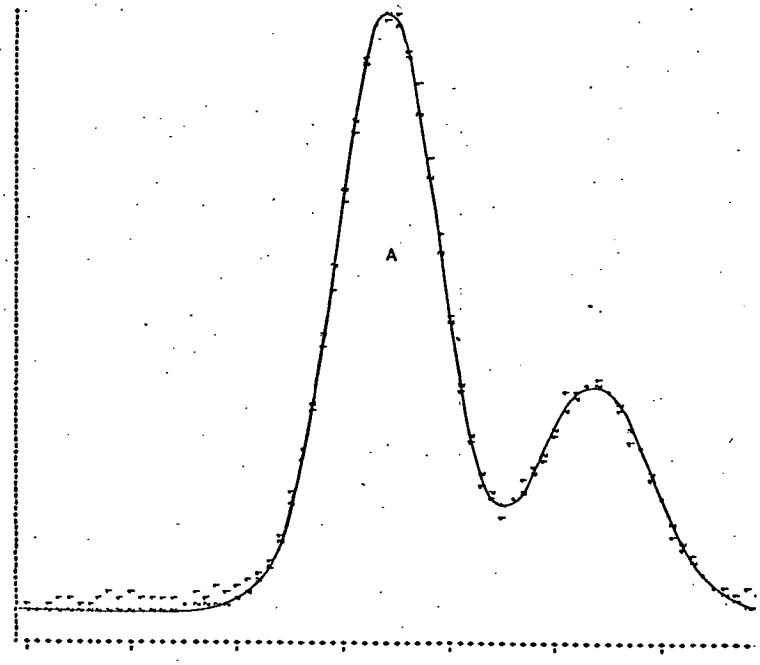

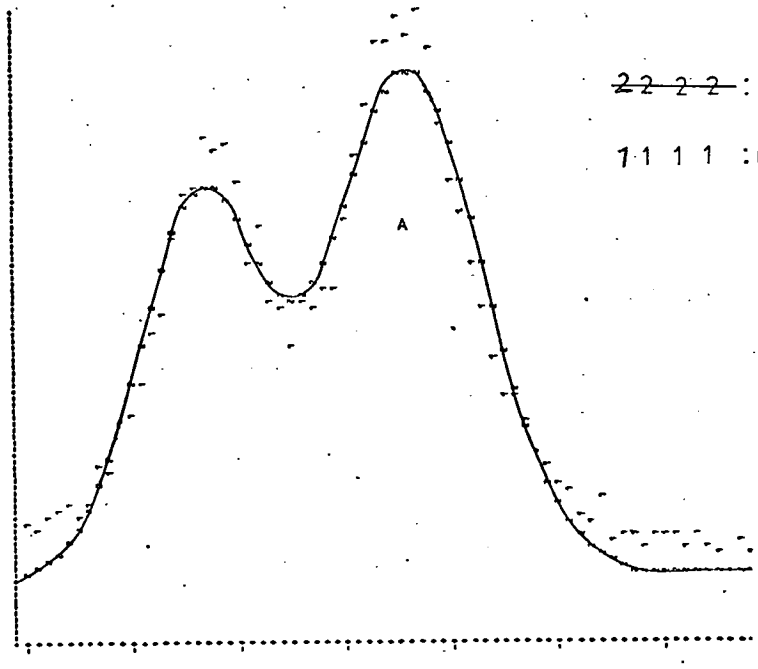

~~2 2 2 2~~ : Calculated profile

1 1 1 1 : Observed profile

$$f(x) = A \exp K\left(\frac{x-x_o}{\Gamma}\right)^2$$

are fitted to each profile, where A is the peak strength, x the position of each data point (relative to the other data points in the scan for each reflection), x_o is the peak position, Γ is the width at half height and $K = -4 \log_e 2$.

The parameters varied for each profile are the position, strength and width at half height of each expected Gaussian in the profile, and an overall background parameter.

The output consists of the final fitted parameters, an estimate of the 'goodness' of fit, and a graphical comparison of the observed and calculated profiles (see Figure 4.3).

Three criteria are used to determine whether the results from the fitting program, for each profile, are acceptable: a) a visual comparison of the observed and calculated profiles showing a close match between the two, b) physically meaningful parameters and c) a value of the function 'Phisum' close to unity, where

$$\text{Phisum} = (\text{CHISQR}/(N_{obs}-1))^{\frac{1}{2}}$$

$$(\text{CHISQR} = \sum_{i}^{N_{obs}} \left(\frac{Y_i - f(x_i)}{\sqrt{Y_i}}\right)^2$$, where Y_i is the measured data point, $f(x_i)$ the calculated data point and N_{obs} is the number of data points in the profile.)

The integrated intensity, I, for a Gaussian spectrum is given by

$$I = \int_{-\infty}^{\infty} Ae^{\frac{-(x-x_o)^2}{\sigma_o}} dx$$

$$= \frac{A\Gamma\sqrt{\pi}}{2\sqrt{\log_e 2}}$$

Therefore, using the fitted parameters relating to each principal Bragg reflection, it is possible to calculate the integrated intensity for each reflection.

A comprehensive estimation of errors, relating to the fitting procedure, for each reflection has not yet been formulated. Therefore, at present, each reflection is given unit weighting.

Having extracted the integrated intensities of all resolvable reflections, the data analysis follows the same form as described in Chapter 3.

The results of applying the technique described in this chapter are presented in Section 5.3.3.

4.5 Discussion

In applying this method to an unpoled and physically unconstrained crystal, it has proved possible to perform an accurate structural investigation of the orthorhombic phase of $Cs(D_{0.57}H_{0.43})_2AsO_4$ at 77^oK (see Section 5.3.3). A limitation of the method is that, as the shearing of the tetragonal cell occurs in the ab plane, it is

necessary to mount the crystal with the c-axis vertical. This results in limited resolution in the vertical plane because it is only possible to collect data from the four layers $0 \leq l \leq 3$ because of the limited tilt angle of the counter on the two-circle diffractometer.

The structure of orthorhombic $Cs(D_{0.57}H_{0.43})_2AsO_4$ is basically the same as the structure of other KH_2PO_4-type materials in the orthorhombic phase (Table 5.8). It is concluded therefore that the method described in this Chapter successfully allows the determination of the structural parameters of $Cs(D_{0.57}H_{0.43})_2AsO_4$ in the orthorhombic phase without having to constrain physically and pole, or powder the sample.

CHAPTER 5

STRUCTURAL STUDIES OF $Cs(D_xH_{1-x})_2AsO_4$ (NOMINAL x = 0.67) IN THE PARAELECTRIC AND FERROELECTRIC PHASES

CHAPTER 5

STRUCTURAL STUDIES OF $Cs(D_xH_{1-x})_2AsO_4$ (NOMINAL x = 0.67) IN THE PARAELECTRIC AND FERROELECTRIC PHASES

5.1 Introduction

In the family of KH_2PO_4-type crystals, K can be replaced by Rb, Cs or NH_4, P can be replaced by As, and H can be replaced by D. This group of isomorphs is structurally one of the simplest of the various materials exhibiting the property of ferroelectricity.

The most extensively studied member of this group of crystals is KH_2PO_4 (hereafter KDP). Its ferroelectric properties were first noted by Busch and Scherrer (1935) who discovered a ferroelectric phase transition at 123°K. The room-temperature structure was determined by West (1930) using X-rays. West found the space-group symmetry of the paraelectric phase to be $I\bar{4}2d$, with four formula units (KH_2PO_4) in the body-centred tetragonal unit cell. Because the distance between nearest oxygens of adjacent PO_4 groups strongly suggests the existence of hydrogen bonds, West proposed the position of the hydrogens to be the eight-fold positions between the oxygens.

The cell dimensions found by West were more accurately determined by Ubbelohde and Woodward (1947) to be: a = b = 7.434Å and c = 6.945A°. Subsequent X-ray studies by de Quervain (1944) and by Ubbelohde and Woodward (1947) established the symmetry of the ferroelectric phase to be that of the orthorhombic space group Fdd2. Frazer and Pepinsky (1953), using X-rays, investigated the structure of KDP

just above and just below the Curie point; in particular they studied the structural changes that occur on going through the transition. Although their results gave indications as to the location of the hydrogen ions, there was no concrete evidence for the location of the protons in either phase. This had to wait for the first neutron-diffraction studies to be made.

A structural analysis of KDP using neutron diffraction was carried out by Bacon and Pease (1953, 1955), by Peterson, Levy and Simonsen (1953), and by Levy, Peterson and Simonsen (1954). The positions of the protons were located conclusively and more accurate parameters for the O ions were obtained.

A projection of the structure in the paraelectric phase is shown in Figure 5.1. The structure can be pictured as being built up from PO_4 tetrahedra and K ions. Each phosphorus ion is surrounded by four oxygens at the corners of a tetrahedron which is nearly but not quite regular, being compressed by about 2% along the c axis. Alternate tetrahedra, as projected on the (001) plane, are rotated in opposite directions about the c axis by approximately 15^{o}. The K and P ions lie vertically above one another, separated by a distance $^{c}/_{2}$. Every PO_4 group is linked to four other PO_4 groups, separated by a distance $^{c}/_{4}$ along c, by hydrogen bonds. The upper oxygens of one tetrahedron lie nearly in the same (001) plane as the lower oxygens of its neighbour and so each of the hydrogen bonds lies very nearly perpendicular to the c-axis.

Figure 5.1 A projection of the structure KH_2PO_4 onto the x-y plane. One unit cell is shown. The structure is built up of PO_4 groups linked by hydrogen bonds (dotted lines) nearly perpendicular to Z. The K ions lie halfway between the P ions along Z. Two possible D,H distributions are shown. One symmetry element is shown.

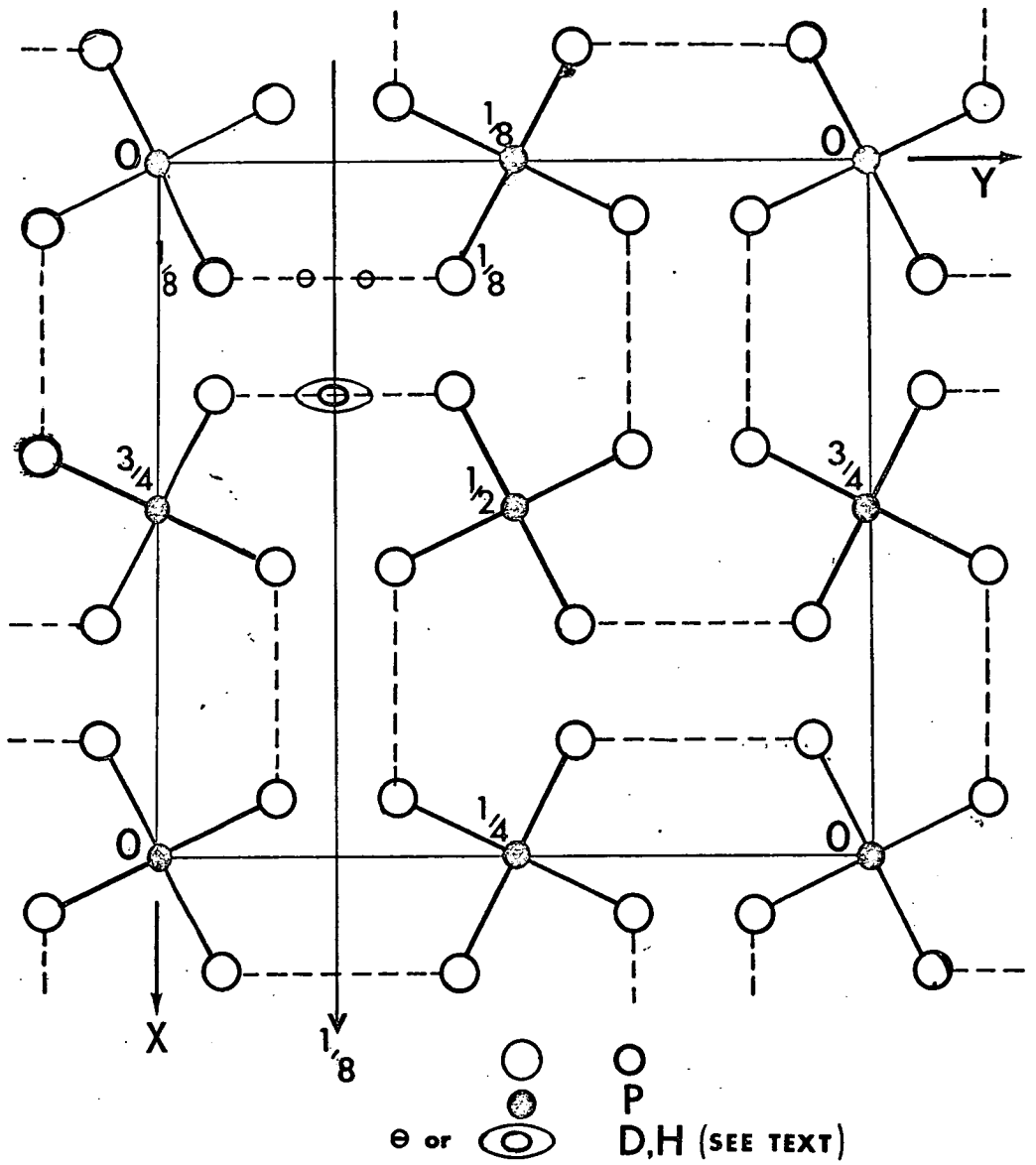
0
1/8
1/8
1/8
0
Y
3/4
1/2
3/4
0
1/4
0
X
1/8
O
P
Θ or
D,H (SEE TEXT)

Each K ion is surrounded by eight oxygens, four belonging to the tetrahedra immediately below and above it and four belonging to tetrahedra in the same (001) plane as the K ion. The positions of the P and K ions are fixed by symmetry, lying on inversion centres on the $\bar{4}$ axis, but the sixteen oxygens are in a set of general positions. The eight hydrogens are in a set of special positions at x, $^1/_4$, $^1/_8$.

In the paraelectric phase, although Bacon and Pease (1953) located the hydrogen sites unambiguously, they concluded that they could not distinguish between the possibilities of the protons being either a) disordered in a double minimum potential well or b) having pronounced thermal motion in a single minimum well along the O-H.....O bond. Bacon and Pease (1955) attempted again to distinguish between the two possibilities for the protons by repeating their measurements at a much lower temperature so that the thermal motion would be reduced, but they still could not distinguish between the two possibilities for the protons.

On a reanalysis of Bacon and Pease's data, Nelmes, Eiriksson and Rouse (1972), using constrained least-squares refinement and significance testing techniques, showed that in the short oxygen-oxygen bonds, the protons are disordered.

Eiriksson, Rouse and Nelmes (1974) and Nelmes and Rouse (1974) collected full three-dimensional neutron data from $K(D_x H_{1-x})_2PO_4$, hereafter DKDP, (x = 0.88) and KDP respectively (both in the tetragonal

phase at 294^{o}K). They were able to conclude that both the deuterium in DKDP and the hydrogen in KDP are disordered over two sites in a double minimum well and that the line joining these sites is inclined at an angle to the oxygen-oxygen line (see Figure 5.2).

Nakano, Shiozaki and Nakamara (1973, 1974), using X-rays, determined the room-temperature crystal structures of KDP and DKDP (x = 0.96) and reported an isotope effect in the length of the O-H....O distance.

The low-temperature ferroelectric phase has an orthorhombic structure with its x- and y-axis in the $[110]$ and $[\bar{1}10]$ directions of the tetragonal cell. With the lowering of symmetry (from $I\bar{4}2d$ to Fdd2) on going through the transition, the ions are released from their special positions in the tetragonal phase. The $\bar{4}$ axes are reduced to rotation diads and all the rotation and screw diads perpendicular to them have disappeared. This results in the K and P ions being able to move in the z direction, the O ions being divided into two independent sets, O(1) and O(2), on the upper and lower edges of the tetrahedra, and the H ions being ordered in general positions. The H ions are ordered in such a way that they are all near 'upper' or 'lower' oxygens, depending on the polarity. Bacon and Pease (1955) demonstrated the ordering of the H ions onto one of two possible sites, and they were also able to show that by reversing $\underline{E}$, the applied electric field, the protons shifted from one set of ordered positions to the other.

Figure 5.2 The hydrogen bond in KH_2PO_4. The bond is viewed down the x-axis and has a two-fold symmetry axis (diad) at its centre $(x, {}^{b}/_{4}, {}^{c}/_{8})$. The open circles denote the oxygen ions. A and B are the sites of the two 'half' hydrogen ions in the double minimum potential well (disorder) model. The line AB is the direction of the principal thermal motion for the single minimum (order) model in which the hydrogen lies on the diad. Δ is the distance from A to B. The approximate location of the phosphorous to which each oxygen is attached is indicated: the x coordinate of the phosophorous is less than that of the oxygen. The angles Θ and ϕ are defined as positive.

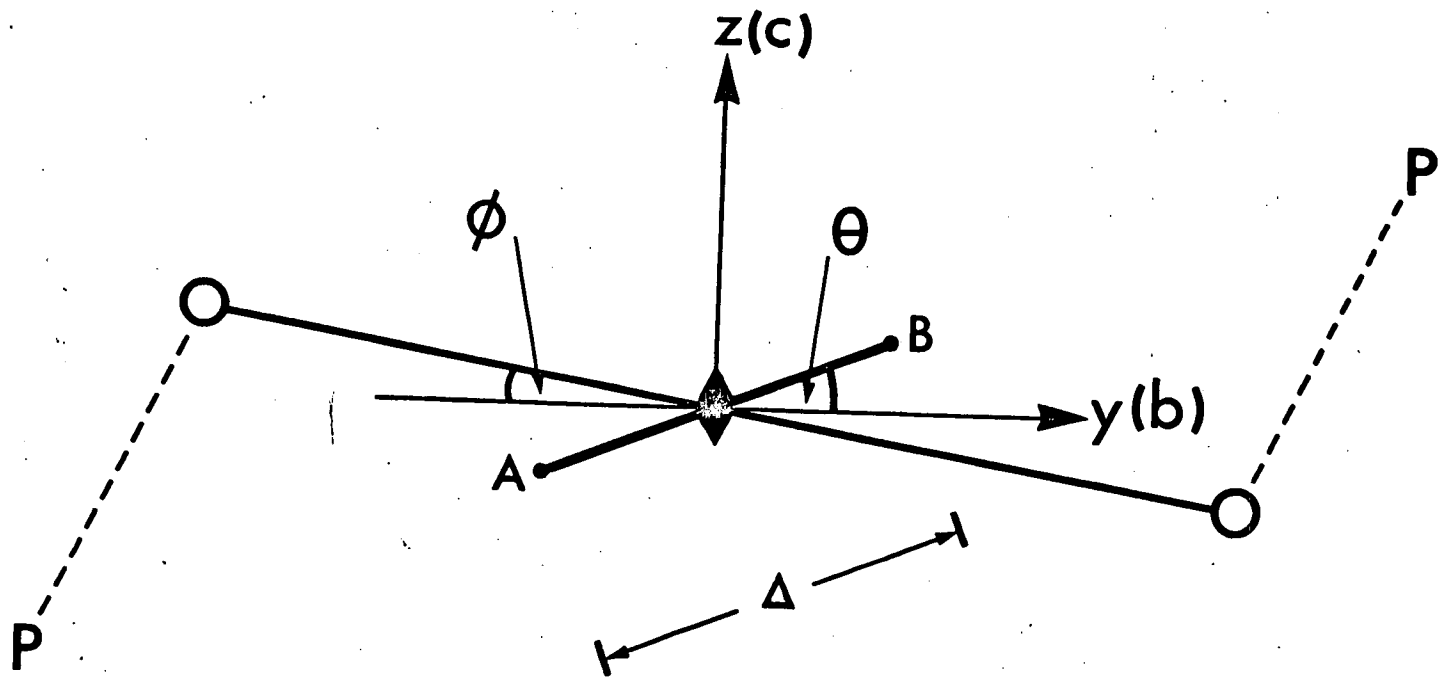

$$\psi = \theta + \phi$$

The P ion moves away from the O ions that the H ions have moved towards, and the K ion moves in the opposite direction to the P ion. There is a slight increase in the O-H.....O distance and a decrease in the O-H bond length. P-O(2) (O(2) is the oxygen towards which the hydrogen has moved) is longer than P-O(1), as would be expected from the movement of the P ion. The framework of the O ions changes very little. As the orthorhombic phase has a polar structure the choice of origin along the z-axis is arbitrary. In the structural work reported later in this chapter, the origin has been chosen such that the z coordinate of the P ion is zero.

The crystals isomorphous with tetragonal KDP also undergo transitions to a phase with lower symmetry at low temperatures. The phase transition in KDP is regarded as one of first order (Bastie, Bornarel, Lajzerowiez, Vallade and Schneider, 1975). Studies of the various isomorphs (Strukov, Vaks, Baddur, Zimenko and Koptsik, 1974; Blinc, Burger and Levstik, 1973; Strukov, Baddur, Zinenko, Mikhailev and Koptsik, 1973) point out that isomorphic and isotopic substitutions lead not only to a displacement of the phase transition temperature, but also to a considerable change in the character of the ferroelectric phase transition. It has been reported that with an increase of the radius of the monovalent metal ion, $K^{+} \rightarrow Rb^{+} \rightarrow Cs^{+}$, the transition becomes more nearly second order, whereas the substitution $P^{5+} \rightarrow As^{5+}$ makes the transition more strongly first order. The substitution H→D increases the first-order nature of the transition and also has a marked effect on the transition temperature.

The transition temperatures of the deuterated crystals are considerably higher than those of their hydrogenous counterparts. This isotope effect emphasises the importance of the hydrogen bond in the mechanism of the KDP-type ferroelectric transition.

The ferroelectric phase transition in $Cs(D_x H_{1-x})_2AsO_4$ (hereafter DCsDA) is observed to be a first order one (Strukov et al, 1973). The transition temperature in DCsDA exhibits the same linear dependence on deuteration (Loiacono, Ladell, Osborne and Nicolosi, 1976) previously observed for $K(D_x H_{1-x})_2PO_4$ (Kaminow, 1965; Baddur, Strukov, Velichko and Setkina, 1973).

Though the ammonium salts $NH_4H_2PO_4$, $NH_4H_2AsO_4$ and their deuterated counterparts are isomorphous with tetragonal KDP, their low-temperature form differs from that of KDP in two important ways. In contrast to KDP, the ammonium salts in the orthorhombic phase (space group $P2_12_12_1$) do not have their x- and y-axes along the base diagonals of the tetragonal cell, but along the sides. The ordering of the hydrogens in these materials is such that each tetrahedron in $NH_4H_2PO_4$ has one H attached to an upper oxygen and one to a lower oxygen (Kelling and Pepinsky, 1955; Hewat, 1973) with the result that the dipoles lie in the (001) plane and the total polarization of the crystal is zero. The crystal is therefore antiferroelectric.

It is known that some of the members of the KDP family possess a form other than the tetragonal and orthorhombic structures discussed above. Room-temperature KDP crystallises in a monoclinic form when

highly deuterated (Ubbelohde, 1939). The existence of high-temperature phase transitions, not associated with thermal decomposition, have since been reported for KH_2PO_4, KD_2PO_4, RbH_2PO_4, RbD_2PO_4, RbH_2AsO_4 and CsD_2AsO_4 (Grunberg, Leven, Pelah and Wiener, 1967; Blinc, Dimic, Kolar, Lahaynar, Stepisnik, Zumer, Vene and Hadgi, 1968; Blinc, O'Reilly, Peterson and Williams 1969; Pereverzeva, Pogosskaya, Poplavko, Pakhomov, Rez and Sil'nitskaya, 1972; Nicholson and Soest, 1974; She and Pan, 1975; Loiacano et al, 1976). All of these compounds are tetragonal at room temperature and transform at high temperature to a structure reported to be monoclinic.

The structure of the room-temperature monoclinic form of DKDP has been determined by Nelmes (1972) using X-rays. The K, P and O ions were located and the D sites inferred from the P-O bond lengths. The positions of the deuterium ions were located in a later study, using neutron diffraction, by Thornley, Nelmes and Rouse (1975). The space group is $P2_1$ and there are eight formula units in the cell. The cell dimensions measured by Nelmes (1972) were $a = 7.45(1)\mathring{A}$, $b = 14.71(2)\mathring{A}$ and $c = 7.14(1)\mathring{A}$ with $\beta = 92.31(1)^{\circ}$. Thomas, Benoit, Herpin and Mercier (1974) carried out an X-ray investigation of the high-temperature monoclinic phase obtained by heating tetragonal DKDP and found the same arrangement of K, P and O ions as in the room-temperature monoclinic study. This is in agreement with Blinc et al (1969) who suggested that the two monoclinic phases are identical.

The high-temperature phase of KH_2PO_4 has now also been shown to be monoclinic by Itoh, Matsubayashi, Nakamura and Motegi (1975). Kennedy, Nelmes, Thornley and Rouse (1976) have reported that the very highly deuterated form of DKDP (monoclinic at room temperature) remains monoclinic down to 6^oK.

Based on the structural analysis of West (1930), Slater (1941) developed a theory of the ferroelectric phase transition in KDP. This microscopic theory proposed a mechanism for the transition in terms of short-range interactions - neglecting the long-range forces. Slater assumed that on every hydrogen bond there are two equal and symmetrically-placed potential wells. The distribution of the hydrogens between these positions is subject to two restricting conditions (according to Slater): a) there is one and only one hydrogen on each bond and b) there are only two hydrogens near any one PO_4 group. He further assumes that of the six possible configurations for each PO_4 group, the two having a dipole moment lying parallel to the ferroelectric c-axis have an energy lower than those with the H arranged so that the dipoles lie perpendicular to the z-axis. The spontaneous polarization P_s, found by minimising the free energy, goes abruptly from zero to its maximum value at T_c. However, all values of P_s between zero and its maximum value are allowed at T_c.

Takagi (1948) modified the Slater theory by allowing the possibility of the existence of groups having one or three hydrogens close to a phosphate ion. This results in the theory predicting a second-order transition.

Though the Slater-type theories obtained experimental support from the structural study of Bacon and Pease (1953, 1955) they had one principal weakness - their failure to predict the increase in the transition temperature on the substitution of D for H.

Pirenne (1949, 1955) was the first to consider the isotope effect. He proposed a model where the kinetic energy of the protons played an important part. Blinc (1960) developed this idea further by considering a double-minimum potential in which tunnelling of the protons (deuterons) in the hydrogen bond is allowed. The tunnelling motion opposes the tendency of the proton to attain the lower-energy configuration thus inhibiting the phase transition. The lighter the particle is, the more easily it can tunnel and so the substitution of D for H can be expected to raise the transition temperature. de Gennes (1963) described the tunnelling process using a pseudospin Ising-type model and this formalism was further developed by Tokunaga and Matsubara (1966) and Tokunaga (1966). These theories predicted a collective motion (tunnelling mode) of the hydrogens which becomes unstable at the phase transition.

The most serious limitation of this approach is that while the motion of the protons is in the a-b plane, the ferroelectric axis is the c-axis. Cochran (1961) emphasised that the motion of the protons could not be considered as being independent of the other atoms.

Cochran (1959, 1960) showed that the phenomenon of ferroelectricity could be directly related to the lattice dynamics of a crystal, in particular that the ferroelectric phase transition could be regarded 'as the result of an instability of the crystal to a normal mode of vibration'. This 'soft' mode is a transverse optic (TO) mode whose frequency tends towards zero as the transition temperature is approached. This idea led to a much more general understanding of the displacive phase transition - first in perovskites and, with further development (Cochran, 1961), order-disorder transitions like that of KDP. The suggestion that the tunnelling mode is the 'soft' mode in KDP and is coupled to one or more phonon modes whose frequencies are almost temperature-independent was made by Cochran in 1969.

Kobayashi (1968) extended the pseudospin tunnelling model to permit coupling to a transverse optic vibrational mode of the K and P ions along the c-axis. This yielded a coupled-mode frequency which becomes soft in much the same manner as Cochran described. According to Kobayashi, KDP-type crystals constitute a 'mixed' type of ferroelectric exhibiting order-disorder phenomena of the hydrogen system and displacive behaviour of the heavy ion system.

Though Barker and Tinkham (1963) showed a relaxation of the dielectric response at relatively low frequencies, using infra-red measurements, the first quantitative measurements supporting the soft-mode approach to KDP were made by Kaminow and Damen (1968). Using Raman scattering, they detected a heavily damped mode in KDP and deduced a $((T-T_c)/T)^{\frac{1}{2}}$ variation for its undamped frequency.

The proton distribution in KDP at room temperature was investigated by Plesser and Stiller (1969) using incoherent neutron scattering. They claimed that the protons tunnelled between two potential minima separated by 0.40(3)Å on the hydrogen bond and that the H-H line was inclined by 6(3)° to the a-b plane.

The ferroelectric transition in DKDP was investigated by Paul, Cochran, Buyers and Cowley (1970) using inelastic coherent neutron scattering. It was found that they could not easily distinguish between the overdamped soft phonon mode and the critical slowing down of the polarization fluctuations in the order-disorder dipolar system.

Skalyo, Frazer and Shirane (1970) determined, by neutron triple-axis spectrometry, the atomic motions of the ferroelectric soft mode in KD_2PO_4. By a careful study of the temperature dependence of the overdamped optic branch, they determined the soft-mode intensity at the zone-centre of 60 Brillouin zones. A least-squares calculation of the inelastic structure factors fitted the intensities well and permitted an evaluation of the relative atomic movements (eigenvectors) of the soft mode.

Further work on the eigenvectors of DKDP was carried out by Wallace, Cochran and Stringfellow (1972). Their results are in good general agreement with those of Skalyo et al (1970).

Wilson (1970) and Wilson and Cummings (1969) have made detailed measurements of the temperature and electric field dependences of the

soft-mode Raman spectrum in KDP. Katiyar, Ryan and Scott (1971) demonstrated that the soft mode in the isomorphous arsenates is strongly coupled to an optic mode of the lattice and Scott and Wilson (1972) pointed out the necessity of including this coupling in the analysis of the Raman scattering measurements in KDP. The temperature dependence of the Raman spectra in KDP have been analysed by She, Brobert, Wall and Edwards (1972) using a coupled-mode analysis. Measurements of the temperature dependence of the coupled-mode systems have also been made in RbH_2PO_4 by Peercy and Samara (1973) and in the isomorphous arsenates by Lowndes, Tornberg and Leung (1974).

Very little structural work has been carried out on the crystals isomorphous with KDP; and inelastic neutron scattering, Raman scattering and other investigations of the ferroelectric phase transition in KDP-type compounds have long depended on the structural parameters for KH_2PO_4 at room temperature.

Further interest was stimulated in DCsDA in particular through the results of Dietrich, Cowley and Shapiro (1974). They appeared to find evidence for a complex domain structure in the ferroelectric phase but these results have since been shown to be attributable to multiple Bragg scattering (Meyer, Dietrich, Nelmes, Hay and Cowley, 1976).

DCsDA is at the 'other end' of the KDP family from KDP itself: potassium and phosphorus are both replaced - by caesium and arsenic respectively; and H by D.

No known structural work has been done on it. For a better understanding of KDP-type transitions, a knowledge of the structural details of the KDP isomorphs is required. In view of this, and also the recent inelastic neutron work on CsDA (Meyer and Dietrich, 1975), the Raman scattering results for DCsDA (Lowndes et al, 1974) and originally the results of Dietrich et al (1974), although no longer valid, a detailed structural investigation of DCsDA in its paraelectric and ferroelectric phases has been undertaken.

5.2 Present Work

Three single-crystal neutron-diffraction experiments have been carried out on $Cs(D_x H_{1-x})_2AsO_4$: 1) the collection of full three-dimensional data at room temperature (tetragonal phase) (Section 5.3), 2) the collection of three-dimensional data in the tetragonal phase, just above the transition, (T_c + 5K), (Section 5.4), and 3) the collection of three-dimensional data in the orthorhombic phase at 77°K (Section 5.5).

The ferroelectric transition is strongly linked with the distribution of the D,H ions along the O-H.....O bond. Because of this, particular attention has been paid to the details of the hydrogen bond during the refinements.

In the tetragonal structure, constrained refinement and significance testing techniques (see Section 3.6.2) have been applied to test the statistical significance of certain structural features of interest.

The following constraints have been applied.

1) The D,H ion is ordered in a special position on a two-fold axis i.e. it lies at the centre of the O-O bond at the point X(H), $^1/_4$, $^1/_8$.

2) The D,H ion lies on the O-O line, i.e. ψ is zero (see Figure 5.2).

3) The Z coordinate of the O ion has the value $^c/_8$ so that the O.....O line is confined to the x-y plane, i.e. ϕ is zero (see Figure 5.2).

4) The AsO_4 group is regular.

5) The x coordinate of the hydrogen = the x coordinate of the oxygen.

The thermal motion of the atoms was investigated using the constraints:

6) that the caesium ion has isotropic thermal motion,

7) that the arsenic ion has isotropic thermal motion,

8) that the oxygen ion has isotropic thermal motion, and

9) that the deuterium, hydrogen ion has isotropic thermal motion.

No constraints have been applied during the refinements of the orthorhombic structure.

5.3 Structural Studies of $Cs(D_x H_{1-x})_2AsO_4$ (nominal x = 0.67)

5.3.1 The tetragonal phase of $Cs(D_x H_{1-x})_2AsO_4$ at room temperature (292^oK)

Single crystal sample CN1 (a 2 mm cube) (see Section 2.1.1) was mounted with its c-axis vertical on a Hilger and Watts

four-circle diffractometer at the PLUTO reactor of A.E.R.E. Harwell. Because of the deliquescence of the sample, and to guard against D→H exchange, the crystal was enclosed in a soda-glass sphere.

The cell dimensions measured at room temperature using an X-ray diffractometer at Edinburgh University were a = 7.985(3)Å and c = 7.893(4)Å.

The neutron wavelength, calibrated from a standard sample of CaF_2, of known cell dimensions, was 1.137(2)Å. A ω-2θ scan, employing normal-beam equatorial geometry, was used to collect intensity data out to $\sin\theta/\lambda = 0.76 Å^{-1}$ ($\theta = 60^{\circ}$). A standard reflection was measured every five reflections, as was a positioning check of the setting angles of the four shafts. The intensity of the standard measured remained constant within two standard deviations. 901 reflections from two octants (h, k, l and $\bar{h}$, k, l) were measured. In general, four symmetry-related reflections were measured. All intensities were Lorentz corrected. No correction was made for the effects of absorption. On averaging over the equivalent reflections, the data were reduced to 265 independent reflections. The intensities of symmetry-related equivalent reflections agreed within counting statistics. The error for each was taken to be the larger of the errors estimated from a) the counting statistics and b) the internal agreement of the contributing symmetry-related reflections.

Least-squares refinement, using the full-matrix least-squares program developed by Dr G S Pawley of this Department, was started from the positional and thermal parameters for KD_2PO_4 at room temperature (Eiriksson, 1974). The coherent neutron scattering lengths used were those listed by Bacon (1972). In the 'standard' refinement (with the deuterium disordered over the two sites of a double-minimum well) - designated Model I - there were 25 variable parameters: a scale factor, an isotropic extinction parameter, 6 positional parameters, 16 anisotropic thermal parameters and the scattering amplitidue of the deuterium. The correctness of the weighting scheme was tested by analysing $\overline{W\Delta^2}$ (see Section 3.6.1) as a function of sin θ, F_o and EXTF. No significant systematic dependence of $\overline{W\Delta^2}$ on either sin θ or F_o was found. To allow for a probably inadequate treatment of extinction, 8 of the strongest reflections, for which EXTF ≤ 0.8 on F_c still showed $F_c > F_o$ (significantly), were omitted.

With the final set of observed structure amplitudes and their estimated errors, listed in Appendix C, refinement converged to an R index of 0.035 with R_ω = 312 (see Section 3.6.1).

The final positional and thermal parameters for the unconstrained disorder model (Model I) are given in Table 5.1.

The scattering length of deuterium refined to a value of $0.22(2) \times 10^{-12}$ cm^{-2} : this corresponds to a mean value of x

Table 5.1

Positional and Thermal Parameters for $Cs(D_xH_{1-x})_2AsO_4$ (x = 0.57) at room temperature (292°K)

The positional parameters are in Å, U_{ij} are in $Å^2$ (the temperature factor is $\exp\left(-2\pi^2 \sum_{ij} H_i H_j U_{ij}\right)$ where $H_i = \frac{h_i}{a}$). Standard deviations are given on the last quoted place. Parameters without errors are determined by symmetry. The lattice parameters : a = 7.985(3)Å, c = 7.893(4)Å.

	X	Y	Z	U_{11}	U_{22}	U_{33}	U_{23}	U_{31}	U_{12}
Cs	0	0	3.946	0.0319(5)	0.0319	0.0232(6)	0	0	0
As	0	0	0	0.0217(3)	0.0217	0.0253(6)	0	0	0
O	1.1621(8)	0.7326(8)	0.971(1)	0.0301(3)	0.0299(4)	0.0370(4)	-0.0076(3)	-0.0117(3)	0.0047(2)
D	1.106 (3)	1.750 (3)	0.926(7)	0.027 (1)	0.023 (3)	0.029 (2)	-0.004 (2)	-0.002 (2)	0.001 (1)

in $Cs(D_xH_{1-x})_2AsO_4$ of 0.57(1). The structure is essentially the same as that determined for DKDP by Eiriksson (1974).

The techniques of constrained refinement and significance testing (Section 3.6.2) have been applied to investigate some important details of Model I - particularly the deuterium bond. This bond is illustrated in Figure 5.2. The constraints tested and the significance levels found for their rejection are given in Table 5.2.

The double-minimum (disorder) model for the deuterium ion is strongly preferred, with the separation of the deuterium onto two sites being very highly significant ($\alpha < 0.001$, $S = 9.5$). That the angle ψ is non zero (see Figure 5.2) - that is that the deuterium ion does not lie on the O.....O line - is highly significant ($\alpha < 0.001$, $S = 8.4$). The tilt of the O.....O line out of the x-y plane is also highly significant ($\alpha < 0.001$, $S = 22.1$). The difference between X(D) and X(O) is highly significant ($\alpha < 0.001$, $S = 30.6$). The anisotropy of the thermal motion of the Cs, As and O ions is very significant ($\alpha < 0.001$, $S = 12.3$, 4.2, 61.2 respectively). The thermal motion of the deuterium ion, however, is not significantly anisotropic ($\alpha = 0.25$). These results are discussed further and compared with results from other structural studies of KH_2PO_4-type crystals in Section 5.4.

5.3.2 The tetragonal phase of $Cs(D_xH_{1-x})_2AsO_4$ at T_c+5^oK ($T_c=208^oK$):

For the experiment at T_c+5^oK, a cuboid-shaped crystal of size

Table 5.2

Comparison of constrained models with Model I for $Cs(D_xH_{1-x})_2AsO_4$ (x = 0.57) at room temperature (292°K)

The number of parameters in Model I is N (=25); the number of parameters in the constrained model is n, less than N by the tabulated N-n. $\mathcal{R}$ is calculated from the tabulated R_ω and the value R_ω (=312) for the standard model as $\mathcal{R} = \left(R_\omega/312\right)^{\frac{1}{2}}$. $\mathcal{R}_\alpha$ was determined for α values of 0.50, 0.25, 0.10, 0.05, 0.025, 0.010, 0.005 and 0.001. The value of α given is the smallest of these for which $\mathcal{R} > \mathcal{R}_\alpha$. $\mathcal{S}$ is defined in Section 3.6.2. The values for the constrained thermal parameters with estimated standard deviations are in $Å^2$.

Constraint	N-n	R_ω	$\mathcal{R}$	α	$\mathcal{R}_\alpha$	$\mathcal{S}$	Constrained Parameters
D at X, $^b/_4$, $^c/_8$	4	500	1.266	0.001	1.040	9.5	
D on O...O line	1	390	1.118	0.001	1.023	8.4	
Z(O) = $^c/_8$	1	535	1.309	0.001	1.023	22.1	
X(D) = X(O)	1	636	1.428	0.001	1.023	30.6	
Cs isotropic	1	429	1.173	0.001	1.023	12.3	$U_{11} = U_{22} = U_{33} = 0.0291(4)$
As isotropic	1	350	1.059	0.001	1.023	4.2	$U_{11} = U_{22} = U_{33} = 0.0228(3)$
O isotropic	5	2730	2.958	0.001	1.044	61.2	$U_{11} = U_{22} = U_{33} = 0.0294(7)$
D isotropic	5	324	1.019	0.25	1.014	0.6	$U_{11} = U_{22} = U_{33} = 0.027\ (1)$

$2 \times 2 \times 4\ mm^3$ - sample CN2 (see Section 2.1.1) - was mounted with its b-axis vertical in a variable temperature cryostat (see Section 3.4) on a Hilger and Watts two-circle diffractometer with tilting counter on the PLUTO reactor of A.E.R.E. Harwell. Normal-beam inclination geometry was employed. As it is possible to collect only a few layers of data in any one mounting of a crystal on a two-circle diffractometer, the mounting of the crystal with the b-axis vertical allows the collection of high-resolution data along both a and c. The transition temperature of the crystal was measured by observing the splitting of the 440 reflection (tetragonal indexing) on slow cooling and the reverse effect on slow heating. It must be noted that only about half the crystal transformed to the orthorhombic structure at this temperature, the rest transforming over a $60^{\circ}K$ temperature range (see Chapter 6). During the data collection the crystal temperature was maintained at $213 \pm 0.5^{\circ}K$, 5° above the ferroelectric phase transition ($208 \pm 0.5^{\circ}K$). A permanent record of the crystal temperature was produced by a chart recorder.

The neutron wavelength was $1.072(2)\mathring{A}$, calibrated by using a CaF_2 single crystal of known cell dimensions. The data were collected using a ω-2θ scan out to $\sin\theta/\lambda = 0.71\mathring{A}^{-1}$ ($\theta=50^{\circ}$). The cell dimensions measured by fitting Bragg reflections at high and low θ were found to be $a = 7.982(7)\mathring{A}$ and $c = 7.889(9)\mathring{A}$. Measurements were made of 396 reflections in the four layers h, k=0-3, l in two octants (h, k, l and h, k, $\bar{l}$).

The data were collected one layer at a time. A 'standard' reflection for each layer, was measured every five reflections. The zero-layer standard was remeasured whenever the layer was changed. The intensities of the standards remained constant within 3 standard deviations. All intensities were Lorentz corrected ($L^{-1} = \sin\chi \sin\gamma$, where χ is the setting angle and γ the tilt angle of the detector) but no correction was made for the effects of absorption. Averaging over symmetry-related reflections, at least two in general, yielded 163 independent reflections - most of the full three-dimensional data set because (h, k, l) and (k, h, l) are equivalent. The intensities of symmetry-related reflections agreed within counting statistics. The error for each was taken to be the larger of the errors estimated from a) the counting statistics and b) the internal agreement of the contributing symmetry-related reflections.

Least-squares refinement was started from the positional and thermal parameters of DKDP at T_c+5^oK (Eiriksson, 1974). As in the room-temperature experiment, the standard disordered refinement (with the deuteriums disordered over two possible sites) was designated Model I. In this model there were 25 variable parameters: a scale factor, an isotropic extinction parameter, 6 positional parameters, 16 anisotropic thermal parameters and the scattering length of the deuterium. The coherent neutron scattering amplitudes were taken from the compilation of Bacon (1972).

The correctness of the weighting scheme was tested by analysing $\overline{W\Delta^2}$ (see Section 3.6.1) as a function of sinθ, F_o, EXTF and layer. No significant systematic dependence of $\overline{W\Delta^2}$ on either sin θ, F_o or EXTF was found. However, the highest layer data (k=3) were found to be over weighted. The weights on all the reflections with k=3 were multiplied by a factor 1.5, resulting in a weights analysis that showed no dependence on layer. The final set of observed structure amplitudes and their estimated errors are listed in Appendix D. The final refinement for the 'standard' unconstrained model converged to an R index of 0.039 with R_ω = 263 (see Section 3.6.1).

The final positional and thermal parameters for Model I are given in Table 5.3. The deuterium scattering length refined to $0.22(2)\times10^{-12}cm^{-2}$ in good agreement with the refined value in the room-temperature experiment. The structure is essentially the same as that determined for DCsDA at room temperature.

Using the techniques of constrained refinement and significance testing (Section 3.6.2), the statistical and physical significance of certain structural features were tested. The constraints tested and the significance levels found for their rejection are given in Table 5.4.

Table 5.3

Positional and Thermal Parameters for $Cs(D_xH_{1-x})_2AsO_4$ (x = 0.57) at T_c+5^oK ($T_c=208^oK$)

The positional parameters are in Å; U_{ij} are in $Å^2$ (the temperature factor is $\exp\left(-2\pi^2 \sum_{ij} H_i H_j U_{ij}\right)$ where $H_i = \frac{h_i}{a}$). Standard deviations are given on the last quoted place. Parameters without errors are determined by symmetry. The lattice parameters : a = 7.982(7)Å, c = 7.889(9)Å.

	X	Y	Z	U_{11}	U_{22}	U_{33}	U_{23}	U_{31}	U_{12}
Cs	0	0	3.945	0.0244(9)	0.0244	0.017 (1)	0	0	0
As	0	0	0	0.0150(6)	0.0150	0.022 (1)	0	0	0
O	1.162(2)	0.733(2)	0.0972(2)	0.0220(6)	0.022(1)	0.0263(6)	-0.0040(6)	-0.0089(7)	0.001(1)
D	1.099(9)	1.742(6)	0.92 (1)	0.023 (3)	0.011(8)	0.018 (3)	-0.004 (5)	-0.005 (4)	-0.003(4)

Table 5.4

Comparison of Constrained Models with Model I for $Cs(D_xH_{1-x})_2AsO_4$ (x = 0.57) at T_c+5^oK ($T_c=208^oK$)

The number of parameters in Model I is N (25); the number of parameters in the constrained model is n, less than N by the tabulated N-n. $\mathcal{R}$ is calculated from the tabulated R_ω as $\mathcal{R}=\left(R_\omega/214\right)^{\frac{1}{2}}$. $\mathcal{R}_\alpha$, α and S are determined as in Table 5.2. The values of the constrained thermal parameters with estimate standard deviations are in $Å^2$.

Constraint	N-n	R_ω	$\mathcal{R}$	α	$\mathcal{R}_\alpha$	S	Constrained Parameters
D at x, $^b/_4$, $^c/_8$	4	266	1.115	0.001	1.069	2.4	
D on O...O line	1	238	1.054	0.001	1.04	2.2	
Z(O) = $^c/_8$	1	341	1.262	0.001	1.04	10.8	
X(D) = X(O)	1	274	1.132	0.001	1.04	5.4	
Cs isotropic	1	246	1.072	0.001	1.04	3	$U_{11} = U_{22} = U_{33} = 0.0217(7)$
As isotropic	1	255	1.092	0.001	1.04	3.8	$U_{11} = U_{22} = U_{33} = 0.0172(6)$
O isotropic	5	572	1.635	0.001	1.077	11.4	$U_{11} = U_{22} = U_{33} = 0.0232(7)$
D isotropic	5	224	1.023	0.5	1.016	0.4	$U_{11} = U_{22} = U_{33} = 0.020\ (2)$

The separation of the deuterium ions onto two sites is significant at the 0.001 level ($S = 2.4$). The line joining the two possible sites is inclined to the O.....O line at a significantly non-zero angle. ($\alpha = 0.001$, $S = 2.2$). The tilt of the O.....O bond out of the x-y plane is highly significant ($\alpha < 0.001$, $S = 10.8$). That X(D) is not equal to X(O) is significant at the 0.001 level ($S = 5.4$). It is >99.9% probable that the thermal motion of the Cs, As and O ions is not isotropic ($S = 3$, 3.8 and 11.4 respectively). The thermal motion of the deuterium ion, however, is not significantly anisotropic ($\alpha = 0.5$).

These features are discussed further and compared with results from the other structural studies of KH_2PO_4-type crystals in Section 5.4.

5.3.3 The orthorhombic phase of $Cs(D_xH_{1-x})_2AsO_4$ at 77°K: Single crystal sample CN3, a cuboid-shaped crystal of dimensions 1.5 x 1.5 x 4 mm^3, (see Section 2.1.1) was mounted with the c-axis vertical in a variable-temperature cryostat (see Section 3.4) on the same Hilger and Watts two-circle diffractometer with tilting counter on the PLUTO reactor at A.E.R.E, Harwell as was used for the experiment with $Cs(D_xH_{1-x})_2AsO_4$ at T_c+5^oK. The transition temperature (208 ± 0.5^oK) for this crystal was determined by observing the splitting of the 440 reflection (tetragonal indexing) on slow cooling. As with the crystal of $Cs(D_xH_{1-x})_2AsO_4$ (CN2) used for the T_c+5^oK

study, only about half the crystal transformed to the orthorhombic phase at the transition temperature, with the rest of the crystal transforming over a 60°K temperature range (see Chapter 6). The value obtained for T_c compared favourably with the value of T_c determined for crystal CN2 - both samples originate from the same parent sample, as did the crystal CN1 for the room-temperature study. The data collection was carried out at 77°K. A continuous record of the crystal temperature was produced by a chart recorder.

Unlike previous single-crystal structural experiments on the orthorhombic phase of KH_2PO_4-type crystals (e.g. Bacon and Pease, 1955), the crystal of $Cs(D_xH_{1-x})_2AsO_4$ was not poled or physically constrained. In this situation there are thus four ferroelectric domains distinguished by their mutual orientation. It is possible to collect data from only one of them using the method described in Chapter 4. This method involves collecting data from only one of the ferroelectric reciprocal lattices in regions in reciprocal space where there is little or no overlap from the other three lattices. Where some degree of overlap exists, the individual reflections are resolved using a curve-fitting technique. As the shearing of the tetragonal cell takes place in the ab plane, the technique can only be applied readily with the tetragonal c-axis vertical. This results in a lower degree of resolution in the vertical plane because of the limited ω range of the tilting counter.

Normal-beam inclination geometry was employed. The neutron wavelength was 1.075(2)Å, calibrated by using a CaF_2 single crystal of known cell dimensions. The cell dimensions measured on the diffractometer were a = 11.516(5)Å, b = 11.103(5)Å and c = 7.78(2)Å. Using an ω-2θ scan, the data were collected in four layers, $0 \leq l \leq 3$. Measurements were made of 633 reflections. However this was reduced to 180 reflections on applying the curve-fitting techniques described in Section 4.4. It was found impossible to resolve the other 453 reflections using the techniques developed for this experiment.

The acceptance of a fitted profile was based on three criteria : a) a low 'Phisum' value (see Section 4.4), b) physically sensible refined profile parameters (e.g. profiles in which one of the fitted Gaussians had a negative width were rejected although the 'Phisum' value was close to one) and c) that the graphing of the observed and calculated profiles were in good visual agreement. Some check on the values of the integrated intensities calculated from the resolved Gaussians was made by calculating manually the integrated intensities of the reflections with very little or no overlap. There was good agreement between these values and the values calculated from the corresponding fitted parameters.

A standard reflection was measured every five reflections. A separate standard reflection was measured for each layer.

The zero-layer standard was remeasured each time the layer was changed. All the standard reflections were reflections that did not suffer from overlap with the reflections from the other ferroelectric domains.

All intensities were Lorentz corrected ($L^{-1} = \sin\gamma \cos\nu$) but no correction was made for the effects of absorption. On averaging over symmetry related equivalents, the data reduced to 120 independent reflections. The intensities of symmetry related reflections agreed within 'counting statistics'.

Least-squares refinement was started from the positional parameters of the tetragonal phase at T_c+5^oK (Table 5.3) transformed to the Fdd2 cell. During the initial refinements, the observed structure amplitudes were given unit weights. An analysis of the values of $\overline{W\Delta^2}$ averaged over small ranges of F_o and sin θ showed a variation with both F_o and sin θ. The introduction of a weighting scheme, such that

$$W = \frac{1}{(a + F_o + cF_o^2)} \qquad \text{(Rollet, 1965)}$$

where $a = 2F_{MIN}$ and $c = \frac{2}{F_{MAX}}$

removed this systematic dependence of $\overline{W\Delta^2}$ on either sin θ or F_o. Refined isotropic extinction factors (see Appendix A) were mostly near unity, being > 0.97 for all reflections.

In the 'standard' refinement there were 39 variable parameters: a scale factor, an isotropic extinction parameter, 10 positional parameters, 26 anisotropic thermal parameters and the scattering length of the deuterium.

The refinement converged to an R index of 0.046 and R_ω= 12.0. The final positional and thermal parameters are given in Table 5.5. The observed structure amplitudes are given in Appendix E. The deuterium scattering length refined to $0.25(3) \times 10^{-12}$ cm^{-2}. Within error, this is in agreement with the values of the refined scattering length in the room-temperature and T_c+5°K studies. The structure is basically the same as that determined for KH_2PO_4 at 77°K by Bacon and Pease (1955). It should be noted, however, that the temperature factors for the arsenic, the two independent oxygen and the deuterium ions are non-positive-definite.

That the deuterium ion is ordered onto one site in the orthorhombic phase was tested in a further refinement. Two deuterium ions, D(1) and D(2), were included in the model, with half the value of the deuterium scattering amplitude, determined in the 'standard' refinement, allocated onto each site. The scattering amplitudes of D(1) and D(2), b(1) and b(2) respectively, were treated as variable parameters in the refinement. It was found that the value of b(2) reduced to zero and the value of b(1) increased to the single value determined in the standard refinement.

Table 5.5

Positional and Thermal Parameters for $Cs(D_xH_{1-x})_2AsO_4$ (x = 0.57) at 77°K

The positional parameters are in Å; U_{ij} are in $Å^2$ (the temperature factor is exp $\left(-2\pi^2 \sum_{ij} H_i H_j U_{ij}\right)$ where $H_i = \frac{h_i}{a}$). Standard deviations are given on the last quoted place. Parameters without errors are determined by symmetry. The lattice parameters : a = 11.516(5)Å, b = 11.103(5)Å, c = 7.87(2)Å.

	X	Y	Z	U_{11}	U_{22}	U_{33}	U_{23}	U_{31}	U_{12}
Cs	0	0	3.98	0.001(1)	0.004(2)	0.03 (2)	0	0	-0.001 (2)
As	0	0	0	0.010(2)	0.006(2)	-0.03 (2)	0	0	-0.001 (2)
O(1)	-1.501(4)	3.086(5)	0.95(3)	0.004(1)	0.007(1)	0.005(23)	-0.002 (3)	-0.007(3)	-0.001 (1)
O(2)	0.318(4)	1.327(5)	0.97(3)	0.010(2)	0.008(2)	-0.02 (2)	0.002 (3)	0.001(3)	-0.0001(12)
D	-0.47 (1)	2.00 (1)	1.01(5)	0.025(5)	0.016(6)	-0.06 (5)	-0.0006(91)	0.027(9)	-0.007 (4)

It is concluded, therefore, that the deuteriums are ordered onto one site consistent with the expected order-disorder transition for KH_2PO_4-type ferroelectrics.

The results from this experiment are discussed in Section 5.4.

5.4 Discussion

The structural studies of the tetragonal phase of $Cs(D_{0.57}H_{0.43})_2AsO_4$ at room temperature and T_c+5^oK (213^oK), show that, though there are small significant differences, the structures are essentially similar to those previously determined for KH_2PO_4 and KD_2PO_4.

A comparison of the tested features of $Cs(D_{0.57}H_{0.43})_2AsO_4$ at room temperature and those of $Cs(D_{0.57}H_{0.43})_2AsO_4$ at T_c+5^oK (213^oK) is given in Table 5.6. It can be seen that the tested features are much more significant at room-temperature, with α often $\ll 0.001$, than at T_c+5^oK. However, it must be noted that the room-temperature data set (265 independent reflections) and the resolution of this data ($\sin\theta/\lambda = 0.76\text{Å}^{-1}$) are greater than the number of independent reflections in and the resolution of the T_c+5^oK data set (163 and 0.71Å^{-1} respectively).

At both temperatures the double minimum (disorder) model is strongly preferred, the D-D line is inclined to the O-O line, the Z(O) does differ from $c/8$ and X(D) does not equal X(O). The thermal motion of the Cs, As and O ions is anisotropic at a high level of significance while the thermal motion of the D ion is probably anisotropic.

Table 5.6

Comparison of Constrained Refinement Results for $Cs(D_xH_{1-x})_2AsO_4$ (x = 0.57) at room temperature (292°K) and at 213°K

α and S are defined in Section 3.6.6.

Constraint	$Cs(D_{0.57}H_{0.43})_2AsO_4$ (292°K) (Section 5.3.1)		$Cs(D_{0.57}H_{0.43})AsO_4$ (213°K) (Section 5.3.2)	
	α	S	α	S
D at x, $^b/_4$, $^c/_8$	0.001	9.5	0.001	2.4
D on O...O line	0.001	8.4	0.001	2.2
Z(O) = $^c/_8$	0.001	22.1	0.001	10.8
X(D) = X(O)	0.001	30.6	0.001	5.4
Cs isotropic	0.001	12.3	0.001	3.
As isotropic	0.001	4.2	0.001	3.8
O isotropic	0.001	61.2	0.001	11.4
D isotropic	0.25	0.6	0.5	0.4

A comparison of the thermal parameters in Tables 5.1 and 5.3 shows that the thermal motion of the As becomes more anisotropic on cooling; the thermal motion is greatest along the c-axis, the direction of the displacement of the As ion at the ferroelectric transition.

Figure 5.3 gives details of the deuterium bond at room temperature and T_c+5^oK. It can be seen that the value of Ø is significantly non-zero and negative at both temperatures. In KH_2PO_4 and KD_2PO_4 Ø is found to be positive (see Figure 5.4).

Inter-ion distances and angles calculated from the positional parameters found for the tetragonal phase of $Cs(D_{0.57}H_{0.43})_2AsO_4$ at room temperature (Section 5.3.1), and $Cs(D_{0.57}H_{0.43})_2AsO_4$ at 213^oK (Section 5.3.2) are given in Table 5.7 along with the corresponding values for $K(D_{0.88}H_{0.12})_2PO_4$ at room temperature (Eiriksson, 1974), $K(D_{0.88}H_{0.12})_2PO_4$ at T_c+5^oK (Eiriksson, 1974), KH_2PO_4 at room temperature (Eiriksson, 1974) and KH_2PO_4 at T_c+5^oK (Kennedy, 1977). The cell dimensions determined by Eiriksson (1977) for $K(D_{0.88}H_{0.12})_2PO_4$ at T_c+5^oK and KH_2PO_4 at room temperature are believed to be inaccurate. The cell dimensions for $K(D_{0.88}H_{0.12})_2PO_4$ at T_c+5^oK have been remeasured (using the same crystal as Eiriksson) and found to be $a = 7.453(4)\mathring{A}$, $c = 6.955(4)\mathring{A}$. Isherwood (1977) has redetermined the cell dimensions for KH_2PO_4 and reports them to be $a = 7.452(1)\mathring{A}$ and $c = 7.973(1)\mathring{A}$. The inter-ion distances for these two materials have been recalculated using the redetermined cell dimensions and the positional parameters quoted by Eiriksson (1974).

Figure 5.3 The deuterium bond in $Cs(D_xH_{1-x})_2AsO_4$ ($x = 0.57$) at room temperature and T_c+5^oK (213^oK).

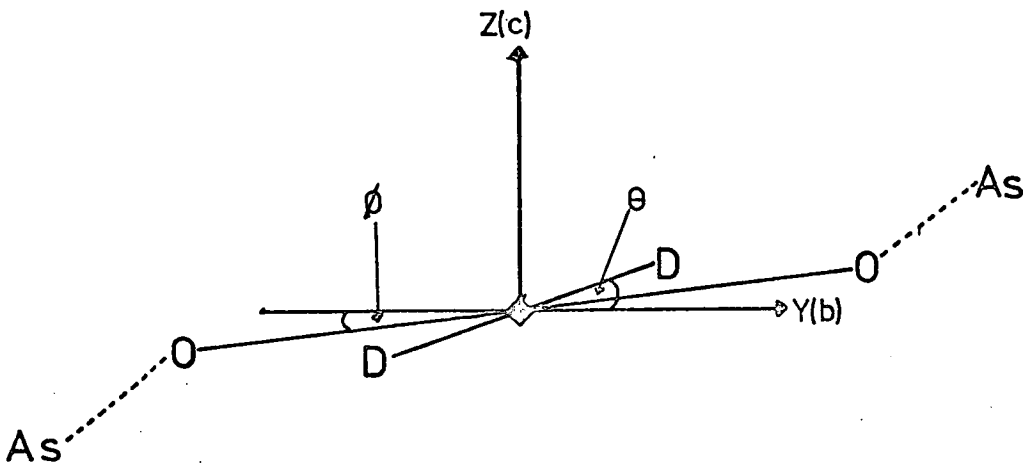

$Cs(D_xH_{1-x})_2AsO_4$ (x=0,57) at R.T. :

$\theta = 14(2)^\circ$

$\phi = -0,7(1)^\circ$

D—D = 0.507(7) Å

O—O = 2.528(4) Å

$Cs(D_xH_{1-x})_2AsO_4$ (x=0.57) at $T_c \pm 5^\circ K$ ($213^\circ K$) :

$\theta = 14(4)^\circ$

$\phi = -0.7(1)^\circ$

D—D = 0.51(1) Å

O—O = 2.524(6) Å

Figure 5.4 The hydrogen, deuterium bond in KH_2PO_4 and $Cs(D_xH_{1-x})_2AsO_4$ (x = 0.57).

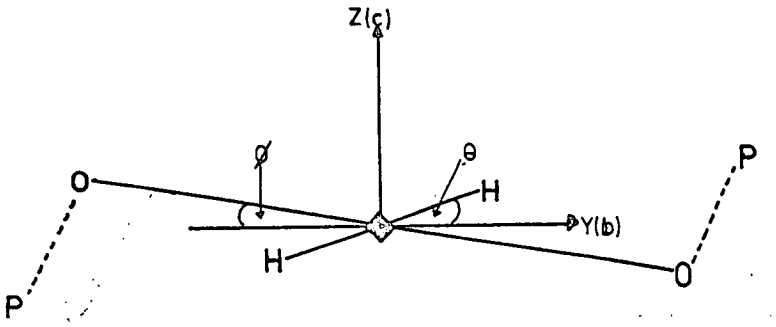

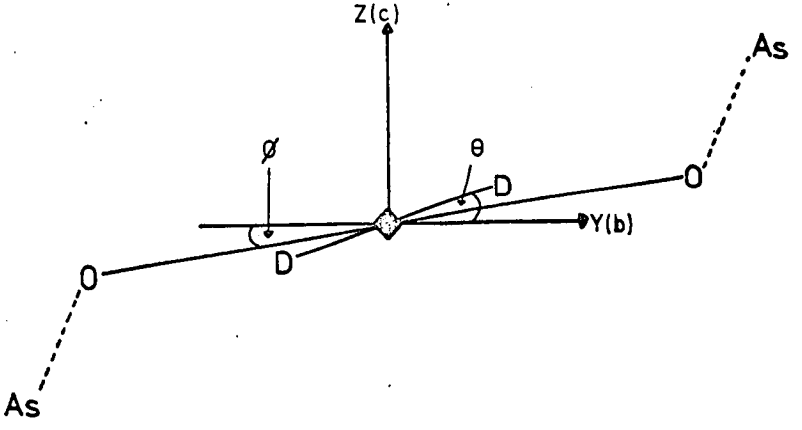

KH_2PO_4 at R.T. :

$\theta = 7(2)^\circ$

$\emptyset = 0.06(9)^\circ$

H——H = 0.381(2) Å

O——O = 2.495(2) Å

KH_2PO_4 at $T_c + 5^\circ K$ (127°K) :

$\theta = 8(2)^\circ$

$\emptyset = 0.6(2)^\circ$

H——H = 0.349(2) Å

O——O = 2.483(2) Å

$Cs(D_xH_{1-x})_2AsO_4$ at R.T. :

$\theta = 14(2)^\circ$

$\emptyset = -0.7(1)^\circ$

D——D = 0.507(7) Å

O——O = 2.528(4) Å

$Cs(D_xH_{1-x})_2AsO_4$ at $T_c + 5^\circ K$ (213°K) :

$\theta = 14(4)^\circ$

$\emptyset = -0.7(1)^\circ$

D——D = 0.51(1) Å

O——O = 2.524(6) Å

From Table 5.7 it can be seen that there is little change in structure resulting from decreasing the temperature except in KH_2PO_4. However, the temperature change in going from room temperature to T_c+5^oK is much greater in KH_2PO_4 (175^oK) than in $Cs(D_{0.57}H_{0.43})_2AsO_4$ (89^oK) and $K(D_{0.88}H_{0.12})_2PO_4$ (78^oK). The distances O.....O, O-D, D...D and As,P-O and angles θ, ϕ in $Cs(D_{0.57}H_{0.43})_2AsO_4$ and $K(D_{0.88}H_{0.12})_2PO_4$ remain unchanged, within error, on decreasing the temperature. On lowering the temperature in KH_2PO_4 the O.....O and H...H distances decrease, the O-H distance increases and the $\frac{H...H}{O.....O}$ ratio decreases by around 8%. The angle ϕ increases in KH_2PO_4 as the temperature is lowered. The angle ϕ is positive in KH_2PO_4 and $K(D_{0.88}H_{0.12})_2PO_4$ and is negative in $Cs(D_{0.57}H_{0.43})_2AsO_4$ (see Figure 5.4).

The investigation of $Cs(D_{0.57}H_{0.43})_2AsO_4$ at 77^oK revealed a structure similar to that found for KH_2PO_4 at 77^oK (Bacon and Pease, 1955).

In Table 5.8 some inter-ion distances for orthorhombic $Cs(D_{0.57}H_{0.43})_2AsO_4$ are given along with the corresponding values for orthorhombic KH_2PO_4 (Bacon and Pease, 1955), $K(D_{0.95}H_{0.05})_2PO_4$ (Kennedy, 1977) and RbH_2PO_4 (Kennedy, 1977). Although the substitution of As for P results in a longer As-O bond compared with the P-O bond, the general features in orthorhombic $Cs(D_{0.57}H_{0.43})_2AsO_4$ are in good agreement with those of the orthorhombic phosphates. The P,As-O(2) (O(2) may also be written O(H)) bond is significantly longer than the P,As-O(1) bond, i.e. the As,P ion has moved away

Table 5.7

Structural Features in Tetragonal $Cs(D_{0.57}H_{0.43})_2AsO_4$, $K(D_{0.88}H_{0.12})_2PO_4$ and KH_2PO_4

Bond lengths and cell dimensions are in Å. Angles are in degrees. Standard deviations are given on the last quoted place.

Structural Features	$Cs(D_{0.57}H_{0.43})_2AsO_4$ (R.T.) (Section 5.3.1)	$Cs(D_{0.57}H_{0.43})_2AsO_4$ (T_c+5°K:213°K) (Section 5.3.2)	$K(D_{0.88}H_{0.12})_2PO_4$ (R.T.) (Eiriksson, 1974)	$K(D_{0.88}H_{0.12})_2PO_4$ (T_c+5°K:213.8°K) (Eiriksson, 1974)	KH_2PO_4 (R.T.) (Eiriksson, 1974)	KH_2PO_4 (T_c+5°K:127°K) (Kennedy, 1977)
O-H,D....O	2.528(4)	2.524(6)	2.523(2)	2.520(4)	2.495(2)	2.483(2)
O-H,D	1.020(4)	1.014(6)	1.041(1)	1.041(4)	1.059(5)	1.066(1)
H,D...H,D	0.507(7)	0.51 (1)	0.448(3)	0.447(4)	0.381(2)	0.349(2)
As,P-O	1.682(2)	1.683(2)	1.543(1)	1.545(4)	1.540(1)	1.541(1)
Ratio $\frac{H,D...H,D}{O.....O}$	0.201(3)	0.202(4)	0.178(1)	0.177(2)	0.153(1)	0.140(1)
θ	14(2)	14(4)	8.5 (4)	10(3)	7(2)	8(2)
ϕ	-0.7 (1)	-0.7 (1)	0.43 (4)	0.6 (3)	0.06 (9)	0.6 (2)
a	7.985(3)	7.982(7)	7.468(1)	7.453(4)	7.452(1)	7.426(1)
c	7.893(4)	7.889(9)	6.979(1)	6.955(4)	6.973(1)	6.926(1)

Table 5.8

Inter-ion Distances in Orthorhombic $Cs(D_{0.57}H_{0.43})_2AsO_4$, $K(D_{0.95}H_{0.5})_2PO_4$, KH_2PO_4 and RbH_2PO_4

Distances are in Å. Standard deviations are given on the last quoted place.

	$Cs(D_{0.57}H_{0.43})_2AsO_4$ (77°K) (Section 5.3.3)	$K(D_{0.95}H_{0.5})_2PO_4$ (4°K) (Kennedy, 1977)	KH_2PO_4 (77°K) (Bacon and Pease, 1955)	RbH_2PO_4 (77°K) (Kennedy, 1977)
O-H....O	2.53(1)	2.538(8)	2.486(4)	2.49(1)
O.....O } 1^ to c	2.84(1)	2.562(8)	2.549(6)	2.55(1)
O(H).....O(H) } 1^ to c	2.73(1)	2.513(8)	2.521(6)	2.51(1)
O - H,D	1.04(1)	1.033(7)	1.05 (1)	1.06(1)
As,P - O(1)	1.67(2)	1.518(6)	1.51 (2)	1.51(1)
As,P - O(2)	1.75(2)	1.571(5)	1.58 (2)	1.58(1)

from the O ions which the H,D ions have moved towards. There is a small distortion of the O_4 (of AsO_4 and PO_4) group in the orthorhombic phase. The O(H)-O(H) distance perpendicular to the c-axis has contracted slightly and the O(1)-O(1) distance has increased.

In all three studies, the refined value for the scattering length of the deuterium indicates an average deuteration level of 57%. The transition temperature indicates a deuteration level of 67% (Loiacono et al, 1976). An anomaly of this nature is to be expected considering the unusual nature of the transition (see Chapter 6) - only part of the crystal transforms to the orthorhombic phase at the nominal transition temperature. The average deuteration level determined by integrating under the curve in Figure 6.1 (the temperature dependence of the integrated intensity of the tetragonal 440 reflection), with the nominal deuteration level taken to be 67%, agrees well with the value indicated by the refined scattering length.

The studies of $Cs(D_{0.57}H_{0.43})_2AsO_4$ at room temperature, T_c+5^oK and 77^oK have shown that the structures are in their essentials and temperature variations like other KH_2PO_4-type materials. Some interesting differences with KH_2PO_4 have been shown - in particular the angle ϕ in $Cs(D_{0.57}H_{0.43})_2AsO_4$ is negative. The small temperature dependence of the inter-ion distances in tetragonal $Cs(D_{0.57}H_{0.43})_2AsO_4$ is similar to that found in KD_2PO_4 and is in contrast with the marked temperature dependence of the inter-ion distances in KH_2PO_4.

In investigating the structure below T_c, the peak-fitting method (Chapter 4) which avoids the need to pole and physically constrain the crystal, has worked well; the orthorhombic structure agrees well with the structure of other orthorhombic KH_2PO_4-type materials. The structural investigations, therefore, have succeeded in providing structural parameters to support other studies of CsD_2AsO_4.

The structural work, however, must be considered in relation to the peculiar nature of the transition (Chapter 6). This feature of $Cs(D_xH_{1-x})_2AsO_4$ is not observed in the structure, though, as no difference in cell dimensions between the deuterated and hydrogenous compounds has been detected (Chapter 6), this is perhaps to be expected. The structural parameters can therefore be regarded as those of the average structure of $Cs(D_{0.57}H_{0.43})_2AsO_4$. The unusual nature of the transition does however bring into question any detailed work on CsD_2AsO_4 (for example dynamical studies of the 'soft' mode) unless great care is taken with crystal growth to achieve microscopic uniformity.

CHAPTER 6

THE TETRAGONAL BRAGG PEAK IN FERROELECTRIC $Cs(D_xH_{1-x})_2AsO_4$

CHAPTER 6

THE TETRAGONAL BRAGG PEAK IN FERROELECTRIC $Cs(D_xH_{1-x})_2AsO_4$

The work reported in this chapter gives details of some investigations into a previously unreported feature of the ferroelectric phase transition in crystals of $Cs(D_xH_{1-x})_2AsO_4$.

Deuteration changes a number of properties of CsH_2AsO_4. The shear angle, when measured away from the transition temperature, increases from $1.75(1)^o$ in CsH_2AsO_4 to $2.0(1)^o$ in $Cs(D_xH_{1-x})_2AsO_4$ (x = 0.57). The transition temperature increases from 143^oK in CsH_2AsO_4 to 227^oK at a deuteration level of 85% (Loiacono et al, 1976). An unexpected change, discovered during the structural studies of $Cs(D_xH_{1-x})_2AsO_4$ (hereafter DCsDA), reported in Chapter 5, is that only part of the deuterated crystal transforms at the nominal transition temperature with the remainder transforming over a 60^oK temperature range.

During the preliminary X-ray investigation of DCsDA, prior to the neutron structural work (see Chapter 5), a small crystal of DCsDA (average dimension 0.2 mm), cut from the parent crystal CP (see Section 2.1), was slowly cooled to determine the transition temperature. The intensities of the Bragg reflections were recorded on X-ray film using a Weissenberg X-ray camera. The transition temperature was recognised by the 'splitting' of the 440 tetragonal reflection. At the transition temperature (208^oK) the crystal sheared as expected to produce four ferroelectric lattices in the orthorhombic phase (see Figure 4.1).

However, from the X-ray film it was apparent that only about half the crystal had transformed at the 'transition' temperature, the rest remaining in the tetragonal phase. This feature was not local to the 440 tetragonal reflection, but was a property of the whole crystal. As the temperature was further reduced, below the nominal transition temperature, more of the crystal gradually transformed to the orthorhombic phase until at a temperature of about 60°K below T_c all the crystal had transformed to the ferroelectric phase. This temperature of about T_c-60°K is very close to the transition temperature (143°K) of undeuterated CsH_2AsO_4.

This is a phenomenon that has not previously been encountered. No record could be found in the literature of a similar effect occurring in any other hydrogen-bonded ferroelectric crystal. In view of this, further studies of the nature and reproducibility of the effect have been carried out to investigate the phenomenon more thoroughly.

Four crystal samples of DCsDA (CN3, CN5, CN6 and CN7 - see Section 2.1.2), all of dimensions 1.5 x 1.5 x 4 mm^3, have been used to investigate the transition using neutrons. Crystal sample CN3 (supplied by Quantum Technology) is the single crystal used for the collection of three-dimensional neutron data in the orthorhombic phase at 77°K (see Section 5.3.3). The crystals CN5, CN6 and CN7 were cut from parent crystals supplied by G Loiacono of Philips Laboratories, USA. The transition temperatures of CN5, CN6 and CN7 (as measured by Loiacono) are 223°K, 192°K and 183°K indicating nominal deuteration levels of 82%, 51.5% and 42.6% respectively (Loiacono et al, 1976). The transition temperature of crystal CN3 is 208°K indicating a nominal deuteration level of 63%.

The average deuteration of CN3 refined to 57% (see Section 5.3.3).

The crystals were each mounted with the c-axis vertical in a variable-temperature cryostat on a Grubb-Parsons MKVI two-circle diffractometer at the DIDO reactor at A.E.R.E., Harwell. The neutron wavelength was 1.090(4)Å. The transition temperature for each crystal was determined by observing the 'splitting' of the tetragonal 440 reflection on slow cooling. The transition temperatures of the crystals CN5, CN6 and CN7 are in agreement with the values determined for these crystals by G Loiacono. For each crystal, scans of the 440 tetragonal reflection were made at regular temperature intervals, from room temperature down to 143°K (the transition temperature of CsH_2AsO_4).

Figure 6.1 shows the variation with temperature of the peak intensity of the 440 tetragonal reflection, for crystal CN3. It can be seen that only 40% of the intensity in the tetragonal high-temperature phase disappears at 208°K: the lost intensity is distributed over the four peaks of the orthorhombic low-temperature phase. The remaining tetragonal peak intensity transfers to the orthorhombic peaks gradually, over a range extending nearly to the transition temperature of CsH_2AsO_4.

A similar graph to that of Figure 6.1 is shown in Figure 6.2 for crystal CN5. Only 20% of the crystal does not transform to the orthorhombic structure at the transition temperature (T_c = 223°K). The temperature range over which the remaining tetragonal peak intensity transfers to the orthorhombic peaks is 40°K - smaller than that found in crystal CN3 (60°K).

Figure 6.1 The temperature dependence of the tetragonal Bragg peak intensity at (440) for crystal sample CN3 of $Cs(D_xH_{1-x})_2AsO_4$.

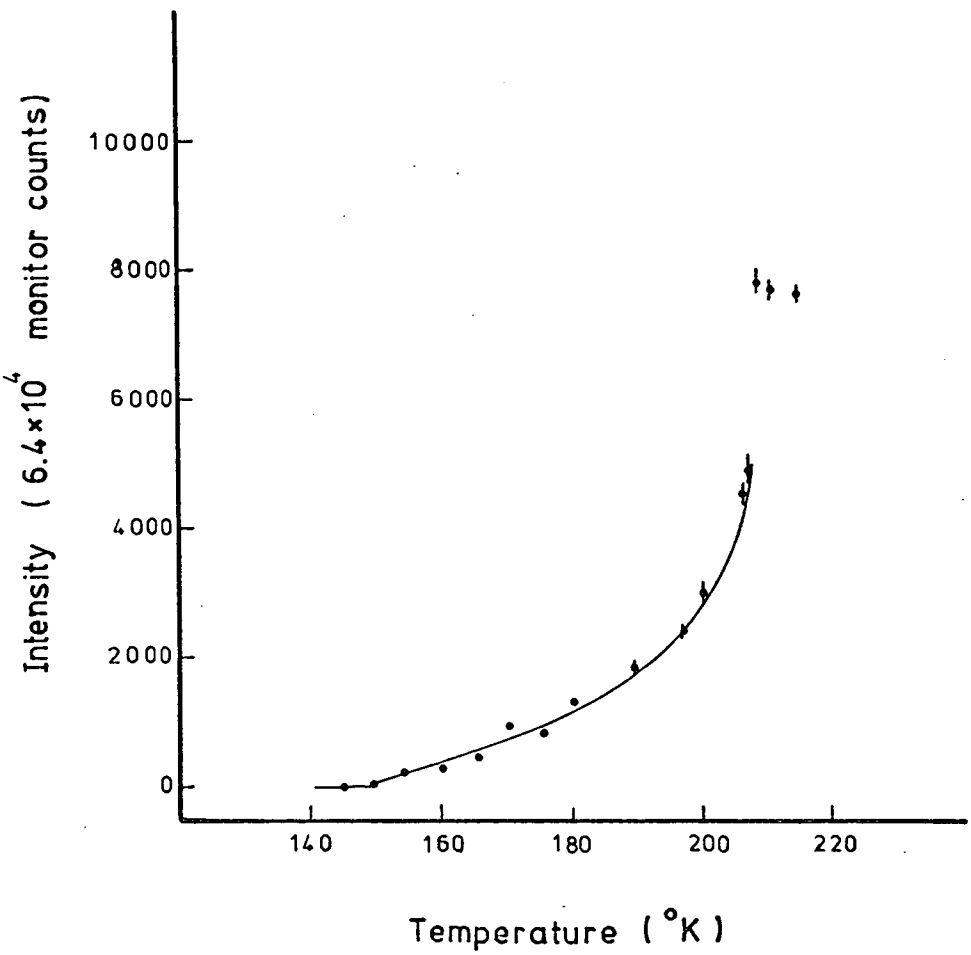
Intensity (6.4×10⁴ monitor counts)
10000
8000
6000
4000
2000
0
140
160
180
200
220
Temperature (°K)

Figure 6.2 The temperature dependence of the tetragonal Bragg peak intensity at (440) for crystal sample CN5 of $Cs(D_xH_{1-x})_2AsO_4$.

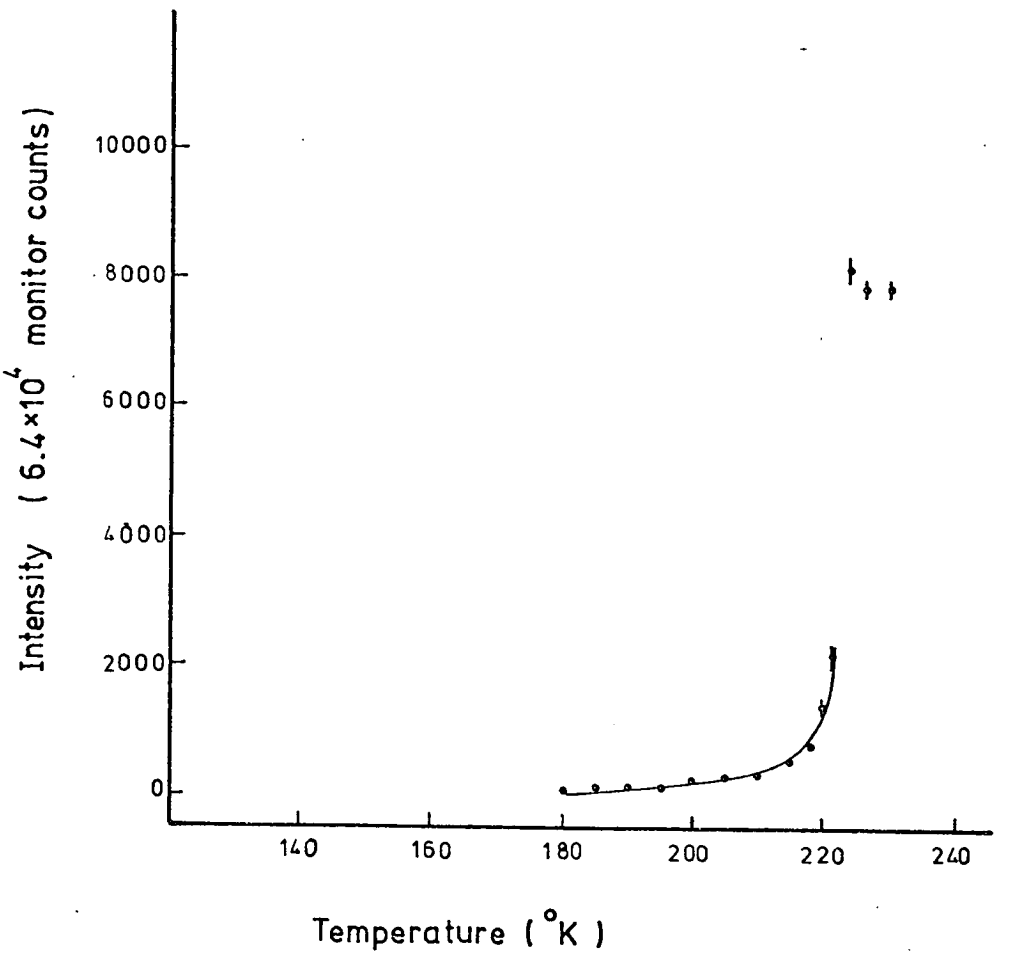
Intensity (6.4×10^4 monitor counts)
10000
8000
6000
4000
2000
0
140
160
180
200
220
240
Temperature (°K)

Preliminary scans of tetragonal reflections in the crystals CN6 and CN7, showed that these two crystals were not single crystals, making quantitative measurements of the variation of the tetragonal peak intensity with temperature impossible. However, though no detailed measurements could be made, it was apparent that, in both cases, not all the crystal transformed at the tetragonal → orthorhombic transition temperature.

At this stage several points can be made. 1) The feature of the tetragonal Bragg peak existing in ferroelectric DCsDA is independent of the source of the crystal, in as much as that crystals from two different suppliers exhibit the phenomenon. However, the effect is more pronounced in the crystal supplied by Quantum Technology Limited. 2) This feature of the transition exists in crystals of varying deuteration levels. 3) Crystals of diverse dimensions (from 0.2 mm to several millimetres) all undergo a similar type of transition.

The fact that such a variety of crystal sizes exhibit quantitatively similar behaviour makes surface rehydrogenation an unlikely explanation. A more likely cause of the observation is that there is an inhomogeneity of the hydrogen-deuterium concentration over regions in the crystal, small in comparison with the smallest sample (0.2 mm).

Crystal CN3 has been examined using the technique of X-ray diffraction topography (Lang, 1959, 1963) to determine if there is any evidence to support the hypothesis of a microstructure relating to an inhomogeneity in the hydrogen-deuterium concentration in DCsDA. This method uses a highly collimated monochromatic beam of X-rays to determine an overall

picture of the distribution of lattice imperfections or irregularities within a crystal. A detailed examination of the rocking curve (the variation of the diffracted intensity as the crystal is slowly rotated through the Bragg reflecting position) for several reflections failed to show any asymmetry in the curves. Asymmetry would be expected if there was any variation in lattice parameters for the deuterated and undeuterated regions in the crystal, resulting in a difference in the Bragg scattering angle. Though the rocking curves failed to indicate any difference in lattice parameter, the X-ray topographs revealed a pattern of varying diffracted intensity when the crystal was scanned in a Bragg-reflecting position. The scattered intensity, forming this pattern, systematically increased or decreased as the crystal was rotated through the Bragg reflecting angle.

The above results, however, have to be regarded as inconclusive with regard to the possible existence of the proposed microstructure. The method of X-ray topography is usually applied to near-perfect crystals, whereas crystals used for structural investigations generally have an angular misorientation of adjacent mosaic blocks measured in minutes of arc (to minimise extinction). This angular misorientation has the effect that, 1) the rocking-curve width will be such that it may conceal small variations in lattice parameter and 2) there will be small variations in the Bragg scattering position. The crystal faces also suffered from some surface damage and these features dominated the X-ray topographs. DCsDA is mechanically soft, making the polishing of crystal faces difficult, and to try to improve the crystal faces by wiping them with D_2O could change the character of the feature being investigated,

therefore no attempt was made to improve the surface quality of the crystal.

A high-resolution X-ray powder camera in the Chemistry Department of this University has been used to determine the lattice parameters of CsH_2AsO_4 and $Cs(D_xH_{1-x})_2AsO_4^-$ (x = 0.57). No detectable difference (within error) was found, with a = 7.985(4)Å and c = 7.893(4)Å in both cases.

At present therefore, there is no conclusive evidence for the existence of a microstructure caused by an inhomogeneous mixing of deuterium and hydrogen concentrations in DCsDA. However it is felt that this is the most likely explanation of the experimental observations and is consistent with the findings of Loiacono (1976) and Isherwood (1976). Loiacono (1976) reports peculiar growth behaviour in DCsDA suggesting cycles of preferential removal of hydrogen from the growth solution followed by an increasing removal of deuterium. In the growth from solution of tetragonal KD_2PO_4, Isherwood (1976) finds that there is a preferential removal of hydrogen while in the growth from solution of monoclinic KD_2PO_4 the deuterium is preferentially removed. Isherwood (1976) also reports that, in the growing of tetragonal KD_2PO_4, as the hydrogen is removed from solution and the deuterium concentration increases, 'whiskers' of monoclinic KD_2PO_4 are formed on the tetragonal crystal.

The transition temperature of 227°K given by Loiacono et al (1976) for a deuterium level of 85% suggests that the deuterium levels for DCsDA samples quoted in the literature have been grossly over-estimated. The work of Isherwood (1976) and Loiacono et al (1976) reveals that the

assumption that the deuterium level for crystals grown from solution is that of the growth solution, results in an over-estimation of the deuteration level in the crystal. If in addition, the pronounced inhomogeneity of the hydrogen-deuterium concentration in DCsDA is a common characteristic of both DCsDA (as it appears to be) and other isomorphs grown from aqueous solution, then further doubt must be attached to the results of previous experiments, particularly in DCsDA.

CHAPTER 7

STRUCTURAL STUDIES OF BORACITES

CHAPTER 7

STRUCTURAL STUDIES OF BORACITES

7.1 Introduction

Boracites are compounds with the chemical formula $M_3B_7O_{13}X$ where M stands for one of the divalent metal ions Mg, Cr, Mn, Fe, Co, Ni, Cu, Zn or Cd and X denotes one of the halogens Cl, Br or I. They are named after the naturally occurring boracite of magnesia. In certain cases it has been found that M can also be monovalent Li and X can be OH, F, NO_3, S, Se or Te. From now on a boracite will be referred to by its metal and its halogen (or substitute) only: for example, Mg-Cl denotes $Mg_3B_7O_{13}Cl$.

Synthesis of boracites in a form suitable for physical studies is difficult. The vapour transport method for crystal growth under reduced pressure developed by Schmid (1965) is currently the most widely used technique. The hydrothermal synthesis technique, however, has yielded better results for the growth of manganese, lithium, chalcogen and hydroxyl boracites (Joubert, Muller, Pernet and Ferrand, 1972). More recently nitrato- (M-NO_3) and fluoro-boracites (M-F) have been obtained at superatmospheric pressures by Bither and Young (1974). The substitution of the halogen by sulphur to give the boracites Mn-S, Mg-S, Fe-S and Cd-S is thought to introduce a charge imbalance.

Fouassier, Levasseur, Joubert, Muller and Haggenmuller (1970) and Levasseur (1973) suggest that the most probable arrangement is $M_3B_7O_{12}$ $(O_{\frac{1}{2}+x}\square_{\frac{1}{2}-x})(S_{1-x}\square_x)$, with $x \simeq 0.15$. More recent work by Gould and Nelmes (1977) on Cd-S suggests that the halogen is in fact replaced by SO_4 rather than S. The result of introducing an oxygen vacancy without apparently changing the structure suggested that M could be a monovalent metal, which led to the preparation of the boracites $Li_4B_7O_{12}X$, where X = Cl, Br or I (Levasseur, Fouassier and Hagenmuller, 1971; Jeitschko and Bither, 1972).

All halogen boracites, with the exception of Cr-Br and Cr-I, which remain cubic at least down to 10°K, transform, on cooling, from a cubic paraelectric phase to a low temperature orthorhombic ferroelectric phase. The space groups of the cubic and orthorhombic phases of Mg-Cl, respectively $F\bar{4}3c$ and $Pca2_1$, are now generally assumed to apply to all the halogen boracites. There is a wide variation in cubic→orthorhombic transition temperature (60-800°K) but for any given metal it generally decreases in the sequence X = Cl→Br→I (Schmid, 1965). An exception to this is when the metal ion is Zn : Zn-Cl, Zn-Br, and Zn-I transform around 786°K, 587°K and 698°K. The transition temperature is relatively independent of the metal.

The cubic structure of Mg-Cl was first determined by Ito, Morimoto and Sadanaga (1951) from X-ray powder intensities at 573°K. The unit cell, with symmetry $F\bar{4}3c$, contains eight formula units ($Mg_3B_7O_{13}Cl$). For convenience of description, one can consider just one-eighth of the cubic unit cell - containing one formula unit.

The cubic framework of oxygen O(1), boron B(1), metal (M) and halogen (X) is shown in Figure 7.1(a). The oxygen O(1) is taken as the origin. It can be seen that the metal (M) and the halogen (X) form three mutually perpendicular sets of chains ...X...M...X...M...X... directed along the three cubic axes ($\bar{4}$ axes). The chains all intersect at the halogen (X) ions, at a site of cubic (23) symmetry, whereas the metal (M) ions, at a site of tetragonal $\bar{4}$ symmetry, are on only one chain. The O(1) ion at the origin is surrounded tetrahedrally by the four B(2) ions - the OB_4 group (Figure 7.1(b)), a coordination unique amongst borate structures (Kriz and Bray, 1971). Along each of the four triads there is a polar sequence O(1)-B(2)...X..... O(1).

The primitive unit cell volume is increased eight times by the introduction of the oxygen O(2) ions in general positions. The B(1) ions have four surrounding O(2) ions forming a tetrahedral BO_4 group with $\bar{4}$ symmetry (Figure 7.1(c)). Each metal (M) ion, at a site with $\bar{4}$ symmetry, forms a very flattened tetrahedron, the MO_4 group, with four surrounding O(2) ions. Along the $\bar{4}$ axis the O(2) ions have coordinates $\pm \varepsilon$ relative to the metal. Each B(2) is in an OBO_3 group, bonded to one O(1) and three O(2) ions labelled O_3^A formed by triad 1 (Figure 7.1(d)). This arrangement in being neither the planar three-fold nor the tetrahedral four-fold boron-oxygen coordination is again unique amongst borates (Waugh, 1968; Kriz and Bray, 1971). The operation of triad 2 on the O(2) labelled B produced another triangle designated the O_3^B group, differing from the O_3^A group in that it is not associated with any boron on the triad. It can be seen from Figure 7.1(c) that the boron-oxygen framework can be represented as BO_4 and OB_4 tetrahedra linked by B-O bonds.

Figure 7.1 The structure of the cubic phase as determined for Mg-Cl by Ito et al (1951). One eighth of the $F\bar{4}3c$ cell is shown, containing one formula unit. (a) the array of oxygen O(1), boron B(1), and halogen (X) and metal (M) ions: some of the $\bar{4}$ axes are marked. (b) the location of the B(2) ions relative to the O(1) and (X) ions; the regular tetrahedral OB_4 group is illustrated for the origin O(1); the triad axes are marked: along each of these there is the polar sequence O(1)-B(2)...X .....O(1). (c) the location of the O(2) ions in general positions; only a few are shown, forming the structural elements BO_4, MO_4 and OBO_3. (d) the OBO_3 configuration around the B(2) ion; the two different O(2) triangles O_3^A and O_3^B are shown.

(after Nelmes and Thornley, 1974)

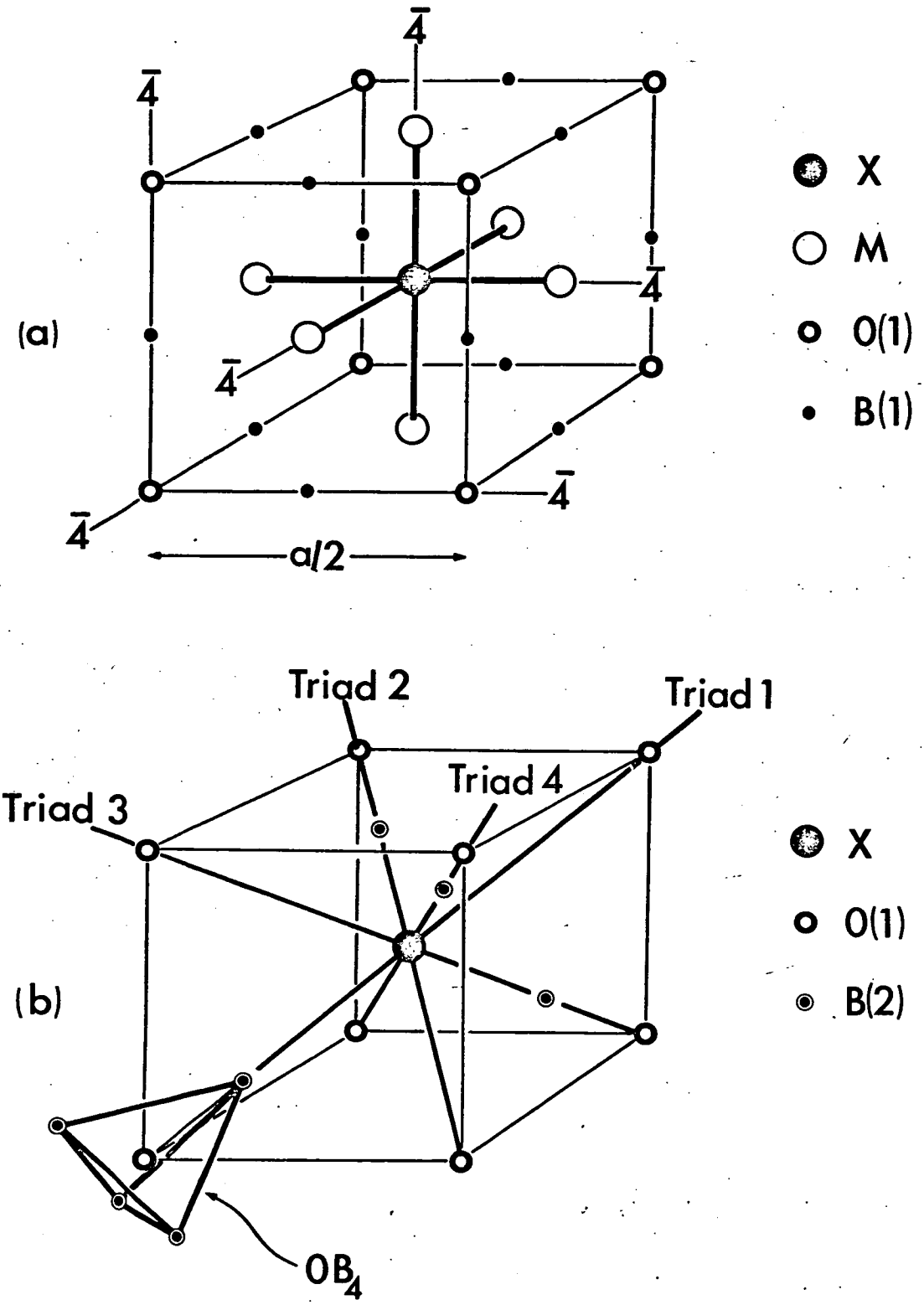
(a)
$\bar{4}$
$\bar{4}$
$\bar{4}$
$\bar{4}$
$\bar{4}$
$\bar{4}$
a/2
X
M
O(1)
B(1)
(b)
Triad 1
Triad 2
Triad 3
Triad 4
OB_4
X
O(1)
B(2)

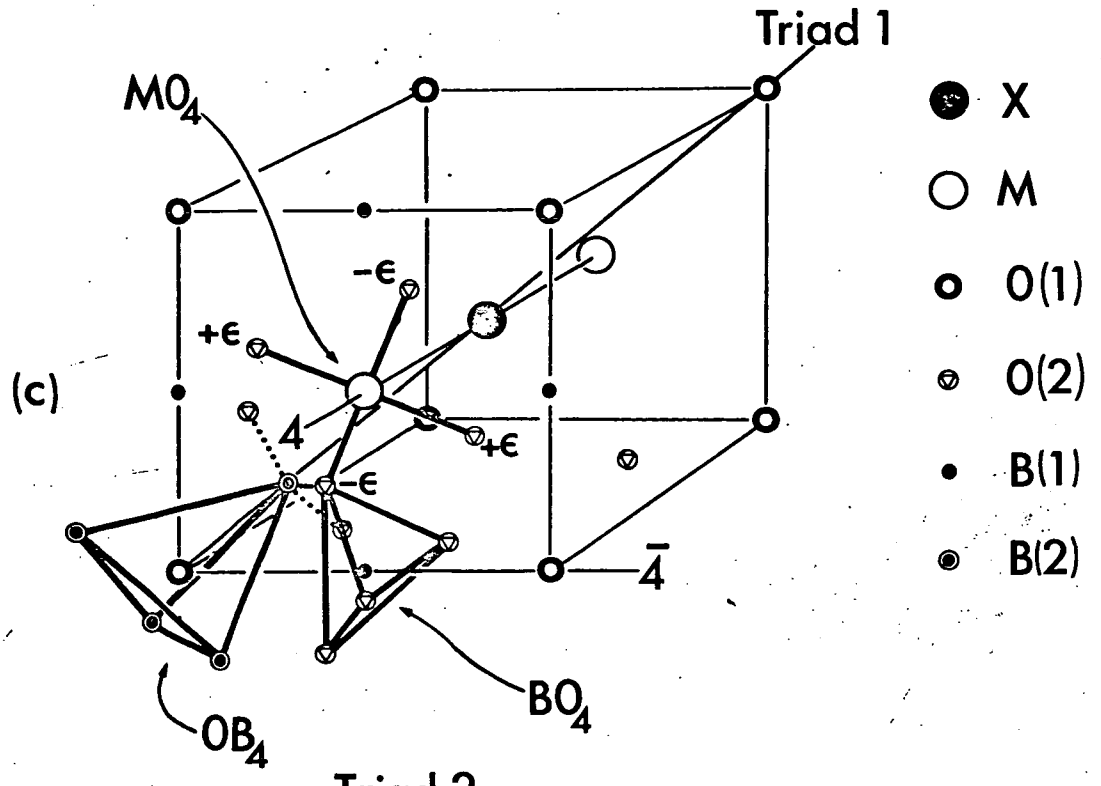
Triad 1
MO_4
(c)
$-\epsilon$
$+\epsilon$
4
$+\epsilon$
$-\epsilon$
$\bar{4}$
BO_4
OB_4
X
M
O(1)
O(2)
B(1)
B(2)

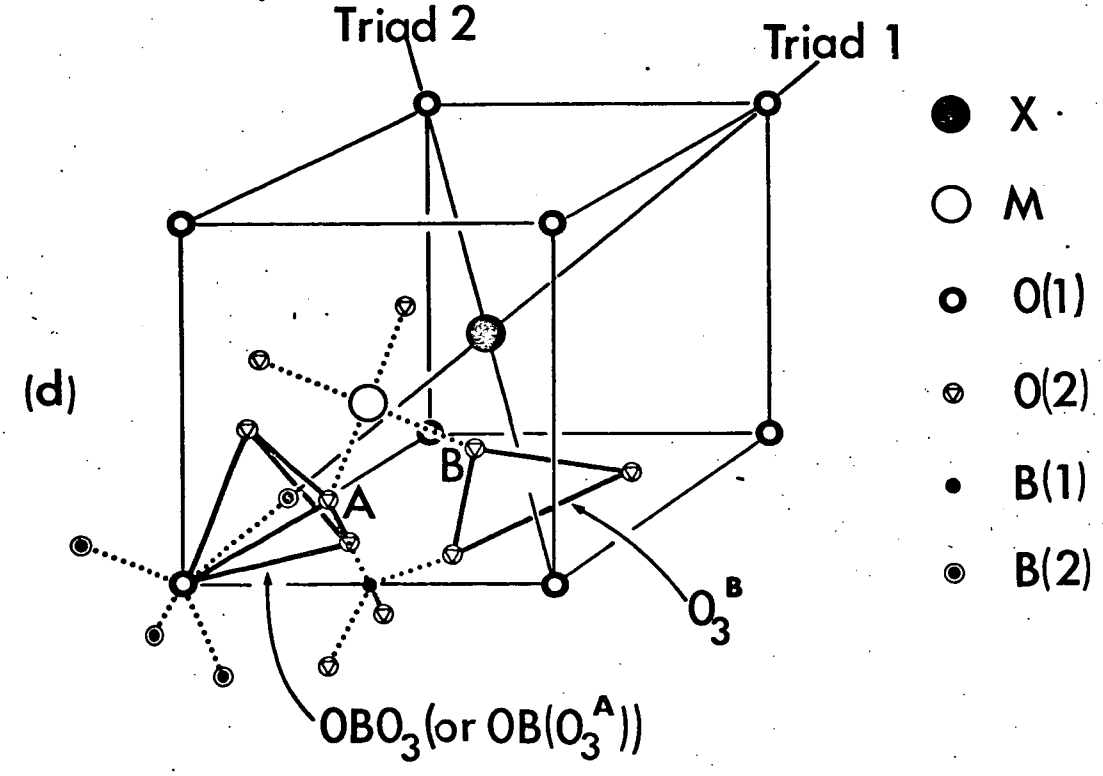
Triad 2
Triad 1
(d)
B
A
O_3^B
OBO_3 (or $OB(O_3^A)$)
X
M
O(1)
O(2)
B(1)
B(2)

The structure is thus a three-dimensional boron-oxygen network interspersed with the chains of metal (M) and halogen (X).

This description of the boracite structure, in the cubic phase, first determined by Ito et al (1951), has now been confirmed in other boracites. For example, similar results have been found

(a) for powdered Ni-I by Becker and Will (1970) using X-rays and neutrons,

(b) for Ni-I (single crystal, B^{11} enriched) by von Wartburg (1973, 1974) from neutron data collected at $77^{o}K$,

(c) for a single crystal of Mg-Cl by Sueno, Clark, Papike and Konnert (1973) from a three-dimensional X-ray study at $673^{o}K$,

(d) for Li-Cl by Jeitschko and Bither (1972) from a three-dimensional X-ray study at $353^{o}K$,

(e) for a single crystal of Cr-Cl by Nelmes and Thornley (1974) from a three-dimensional X-ray study at room temperature,

(f) for a single crystal of Ni-I by Nelmes and Thornley (1976) - a room temperature, three-dimensional X-ray study, and

(g) for a single crystal of Cu-Cl (B^{11} enriched) by Thornley, Nelmes and Kennedy (1976) from a three-dimensional neutron study at $390^{o}K$.

Nelmes and Thornley (1974) compared their calculated inter-ion distances with those of structural studies of cubic boracites carried out prior to their study. They concluded that the boron-oxygen configuration varies little with different metal and halogen ions, with temperature difference, and even with the creation of O(1) vacancies in Li-Cl. The greatest variation among the cubic boracites studied is in the dimensions of the BO_4 group.

Ito et al (1951) determined the orthorhombic structure of Mg-Cl. The space group is $Pca2_1$ with four formula units in the unit cell. It was assumed that the orthorhombic phase differed from the cubic phase only in the position of the metal (M) and halogen (X) ions - that is, Ito et al took the boron-oxygen framework to be the same as in the cubic phase. This assumption was also made by von Wartburg in his determination of the orthorhombic structure of Ni-I (1974).

However, Dowty and Clark (1972) in a full three-dimensional X-ray study of a single crystal of Mg-Cl in its orthorhombic phase obtained displacements for the boron and oxygen ions of the same order of magnitude as the displacements of the metal and halogen ions. Similar displacements have also been confirmed in orthorhombic Cu-Cl (Thornley, Nelmes and Kennedy, 1976) and Fe-I (Nelmes, 1978). These studies show that in the transformation to the orthorhombic phase, the OB_4 and OBO_3 groups are lost; only three of the B(2) ions remain bonded to the O(1) ion, the fourth, designated B(2)-4, is three-fold coordinated to the O(2) ions.

The B-O framework therefore adopts the conventional B-O bonding system in contrast to the hybrid forms of the cubic phase. The halogen (X), O(1) and B(2)-4 ions are displaced along the triads of the cubic phase with O(1) moving in the opposite direction to X and B(2). All halogen ions lying in the same (100) plane move in the same direction which is alternatively $[111]$ and $[\bar{1}\bar{1}1]$ for successive planes. The metal ions are displaced along the direction of the $\bar{4}$ axis they lie on in the cubic phase. The relative movements of the M and X ions with respect to the cubic positions are shown in Figure 7.2.

Schmid and Trooster (1967) and Trooster (1969), on the basis of Mossbauer studies of the orthorhombic phases of Fe-Cl, Fe-Br, Fe-I and ^{57}Fe doped Ni-Cl and Ni-Br, predicted that there would be two distinct types of metal ion site. Dowty and Clark (1973), however, found no pronounced differences between the three symmetrically inequivalent M sites. This has also been found to be the case for the Cu ions in Cu-Cl (Thornley et al, 1976). Nelmes (1978), however, obtained a different atomic arrangement around Fe(1) from that around Fe(2) and Fe(3) in the structure determination of orthorhombic Fe-I. Differences in the metal ion sites are also suggested in studies by Rivera, Bill and Lacroix (1976, 1976a) of E.P.R. spectra of Mn^{2+} in orthorhombic Mg-Cl and Zn-Cl and in studies by Zheludev et al[(1)] (1975) of Mossbauer spectra of ^{57}Fe doped Mn-Cl and Co-Cl. At least 2 M sites were distinguished in E.P.R. spectra of Ni^{+} in orthorhombic Cd-Cl and Cd-I and of Mn^{2+} in orthorhombic Cd-Cl (Baberschke, Reich and Dormann, 1970).

---

(1) Zheludev, Perekalina, Pyl'nev, Smirnovskaya, Belov, Kostov and Yarmukhamedov

Figure 7.2 Structural changes at the cubic to othorhombic phase transition in boracite. One unit cell of the cubic phase, without the boron-oxygen skeleton, is shown. The arrows on the metal and halogen ions indicate the direction of their movements during the transition to the orthorhombic phase (see text). The three different metal environments created are indicated.

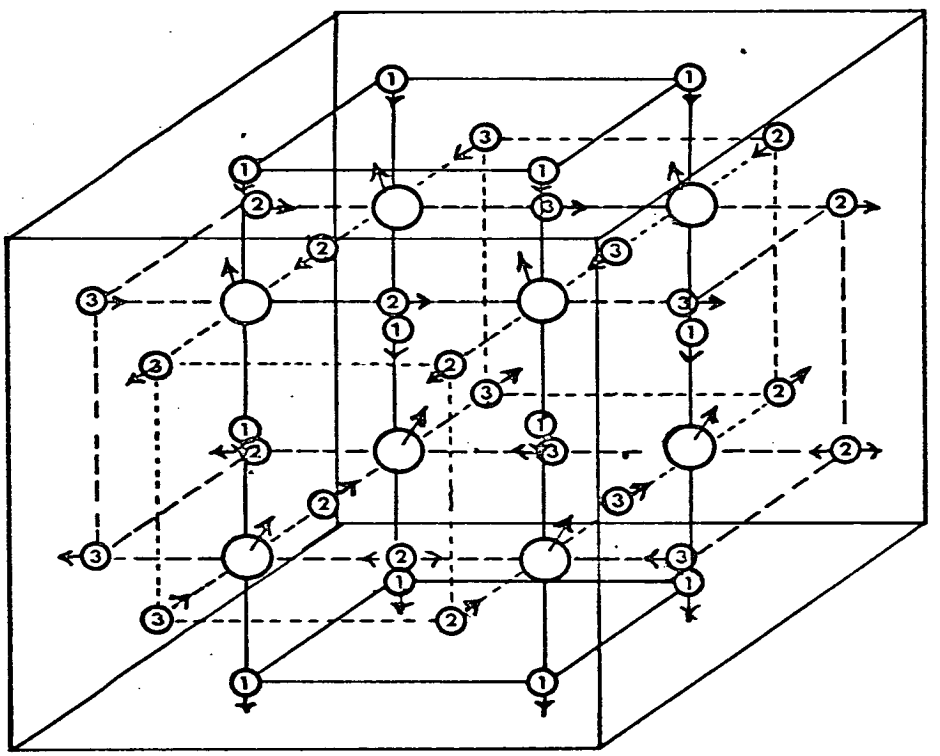

Halogen

Metal

It would therefore appear, on present evidence, that there are at least two distinguishable types of orthorhombic boracite structures.

On further cooling, a rhombohedral phase, space group R3c, has been found to exist in Fe-Cl, Fe-Br, Fe-I, Co-I and Zn-Cl (Schmid and Trooster, 1967). Dowty and Clark (1972), in a full three-dimensional X-ray study of the rhombohedral phase of a single crystal of ericite, $(Fe_{0.8}Mg_{0.2})_3B_7O_{13}Cl$, identified only one M site and showed it to be slightly different from all the M environments in orthorhombic Mg-Cl. This is in contrast with the Mossbauer studies of Schmid and Trooster (1967) who identified the single M site in rhombohedral Fe-Cl, Fe-Br and Fe-I with one of the two distinguishable M sites in the orthorhombic phase. In agreement with Schmid and Trooster (1967), Rivera, Bill and Lacroix (1976a) in their study of the E.P.R. spectra of Mn^{2+} in Zn-Cl identified the single M site in trigonal Zn-Cl and associated it with one of the M sites in orthorhombic Mg-Cl (Rivera et al, 1976).

Schmid, Kliegl and Kobayashi (1969) found that the crystals Zn-Cl, Co-Cl and Fe-Cl undergo a transition to a monoclinic phase, space group Pa, between their orthorhombic and rhombohedral phases. Further work by Kobayashi, Sato and Schmid (1972) has shown that, in Fe-I, two stable monoclinic phases appear separately depending on the history of the temperature change of the crystal. The transition to one phase, monoclinic I, occurs on cooling between the temperatures 203°K and 191°K, and the other, monoclinic II, with increasing temperature between 205°K and 218°K. The two monoclinic phases differ slightly in lattice parameter, thermal expansion coefficient and optical birefringence.

Although no structural investigations of the monoclinic phases have been made to date, Kobayashi et al (1972) have proposed a model for the monoclinic phase of Fe-I and Rivera et al (1976a) a slightly different model for Zn-Cl.

At present there is little information published on either the structure or the phase changes of the chalcogen or hydroxyl boracites. Room-temperature X-ray powder patterns of Mg-S, Mn-S, Mn-Se, Mn-Te, Fe-S, Fe-Se, Cd-S, Cd-Se and Mn-OH all imply a crystal structure similar to the cubic halogen boracites (Muller, 1970; Fouassier et al, 1970; Joubert et al, 1972; Levasseur, 1973; Levasseur et al, 1973a). Although the oxygen framework is found to be similar to that in the cubic halogen boracites, Levasseur (1973), from a single-crystal study of Cd-S, found the Cd and S displacements to differ from the metal and halogen in the halogen boracites and deduced the space group to be P3c1. This possible difference from the halogen boracites was supported by Mossbauer studies of Fe-S which indicated a more complicated structure than $F\bar{4}3c$ (Levasseur et al, 1973a). Nelmes and Gould (1978), however, from a single-crystal X-ray study of Cd-S found no evidence against the usual cubic symmetry $F\bar{4}3c$. They also found that the metal ion, Cd, was disordered over two sites, 1Å apart, along the $\bar{4}$ axis. From the evidence of Fourier maps, Nelmes and Gould (1978) propose that, rather than S, X is more likely to be the SO_4 radical. From E.P.R. spectra of Mn^{2+} in rhombohedral Mg-OH, Rivera, Bill and Lacroix (1976b) concluded that the rhombohedral structure was similar to that found in Zn-Cl.

The determination of the crystal structure of boracites is complicated by the phenomenon of 'growth sectors'. In the cubic phase, boracites grow at different rates along ⟨100⟩, ⟨111⟩ and ⟨110⟩ (Schmid, 1969). The resulting growth pyramids often exhibit different physical properties. The birefringence, dichroism, optical absorption, growth rate and electrical conductivity increase through the sectors in the order ⟨100⟩, ⟨111⟩, ⟨110⟩. The difference in the magnitude of these effects increases as X = Cl→Br→I (Nelmes, 1974).

Nelmes and Thornley (1976) collected full three-dimensional X-ray data from a [100] growth sample and a [110] growth sample of Ni-I. They found no departure from cubic symmetry for either growth sector. Nelmes and Thornley (1976) also concluded that the appearance of birefringence in the [110] growth sector of Ni-I could not be attributed to uniaxial strain, screw dislocation or quadrupole transitions in Ni^{2+} and so the origin of the phenomenon remains uncertain.

Boracites are of interest because they exhibit unusual ferroelectric, magnetic, dynamical and structural properties (Nelmes, 1974). Because of its pseudocubic symmetry and unusual twinning characteristics (see Schmid, 1969), the mineral boracite (Mg-Cl) was attracting interest as early as the 18th century (Mellor, 1924). The phenomena of pyro- and piezo-electricity were first demonstrated for natural boracite by C Friedel, P Curie and J Curie (1880, 1883). Ferroelectricity of the orthorhombic phase was first claimed to be demonstrated for natural Mg-Cl by Le Corre in 1957 but his conclusions were cast in some doubt following further work by Jona (1959) and Sonin and Zheludev (1963),

who in fact suggested that natural Mg-Cl was not ferroelectric, but antiferroelectric. The first conclusive demonstration of ferroelectricity resulted from the observation of domain switching in Ni-Cl (Ascher, Schmid and Tar, 1964) confirming that the orthorhombic phase of Ni-Cl was ferroelectric. Since Ascher et al's experiment on Ni-Cl ferroelectricity has been demonstrated for orthorhombic Ni-I (Ascher, Rieder, Schmid and Stossel, 1966), Fe-I (Kobayashi, Schmid and Ascher, 1968), Ni-Br, Mn-Cl and Zn-Cl (Zimmermann, Bollmann and Schmid, 1970), Co-I (Smutny and Fousek, 1970), Co-Br, Zn-Br, Zn-I, Cr-Cl and Cu-Cl (Schmid, 1974) and Cu-Br (Drozhdin, Bochkov, Gavrilova, Popora, Kopstik and Norvik, 1975); for rhombohedral Zn-Cl, Fe-Cl, Fe-Br, Fe-I and Co-Cl (Schmid, 1970); for monoclinic Zn-Cl (Zimmermann et al, 1970) and it is now generally assumed that ferroelectricity is a property common to all halogen boracites below the cubic→orthorhombic transition.

The cubic (paraelectric)↔ orthorhombic (ferroelectric) phase transition in boracites is an example of a coupled phase transition. The primary order-parameter is not the spontaneous polarization but the normal coordinate of a zone boundary soft mode (Ascher, 1970; Dvorak and Petzelt, 1971). Instability in such a mode can induce through anharmonic coupling to q=o optic and acoustic modes, spontaneous polarization and spontaneous strain as second order parameters varying as $(T-T_c)$ in the ferroelectric phase.

Two soft modes were found in the orthorhombic ferroelectric phase of Cr-Cl by Lockwood (1975) and of Cu-Cl by Lockwood and Syme (1977). The soft-mode behaviour in both is similar except that for Cu-Cl the modes are more heavily damped.

The heavier damping in Cu-Cl indicates a greater degree of anharmonic thermal motion in this boracite. According to Lockwood (1977) the low-frequency wing feature observed in the cubic phase arises predominately from one-phonon scattering and implies some kind of dynamic disorder. This wing feature persists into the orthorhombic phase and finally disappears at around T_c-50^{o}K. The damping of low-frequency phonons observed in Raman spectra of Ni-I, Cr-Cl and Cu-Cl increases on replacing I with Cl and for the chlorides is greater in Cu-Cl. A soft mode has been observed in Raman spectra of the cubic phase of Ni-I (Murray and Lockwood, 1977). This feature, which was not observed in the cubic phase of Cr-Cl or Cu-Cl, suggests that the improper ferroelectric transition in Ni-I differs from that of the other boracites (Murray and Lockwood, 1977).

Felix (1973) and Felix, Lambert, Comès and Schmid (1974) found X-ray diffuse scattering in the cubic phase, concentrated in reciprocal lattice planes perpendicular to the ⟨100⟩ directions of the cubic cell in crystals of Ni-I, Fe-Br, Cr-Cl and Cu-Cl. As with the wing feature in the Raman spectra (see above), this scattering is very weak below T_c-50^{o}K but becomes more pronounced as T_c is approached and also acquires a marked modulation within the planes. The sharpness of the planes and the strength of the modulation within the planes increases as X = I→Br→Cl and is greater in Cu-Cl than in Cr-Cl. These results can be interpreted in terms of short-range ordering in which the displacements of the metal and halogen ions in unit cells are similar to those found for the orthorhombic phase (Ito et al, 1951; Thornley et al, 1976) but in each sub-cell, containing one formula unit, M and X each occupy only one of their possible sites (Felix, 1973).

Alternatively however, the diffuse X-ray scattering results could be interpreted in terms of highly anisotropic dynamics (see Nelmes, 1974).

That the metal and halogen ions are disordered in the cubic phase was suggested by Ito et al (1951), Schmid (1970) and Ascher (1970). The halogen (X) is on a site of 23 symmetry; along each of the four triads passing through this site there is the polar sequence O(1)-B(2)...(X) ....O(1). The suggestion was that the halogen ions move in a saddle like potential with four minima displaced from the mean position by δ along $[111]$, $[\bar{1}\bar{1}1]$, $[1\bar{1}\bar{1}]$ and $[\bar{1}1\bar{1}]$ - i.e. along the 4 triads, towards the O_3^B oxygens (see Figure 7.1(b) and (d)). The proposed disorder for the metal, site symmetry $\bar{4}$, is between two minima, along the $\bar{4}$ axis, displaced by γ from the mean position. For the metal ion at ($^a/_4$, $^a/_4$, 0), the $\bar{4}$ axis is along the z axis and the disordered positions are thus ($^a/_4$, $^a/_4$, $\pm\gamma$). It is then assumed that the halogen and metal ions order onto one of their cubic-phase sites at the cubic→orthorhombic transition.

Support for this disordered model came from experiments by von Wartburg (1973, 1974) on cubic Ni-I at 77°K who refined $\delta \sim 0.7$ Å and $\gamma \sim 0.2$ Å; by Sueno et al (1973) on cubic Mg-Cl at 673°K who refined $\delta \sim 0.3$ Å and $\gamma \sim 0.2$ Å; and by Trooster (1969) on Fe boracites and ^{57}Fe doped Ni boracites, who revealed the marked anisotropy of the thermal motion of the metal ion, greatest along the $\bar{4}$ axis on which it is sited, and showed that the degree of anisotropy increases as X = I→Br→Cl.

Nelmes and Thornley (1974, 1976), however, in single-crystal studies of the cubic phase of Cr-Cl and Ni-I at room temperature showed that neither the halogen nor the metal moves between potential minima separated by the amounts $\geq$ 0.4 Å previously suggested and concluded that, within the resolution of their data, both ions move in single-minimum potential wells. Thornley, Kennedy and Nelmes (1976) concluded that there was no structural study of a cubic boracite for which it is necessary to postulate disorder of the metal and halogen ions in order to explain the experimental results. These conclusions are supported by the value of the entropy change measured for the cubic → orthorhombic transition in Co-I by Smutny (1972) - this change being much smaller than would be expected if the halogen and metal ions were ordered onto their suggested disorder sites (Felix, 1973) - and also by Rivera, Bill, Weber, Lacroix, Hochstrasser and Schmid (1974) who from E.P.R. Spectra on Zn-Cl, Zn-Br, Zn-I and Mg-Cl showed that the M site is axially symmetric. Thornley and Nelmes (1976) argued that all previous disorder results could be shown to be spurious.

As the value of the entropy change for the cubic → orthorhombic transition in Co-I (Smutny, 1972) is seen as supporting the argument against the metal and halogen being disordered in the cubic phase, it was decided to determine the crystal structure of Co-I in the cubic phase at room temperature; details of this experiment are given in Section 7.3.

To date structural work has been confined to the chlorine and iodine halogen boracites - no detailed structural investigation has been carried out on any bromine boracite.

Nelmes et al (1974, 1976) and Thornley et al (1976) have found that the third cumulant (see next section and Appendix B) on the Cl ion in Cu-Cl is greater than that on the Cl ion in Cr-Cl, both of which are greater than the value of the third cumulant on the I ion in Ni-I. Therefore, to extend further the investigation of the possible disorder of metal and halogen ions and to gain a more complete view of halogen boracite structures, it was decided to carry out a detailed structural investigation of copper bromine boracite. This boracite is cubic at room temperature (a limitation of the available equipment for X-ray work) and is related to Cu-Cl in that only the halogen is replaced. (extensive structural and dynamical work has been carried out on Cu-Cl by Edinburgh colleagues.) The details of this experiment are given in Section 7.4 and the conclusions drawn from both the above experiments are given in 7.5.

7.2 Present Work

The work presented here forms part of the programme of detailed structural investigations of phase transitions in boracites (of which results achieved already have been summarised above) instigated by Dr R J Nelmes of this Department.

As mentioned previously, the thermal motion of the ions, especially of the halogen and metal ions, is of particular interest. Ito et al (1951) and later Schmid (1970) suggested that the halogen ions move in a saddle-like potential in the cubic phase with four minima displaced by δ from their mean position towards the O_3^B oxygens, i.e. along $[111]$, $[\bar{1}\bar{1}1]$, $[1\bar{1}\bar{1}]$ and $[\bar{1}1\bar{1}]$.

Ascher (1970) suggested that the metal ion, as well as the halogen, is disordered in the cubic phase, having two minima displaced by δ along the $\bar{4}$ axis from the mean position.

By displacing the halogen ion along one triad to a position (U,U,U) and including the parameter U as a variable in the refinement, it is possible to test this disorder model directly. The small magnitude of δ, the proposed metal displacement, and parameter correlation prevent a similar test being successful for the disorder model of the metal ion.

As an alternative to disorder (i.e. more than one potential minimum) it can be considered that some ions have anharmonic thermal motion in a single-minimum well. To investigate possible anharmonicity in the thermal motion of the metal and halogen ions, higher-cumulant parameters are considered (see Appendix B) and the least-squares refinement program has been modified to allow refinement of third and fourth cumulants (describing anharmonic thermal motion) in addition to the normal positional and anisotropic harmonic thermal parameters (first and second cumulants respectively).

The independent non-zero elements for the metal, halogen and B(2) sites in cubic boracites are given in Table 7.1.

The halogen ions occupy sites of cubic (23) symmetry. The anharmonic thermal motion may therefore be described by one third-cumulant parameter and two fourth-cumulant parameters.

Table 7.1

Independent elements of the third- and fourth-cumulant tensors

Elements not listed are zero by symmetry. The relationships for the metal (M) apply to the $(\frac{1}{4},\frac{1}{4},0)$ sites with $\bar{4}$ along z. The symbol $\circlearrowright$ indicates that the given element is equal to all others obtained by cyclic permutation, e.g. $1233 \circlearrowright 1233 = 2311 = 3122$.

Ion	Site Symmetry	Cumulant	Elements	Number of Independent Elements
M	$\bar{4}$	$3_K\, j\, k1$	$233 = -113,\ 123$	2
		$4_K\, j\, k1m$	$1111 = 2222,\ 3333,$ $1122 = -2111,\ 1122,$ $2233 = 3311$	5
X	23	$3_K\, j\, k1$	123	1
		$4_K\, j\, k1m$	$1111\circlearrowright,\ 1133\circlearrowright$	2
B(2)	3	$3_K\, j\, k1$	$111\circlearrowright,\ 112\circlearrowright,\ 113\circlearrowright,\ 123\circlearrowright$	4
		$4_K\, j\, k1m$	$1111\circlearrowright,\ 1112\circlearrowright,\ 1113\circlearrowright$ $1122\circlearrowright,\ 1233\circlearrowright$	5

The third cumulant, 123, describes a distortion of the potential well of the halogen such that the potential is softened along $[111]$, $[\bar{1}\bar{1}1]$, $[1\bar{1}\bar{1}]$ and $[\bar{1}1\bar{1}]$ and hardened along $[\bar{1}\bar{1}1]$, $[11\bar{1}]$, $[\bar{1}11]$ and $[1\bar{1}1]$ - or vice versa depending on the sign. This is of particular interest as this is the proposed direction of δ .

For the metal ion site, with $\bar{4}$ symmetry, there are two third-cumulant and five fourth-cumulant parameters. The potential along the $\bar{4}$ axis is described by the 3333 fourth cumulant and as this is the proposed direction of γ is of particular relevance.

The statistical significance of certain structural features of interest in both Co-I and Cu-Br has been determined using constrained refinement and significance-testing techniques (see Section 3.6.2). The following constraints were used to investigate particular aspects of the boron-oxygen framework,

1) the O(2) - O(2) distances in the BO_4 group are all equal and are also equal to the O(2) - O(2) distance in the O_3^A group,
2) the BO_4 tetrahedron is regular - with cubic ($\bar{4}3m$) symmetry, and
3) the B(1) - O(2) distance in BO_4 equals the B(1) - O(2) distance in OBO_3.

The thermal motion of all the ions was investigated using the constraint,

4) that the metal ion has isotropic thermal motion,
5) that the B(2) ion has isotropic thermal motion,
6) that the O(2) ion has isotropic thermal motion, and
7) that the B(1) ion has isotropic thermal motion.

7.3 The Cubic Phase of Cobalt Iodine Boracite, $Co_3B_7O_{13}I$, at Room Temperature (291°K)

7.3.1. Experiment: A crystal of cobalt iodine boracite was supplied by Dr H Schmid of the Battelle Institute, Geneva (see Section 2.2.1 for crystal details). X-ray intensity data were collected at 291°K on a Hilger and Watts four-circle diffractometer in the Physics Department of York University using Zr-filtered Mo $K\alpha$ radiation. The lattice parameter, determined by fitting Bragg reflections at high and low θ, was found to be 12.119(3) Å. In a single octant, giving six equivalent reflections in general, all reflections out to $\frac{\sin\theta}{\lambda} = 0.99$ Å^{-1} ($\theta = 45°$) were measured and recorded as integrated intensities. Throughout data collection, three standard reflections were measured at two-hourly intervals and these reflections did not vary by more than two standard deviations throughout the experiment. Where occasional fluctuations of the incident intensity were detected, the corresponding data were deleted. To avoid the problems introduced by the β-filter absorption edge (Nelmes, 1975), measurements were made with unfiltered radiation in the range $\theta \leq 20°$ (DATA 1); for $15° \leq \theta \leq 45°$ measurements were made (DATA 2) using Zr-filtered radiation. All intensities were LP-corrected and then corrected for absorption using the ABSCOR program of the XRAY 72 system (Stewart, 1972). On averaging over symmetry-related reflections, the data reduced to 362 independent structure amplitudes. The error for each was taken to be the larger of the errors estimated

from (a) the counting statistics and (b) the internal agreement of the contributing symmetry-related reflections. Thus a standard deviation, $\sigma(F_o)$, was derived for each F_o. For a few reflections these first estimates of $\sigma(F_o)$ were altered in the initial stages of refinement, as explained later in Section 7.3.2. The observed structure aplitudes and their final estimated errors are listed in Appendix F.

7.3.2 Refinements and Constraints: Structure refinement was started from the values obtained for Cr-Cl at room temperature (Nelmes and Thornley, 1974) using the full-matrix least-squares program developed by Dr G S Pawley of this department. Initially 21 parameters were refined : 2 scale factors (for DATA1 and DATA2), and isotropic extinction parameter, the 4 independent positional parameters and the 14 independent harmonic thermal parameters. Neutral-atom form factors were used (Doyle and Turner, 1968). Because of a probably inadequate treatment of extinction - in the neglecting of path-length variation and angle-dependence of extinction in the theory of Zachariasen (1967) - five of the strongest reflections, with extinction factors <0.7 on F_c still showed $F_c > F_o$ significantly, and were omitted. The ratio of the scale factors of the two data sets and the relative magnitudes of the structure amplitudes of reflections common to both data sets were used to scale DATA2 to DATA1. The reflections common to both sets were averaged and only one scale factor was then refined.

This produced a final set of 338 observed structure amplitudes, F_o, each with a weight $W_i = \frac{1}{\sigma^2(F_o)}$. The correctness of these weights was tested by analysing $W\Delta^2$ as a function of sin θ, F_o and EXTF (see Section 3.6.1). There should be no significant dependence on sin θ, F_o or EXTF. To achieve this it was necessary to increase the $\sigma(F_o)$ estimated for 5 reflections for which no equivalent reflections had been measured. If $\sigma(F_o)_i$ was less than 0.02, then $\sigma(F_o)_i$ was set equal to 0.02 $(F_o)_i$, otherwise no change was made.

With the inclusion of the real and imaginary parts of the anomalous scattering for cobalt and iodine (Cromer, 1965), the two possible absolute orientations were refined, giving an $\mathcal{R}$ ratio of 1.42 (see Section 3.6.2). As $\mathcal{R}(0.001) = 1.018$ then the orientation giving the lower value of R_w could be taken to be the correct one at a very high level of significance. The model thus reached with 20 parameters - a scale factor, an isotropic extinction parameter, 4 independent positional parameters and 14 independent harmonic thermal parameters - was designated Model I.

The correction factor on F_c, for extinction, $y^{\frac{1}{2}}$ (see Appendix A), was > 0.95 for 308 (91%) of the reflections and $0.7 < y^{\frac{1}{2}} < 0.95$ for the remaining 30 (9%) reflections used in the refinement. For the 5 reflections omitted from the refinement, $0.52 < y^{\frac{1}{2}} < 0.7$.

The refinement of Model I converged to an $\mathcal{R}$ index of 3.2%, and $R_{w} = 197$ ($\mathcal{R}$ and R_{w} are defined in Sections 3.6.1 and 3.6.2). The final positional and thermal parameters and their estimated standard deviations are given in Table 7.2.

Further models, with constraints (hence with less paramaters) or with cumulants (as extra parameters) based on the final parameters from Model I were refined and tested. The absolute orientation found for Model I was adopted throughout.

The fit obtained for each constrained model is compared with Model I as shown in Table 7.3. It can be seen that all the short O(2)-O(2) distances cannot be considered as being unequal ($\alpha = 0.5$). The distortion of the BO_4 group, by compression along the $\bar{4}$ axis is not at all significant ($\alpha < 0.5$). The difference between the B(1)-O(2) distance in the BO_4 group and the B(2)-O(2) distance in OBO_3 is very significant ($\alpha = 0.001$, $S = 16$). The anisotropy of the thermal motion of the cobalt is clearly very highly significant. Although the thermal anisotropy of the B(2) and O(2) is highly statistically significant, S has the marginal values of 2.2 and 2.1 respectively. The thermal motion of B(1) is not significantly anisotropic.

The significance levels obtained for the inclusion of third and fourth cumulants for the Co, I and B(2) ions are given in Table 7.4.

Table 7.2

Positional and thermal parameters for $Co_3B_7O_{13}I$ at room temperature

The positional parameters are in Å, U_{ij} are in $Å^2$ (the temperature factor is $\exp(-2\pi^2 \sum_{ij} H_i H_j U_{ij})$ where $H_i = h_i/a$) and B is in $Å^2/8\pi^2$ units. Standard deviations are given on the last quoted place. Parameters without errors are determined by symmetry. The lattice parameter a = 12.119(3)Å.

	X	Y	Z	U_{11}	U_{22}	U_{33}	U_{23}	U_{31}	U_{12}	B
O(1)	0	0	0							0.70(4)
I	3.0297	3.0297	3.0297							0.866(8)
Co	3.0297	3.0297	0	0.0065(1)	0.0065	0.0218(2)	0	0	0	
B(1)	3.0297	0	0	0.0053(8)	0.0064(6)	0.0064	0	0	0	
B(2)	0.966(2)	0.966	0.966	0.0086(5)	0.0086	0.0086	0.0021(6)	0.0021	0.0021	
O(2)	2.185(1)	0.238(1)	1.171(1)	0.0051(4)	0.0070(4)	0.0052(4)	0.0000(4)	0.0006(4)	0.0016(4)	

Table 7.3

Comparison of constrained models with Model I for $Co_3B_7O_{13}I$ at room temperature

The number of parameters in Model I is N (=20); the number of parameters in the constrained model is n, less than N by the tabulated N-n. $\mathcal{R}$ is calculated from the tabulated $^{R}\omega$ as $\mathcal{R} = (^{R}\omega/197)^{\frac{1}{2}}$. $\mathcal{R}_\alpha$, α and $\mathcal{S}$ are determined as in Table 5.2. The values for the constrained parameters are given with estimated standard deviations: distances are in Å, and thermal parameters U_{ii} are in $Å^2$, as defined in Table 7.2.

Constraint	N-n	$^{R}\omega$	$\mathcal{R}$	α	$\mathcal{R}_\alpha$	$\mathcal{S}$	Constrained Parameters
1	2	198	1.003	0.5	1.002	0.4	O-O = 2.388(1)
2	1	197	1.001	-	-	-	B-O = 1.463(1)
3	1	268	1.167	0.001	1.018	15.97	B-O = 1.450(3)
4	1	3366	4.139	0.001	1.018	296	$U_{11} = U_{22} = U_{33} = 0.0102(4)$
5	1	206	1.024	0.001	1.018	2.25	$U_{11} = U_{22} = U_{33} = 0.0086(5)$
6	5	217	1.051	0.001	1.033	2.105	$U_{11} = U_{22} = U_{33} = 0.0057(2)$
7	1	198	1.003	0.25	1.002	0.302	$U_{11} = U_{22} = U_{33} = 0.0060(5)$

Table 7.4

Comparison of third- and fourth-cumulant models with Model I for $Co_3B_7O_{13}I$ at room temperature

The number of parameters in Model I is n(=20); the number of parameters in the cumulant model is N, greater than n by the tabulated (N-n). $\mathcal{R}$ is calculated from the tabulated R_ω as $\mathcal{R} = (197/R_\omega)^{\frac{1}{2}}$: compare Table 7.3. $\mathcal{R}_\alpha$, α and $\mathcal{S}$ are determined as in Table 5.2.

Model Number	is Model I plus	N-n	R_ω	$\mathcal{R}$	α	$\mathcal{R}_\alpha$	$\mathcal{S}$
1	$^3\underline{\underline{K}}$ (I)	1	195	1.004	0.1	1.004	0.42
2	$^3\underline{\underline{K}}$ (B(2))	4	192	1.012	0.25	1.009	0.55
3	$^3\underline{\underline{K}}$ (Co)	2	189	1.019	0.005	1.019	1.43
4	$^4\underline{\underline{K}}$ (I)	2	193	1.009	0.1	1.007	0.62
5	$^4\underline{\underline{K}}$ (B(2))	5	190	1.018	0.1	1.015	0.72
6	$^4\underline{\underline{K}}$ (Co)	5	186	1.029	0.005	1.027	1.17

The third cumulant on Co is significant at the 0.005 level, though S is less than 2. The inclusion of all the third cumulants of I is significant only at the 0.1 level and of B(2) is significant only at the 0.25 level. The fourth cumulant of Co is significant at the 0.005 level, though S is less than 2.

Significance levels for the inclusion of individual cumulant parameters for cobalt were obtained in some further refinements. The low level of significance of the third and fourth cumulant parameters for I and B(2) did not warrant further testing. The results are given in Table 7.5. For the cobalt ion, there are two third-cumulant parameters. The 123 parameter is significant at the 0.05 level (S =0.6) and the 223 = -113 parameter is significant at the 0.01 level (S =1.2). There are five fourth-cumulant parameters. The 1122 parameter is the most significant - at the 0.005 level (S =1.3). The 1111=2222 parameter is significant only at the 0.1 level. The 3333, 1222 = -2111 and 2233=3311 parameters are not significant ($\alpha > 0.5$).

Apart from some of the third- and fourth-cumulant parameters for cobalt, it is clear that the inclusion of anharmonicity in the thermal motion does not give a significantly improved fit.

Table 7.5

Some individual higher-cumulant parameters and significance levels for Co in $Co_3B_7O_{13}I$ at room temperature

The third cumulants are given as C^{jkl} (in $Å^3$) and the fourth cumulants are given as d^{jklm} (in $Å^4$) (see Johnson (1970)). The standard deviations are given on the last decimal place.

Third Cumulants

Ion	jkl	C^{jkl}	α	S
Co	223 = -113	0.007(2)	0.01	1.21
	123	-0.006(3)	0.05	0.6

Fourth Cumulants

Ion	jklm	d^{jklm}	α	S
Co	1111 = 2222	-0.004(2)	0.1	0.4
	1122	-0.0026(9)	0.005	1.3

By displacing the iodine ion a distance δ from its mean position along the triad, away from the B(2) ion, to a position (u,u,u) and by omitting all third and fourth cumulants, the disorder model suggested for the halogen ion in cubic boracites can be tested directly. The parameter u is included as a variable in the refinements. The displacement δ ($= \sqrt{3}(u - {}^{a}/_{4})$, though it refined to a value of 0.12(1) Å, was strongly correlated (-0.91) with the isotropic temperature factor B for I which dropped from 0.87(1) Å^2 to 0.46(2) Å^2 during the refinement. There was no improvement in fit compared with Model I.

7.3.3 Structure: The crystal structure of cobalt iodine boracite in its cubic phase at room temperature is basically the same as that determined for other cubic boracites (see Section 7.1), e.g. Mg-Cl (Sueono et al, 1973), Cr-Cl and Ni-I (Nelmes and Thornley, 1974, 1976), Cu-Cl (Thornley et al, 1976). The final positional and thermal parameters are given in Table 7.2. Some calculated inter-ion distances for Co-I are given in Table 7.10 and are compared and contrasted in Section 7.5 with equivalent values obtained from other studies.

It has been shown that the O(2)-O(2) distance across the $\bar{4}$ axis cannot be regarded as being significantly different from the O(2)-O(2) distance along the $\bar{4}$ axis in the BO_4 group (see Figure 7.1(c)).

In Cu-Cl the O(2)-O(2) distance across the $\bar{4}$ axis is significantly ($\alpha \leq 0.001$) longer than the O(2)-O(2) distance along the $\bar{4}$ axis (Thornley et al, 1976) and for the same constraint in Cr-Cl and Ni-I, $\alpha = 0.001$ (Nelmes and Thornley, 1974, 1975). Similar differences occur between Co-I and Cr-Cl, Cu-Cl and Ni-I in that in Co-I there is no indication of the BO_4 group being distorted from cubic ($\bar{4}3m$) symmetry whereas the small distortion of the BO_4 group in the other three is highly significant ($\alpha = 0.001$). The B(1)-O(2) distance in the BO_4 group in Co-I is longer than the B(2)-O(2) distance in the OBO_3 group. The O(2) ions are displaced out of the plane defined by O(1), B(1) and Co by $\epsilon = 0.238(1)$ Å which means that the O_3^A triangle is slightly smaller than the O_3^B triangle.

The thermal motion of the cobalt ion is highly anisotropic with the much higher value along the $\bar{4}$ axis (0.022(1) $Å^2$) perpendicular to the almost planar O(2) array of the CoO_4 group (see Figure 7.1(c)), than at right angles to the $\bar{4}$ axis (0.006(1) $Å^2$). The anisotropy in the thermal motion of B(2) and O(2) is highly statistically significant ($\alpha = 0.001$) though S is only 2. The B(2) thermal parameters correspond to 0.013(1) $Å^2$ along [111] and 0.007(1) $Å^2$ perpendicular to [111]. (The eigenvalues for the B(2) ion are ($U_{11} + 2\,U_{23}$) along the triad and ($U_{11} - U_{23}$) perpendicular to the triad.) The significance level of the anisotropy of the thermal motion of B(1) is only 0.25.

The investigation of deviations from purely harmonic thermal motion for the Co, I and B(2) ions revealed little of statistical significance - the main exceptions being the third- and fourth-cumulant parameters for Co which were significant at the 0.005 level.

The possibility that the iodine ion is disordered over four sites displaced by δ from the mean position $(\frac{1}{4},\frac{1}{4},\frac{1}{4})$ along $[111]$, $[\bar{1}1\bar{1}]$, $[1\bar{1}\bar{1}]$ and $[\bar{1}\bar{1}1]$ was not found to be significant at any level. The suggested disorder of the cobalt ion could not be tested directly because of the almost complete correlation between the displacement δ and the thermal parameter along $\bar{4}$ (U_{33}). However, the low statistical significance ($\alpha=0.1$) of the 3333 fourth-cumulant parameter which describes anharmonicity in the Co ion's potential along the $\bar{4}$ axis makes a ron-zero δ rather unlikely.

7.4 The Cubic Phase of Copper Bromine Boracite, $Cu_3B_7O_{13}Br$, at Room Temperature (291°K)

7.4.1. Experiment: A crystal of copper bromine boracite was supplied by Dr H Schmid of the Battelle Institute, Geneva (see Section 2.2.2). The experiment was performed on a Hilger and Watts X-ray four-circle diffractometer in the Physics Department of York University.

X-ray intensity data were collected using Zr-filtered Mo K_α radiation and recorded as integrated intensities.

The lattice parameter, determined by fitting Bragg reflections at high and low θ, was found to be 11.955(3) Å . In a single octant, giving six equivalents in general, all reflections out to $\frac{\sin\theta}{\lambda} = 1.07$ Å^{-1} ($\theta = 50^{\circ}$) were measured. At two-hourly intervals throughout data collection three standard reflections were measured. Where occasional fluctuations of the incident intensity were detected, the corresponding data were deleted. The intensity of the standard reflection did not vary by more than two standard deviations. As in the experiment on Co-I, the low-angle data (DATA1) ($\theta \leq 25^{\circ}$) were collected using unfiltered radiation to avoid the problems introduced by the β-filter absorption edge (Nelmes, 1975); for $15^{\circ} \leq \theta \leq 35^{\circ}$ measurements were made (DATA2) using Zr-filtered radiation. The reflections for which h, k and l are all odd result from scattering from oxygen ions only. These reflections are therefore very weak and at high angles prove to be unmeasurable. In the range $35^{\circ} \leq \theta \leq 50^{\circ}$ only the reflections for which h, k and l are all even were collected - these data forming part of DATA2. All intensities were LP-corrected and then corrected for absorption using the ABSCOR program of the XRAY 72 system (Stewart, 1972). Because of the hardness of the material, the cutting of the crystal of Cu-Br used for the experiment resulted in some of the crystal faces having re-entrant angles. The ABSCOR program does not allow for this with the result that there was, in the case of some reflections, a disagreement in intensity between absorption-corrected symmetry-related reflections of up to 10%.

On averaging over symmetry-related reflections, the data reduced to 361 independent structure amplitudes. The error for each was taken to be the larger of the errors estimated from (a) the counting statistics and (b) the internal agreement of the contributing symmetry-related reflections. Thus a standard deviation, $\sigma(F_o)$, was derived for each F_o. For a few reflections these first estimates of $\sigma(F_o)$ were altered in the initial stages of refinement. The observed structure amplitudes and their final estimated errors are listed in Appendix G.

7.4.2 Refinements and Constraints: Structure refinement was started from the values obtained for Cr-Cl at room temperature (Nelmes and Thornley, 1974) using the full-matrix least-squares program developed by Dr G S Pawley of this department. Neutral atom form factors were used (Doyle and Turner, 1968) with the real and imaginary parts of the anomalous scattering included for Cu and Br (Cromer, 1965). After the initial refinements 24 reflections with large extinction factors (< 0.7) on F_c still showed $F_c > F_o$ significantly and were omitted from subsequent refinements. In the case of large extinction it was felt that the corrections were inadequate - perhaps in that the Zachariasen (1967) treatment, incorporated in the least-squares program, neglects path-length variation and the angle-dependence of extinction. Up to this point two data sets DATA1 and DATA2 had been included in the refinement, each with its own scale factor.

The ratio of the scale factors of the two data sets and the relative magnitude of the structure amplitudes of reflections common to both data sets were used to scale DATA2 to DATA1. The reflections common to both sets were averaged and only one scale factor was then refined. This produced a final set of 313 observed structure amplitudes, $(F_o)_i$, each with a weight $W_i = \frac{1}{\sigma^2(F_o)_i}$. As in the experiment on Co-I, the validity of the weighting scheme was tested by analysing $\overline{W\Delta^2}$ over small ranges of sin θ, F_o and EXTF (see Section 3.6.1). As in Section 7.3.2, the $\sigma(F_o)$ for some of the strongest reflections had to be increased and again $\sigma(F_o)_i$ was set to a minimum of $0.02(F_o)_i$.

With the inclusion of the anomalous dispersion of the copper and bromine, the two possible absolute orientations were refined, giving an $\mathcal{R}$ ratio of 1.98. As $\mathcal{R}(0.001) = 1.046$, then the orientation giving the lower value of R_ω could be taken to be the correct one at a very high level of significance.

The final 'standard' refinement, with 20 variable parameters - a scale factor, an isotropic extinction parameter, 4 independent positional parameters and 14 independent harmonic thermal parameters - converged to an $\mathcal{R}$ index of 4.4% and $R_\omega = 160$ (see Sections 3.6.1 and 3.6.2).

The correction factor on F_c, for extinction, $y^{\frac{1}{2}}$ (see Appendix A), was > 0.95 for 260 (83%) of the reflections and $0.7 < y^{\frac{1}{2}} < 0.95$ for the remaining 53 (17%) reflections. For the 24 reflections omitted from the refinement $0.38 < y^{\frac{1}{2}} < 0.7$.

The final positional and thermal parameters and their estimated standard deviations are given in Table 7.6.

Further models have been refined and tested in which constraints are applied (less parameters than Model I) or in which additional parameters are included (higher cumulants). The absolute orientation found for Model I was adopted throughout.

The resulting fit obtained for each hypothesis is compared with Model I as shown in Table 7.7. It can be seen that the distortion of the oxygen framework from a configuration with all the short O(2)-O(2) distances the same is highly significant ($\alpha = 0.001$, $S = 16.9$). Similarly the distortion of the BO_4 group, by compression along the $\bar{4}$ axis is highly significant ($\alpha = 0.001$, $S = 18.3$) as is the difference between the B(1)-O(2) distance in the BO_4 group and the B(2)-O(2) distance in OBO_3 ($\alpha = 0.001$, $S = 20.8$). The anisotropy of the thermal motion of the Cu, B(2) and O(2) are all significant at the 0.001 level. For B(1) the thermal motion is significantly anisotropic only at the 0.025 level.

Table 7.6

Positional and thermal parameters for $Cu_3B_7O_{13}Br$ at room temperature

The positional parameters are in Å, U_{ij} are in $Å^2$ (the temperature factor is $\exp(-2\pi^2\sum_{ij} H_i H_j U_{ij})$ where $H_i = h_i/a$) and B is in $Å^2/8\pi^2$ units. Standard deviations are given on the last quoted place. Parameters without errors are determined by symmetry. The lattice parameter a = 11.955(3)Å.

	X	Y	Z	U_{11}	U_{22}	U_{33}	U_{23}	U_{31}	U_{12}	B
O(1)	0	0	0							0.50(4)
Br	2.989	2.989	2.989							0.86(1)
Cu	2.989	2.989	0	0.0042(1)	0.0042	0.0196(2)	0	0	0	
B(1)	2.989	0	0	0.007 (1)	0.0042(6)	0.0042	0	0	0	
B(2)	0.961(2)	0.961	0.961	0.0071(5)	0.0071	0.0071	0.0027(6)	0.0027	0.0027	
O(2)	2.157(2)	0.213(1)	1.192(2)	0.0035(5)	0.0040(5)	0.0040(6)	0.0010(3)	0.0007(4)	0.0017(3)	

Table 7.7

Comparison of constrained models with Model I for $Cu_3B_7O_{13}Br$ at room temperature

The number of parameters in Model I is N(=20); the number of parameters in the constrained model is n, less than N by the tabulated N-n. $\mathcal{R}$ is calculated from the tabulated R_ω as $\mathcal{R} = (R_\omega/_{160})^{\frac{1}{2}}$. $\mathcal{R}\alpha$ and α and $\mathcal{S}$ are determined as in Table 5.2. The values for the constrained parameters are given with estimated standard deviations: distances are in Å, and thermal parameters U_{ii}, are in $Å^2$, as defined in Table 7.6.

Constraint	N-n	R_ω	$\mathcal{R}$	α	$\mathcal{R}\alpha$	$\mathcal{S}$	Constrained parameters
1	2	257	1.268	0.001	1.024	16.8	O-O = 2.380(2)
2	1	234	1.211	0.001	1.019	18.3	B-O = 1.466(4)
3	1	245	1.239	0.001	1.019	20.8	B-O = 1.450(4)
4	1	2286	3.783	0.001	1.019	242	$U_{11} = U_{22} = U_{33} = 0.0079(5)$
5	1	177	1.052	0.001	1.019	4.5	$U_{11} = U_{22} = U_{33} = 0.0066(6)$
6	5	183	1.071	0.001	1.036	2.7	$U_{11} = U_{22} = U_{33} = 0.0040(3)$
7	1	163	1.010	0.025	1.009	0.9	$U_{11} = U_{22} = U_{33} = 0.0044(6)$

The significance levels obtained for the inclusion of third- and fourth-cumulant parameters for the Cu, Br and B(2) ions are given in Tables 7.8 and 7.9.

The third cumulant on Cu is significant only at the 0.25 level. The fourth-cumulant tensor on Cu is significant at the 0.005 level, though $S = 1.4$.

The third cumulant on Br is not significant and the fourth cumulant is significant only at the 0.25 level.

The inclusion of the third cumulant on B(2) is significant only at the 0.1 level. The fourth-cumulant tensor on B(2) is significant at the 0.025 level.

The low level of significance of the third and fourth cumulants did not warrant further testing except in the case of the fourth cumulant on Cu, the results of which are given in Table 7.9. There are five fourth-cumulant parameters. The 1122 is the most significant - at the 0.025 level. The 2233 = 3311 parameter is significant at the 0.05 level. The 1222 = -2111 parameter is only significant at the 0.1 level and the 1111 = 2222 parameter at the 0.5 level. The 3333 parameter is not significant ($\alpha > 0.5$).

Table 7.8

Comparison of third- and fourth- cumulant parameters with Model I for $Cu_3B_7O_{13}Br$ at room temperature

The number of parameters in Model I is n(=20); the number of parameters in the cumulant model is N, greater than n by the tabulated (N-n). $\mathcal{R}$ is calculated from the tabulated R_ω as $\mathcal{R} = (160/R_\omega)^{\frac{1}{2}}$: compare Table 7.7. $\mathcal{R}_\alpha$, α and $\mathcal{S}$ are determined as in Table 5.2.

Model Number	is Model I plus	N-n	R_ω	$\mathcal{R}$	α	$\mathcal{R}_\alpha$	$\mathcal{S}$
1	$^3\underline{\underline{K}}$ (Br)	1	160	0.99	+		
2	$^3\underline{\underline{K}}$ (B(2))	4	154	1.016	0.1	1.014	0.7
3	$^3\underline{\underline{K}}$ (Cu)	2	158	1.006	0.25	1.005	0.4
4	$^4\underline{\underline{K}}$ (Br)	2	158	1.006	0.25	1.005	0.4
5	$^4\underline{\underline{K}}$ (B(2))	5	153	1.023	0.025	1.023	0.9
6	$^4\underline{\underline{K}}$ (Cu)	5	1.49	1.034	0.005	1.030	1.4

+ $\mathcal{R} < \mathcal{R}_\alpha$ even for $\alpha = 0.5$

Table 7.9

Individual fourth-cumulant parameters and significance levels for Cu in $Cu_3B_7O_{13}Br$ at room temperature

The fourth cumulants are given as d^{jklm} (in $Å^4$). Standard deviations are given on the last decimal place.

Fourth Cumulants

Ion	jklm	d^{jklm}	α	S
Cu	1111 = 2222	0.001(2)	0.5	0.1
	3333	0.002(5)	+	
	1222 = -2111	-0.006(3)	0.1	0.5
	1122	0.0022(9)	0.025	1.0
	2233 = 3311	0.0017(8)	0.05	0.6

+ $R < R_\alpha$ even for $\alpha = 0.5$

The disorder model suggested for the halogen ion was tested by displacing the Br ion a distance δ from its ($^a/_4$, $^a/_4$, $^a/_4$,) site along [111] to a position (U,U,U), the parameter U then being included as a parameter in the refinement. The displacement δ ($=\sqrt{3}$ (U - $^a/_4$)) refined to a value of -0.03(1) Å and was very highly correlated (0.98) with the isotropic temperature factor for Br which changed from 0.86(1) Å^2 to 1.2(1) Å^2 during the refinement. There was no improvement in fit compared with Model I.

7.4.3 Structure: The crystal structure of copper bromine boracite in its cubic phase at room temperature is basically the same as that found for the cubic phase of all other boracites investigated so far. The final positional and thermal parameters and estimated errors are given in Table 7.6. The bond lengths and inter-ion distances calculated from these positional parameters are given in Table 7.10 and are compared and contrasted in Section 7.10 with equivalent values obtained from other studies.

The O(2)-O(2) distance across the $\bar{4}$ axis has been shown to be significantly longer than the O(2)-O(2) distance along the $\bar{4}$ axis in the BO_4 group (see Figure 7.1(c)). Similarly, the distortion of the BO_4 group from cubic ($\bar{4}3m$) symmetry has been shown to be highly significant. Similar results are found for Cu-Cl, Cr-Cl and Ni-I (Thornley et al, 1976; Nelmes and Thornley, 1974, 1976) although in Co-I neither feature is significant (see Section 7.3.3).

The B(1)-O(2) distance in the BO_4 group is longer than the B(2)-O(2) distance in the OBO_3 group. The O(2) ions are displaced out of the plane defined by O(1), B(1) and Cu by $\xi = 0.213(1)$ Å.

The marked anisotropy of the thermal motion of the Cu, B(2) and O(2) ions has been tested and shown to be highly significant, however that of the O(2) ion is of marginal physical significance. The value of the thermal motion of the Cu along the $\bar{4}$ axis (0.0196(2) $Å^2$) perpendicular to the almost planar O(2) array of the CuO_4 group (see Figure 7.1(c)) is much higher than the value perpendicular to the $\bar{4}$ axis (0.0042(1) $Å^2$). The B(2) thermal parameters correspond to 0.012(1) $Å^2$ along $[111]$ and 0.0044(8) $Å^2$ perpendicular to $[111]$. The thermal motion of B(1) is significantly anisotropic at the 0.025 level.

In general, the inclusion of third- and fourth-cumulant parameters did not give a significantly improved fit, the main exception being the inclusion of the fourth-cumulant tensor for copper which was significant at the 0.005 level.

The suggested disorder of the Br ion over four sites displaced δ from the mean position $(\frac{1}{4}, \frac{1}{4}, \frac{1}{4})$ along $[111]$, $[\bar{1}\bar{1}1]$, $[1\bar{1}\bar{1}]$ and $[\bar{1}1\bar{1}]$ was not found to be significant at any level though the very high correlation with the Br isotropic thermal parameter makes this test unsatisfactory.

Because of the high correlation between the thermal parameter along $\bar{4}$ (U_{33}) and the displacement γ, the possible disorder of the Cu ion could not be tested directly. However, the 3333 fourth-cumulant parameter which describes anharmonicity in the Cu ion's potential along the $\bar{4}$ axis, the direction of the proposed disorder, was not statistically significant (as is found in Co-I - see Section 7.3.3) thus making a non-zero γ rather unlikely.

7.5 Discussion

The crystal structures for Co-I and Cu-Br boracites, in their cubic phases, have been found to be essentially the same as that found for previous boracite studies. The inter-ion distances calculated from the atomic positions obtained in Sections 7.3 and 7.4 are given in Table 7.10 along with the corresponding distances for other cubic boracites - Cu-Cl (Thornley et al, 1976), Mg-Cl (Sueno et al, 1973), Cr-Cl (Nelmes and Thornley, 1974), Ni-I (Nelmes and Thornley, 1976) and Ni-I (Thornley et al, 1976a).

A comparison of the values given in Table 7.10 shows how remarkably little the boron-oxygen framework varies with different metal and halogen ions and with temperature. Within the BO_4 group the B(1)-O(2) distances agree well for the various studies though there is a marked difference in the O(2)-O(2) dimension across the $\bar{4}$ axis, with values ranging from 2.390(2) Å in Co-I to 2.444(4) Å in Mg-Cl. (It must be noted that part of this variation will be attributable to the studies being carried out at differing temperatures.)

Table 7.10

Inter-ion distances for Co-I and Cu-Br compared with some other structural studies of cubic boracites

Where it is known, standard deviations are given on the last quoted place. $O(2)^A$ and $O(2)^B$ are oxygen ions belonging to the O_3^A and O_3^B groups respectively. ε is half the height of the MO_4 group. Oxygen-oxygen distances marked +, and boron-oxygen distances marked ∓ have been compared by constrained refinement and significance testing. Distances are in Å.

			Co-I (291°K) Section 7.8	Cu-Br (291°K) Section 7.9	Cu-Cl (390°K) Thornley et al (1976)	Mg-Cl (673°K) Sueno et al (1973)	Cr-Cl (291°K) Nelmes et al (1974)	Ni-I (293°K) Nelmes et al (1976)	Ni-I (77°K) Thornley et al (1976a)
BO_4	B(1)-O(2)	∓	1.463(1)	1.469(3)	1.469(2)	1.472(3)	1.465(1)	1.465(3)	1.464(1)
	O(2)-O(2) across $\bar{4}$	+	2.390(2)	2.422(4)	2.435(4)	2.444(4)	2.398(2)	2.403(4)	2.397(8)
	O(2)-O(2) along $\bar{4}$	+	2.390(2)	2.387(4)	2.382(4)	2.384(4)	2.390(2)	2.389(4)	2.386(2)
OBO_3	O(1)-O(2)		2.490(2)	2.474(3)	2.488(3)	2.519(5)	2.498(2)	2.482(3)	2.474(2)
	B(2)-O(2)	∓	1.434(3)	1.429(4)	1.431(4)	1.437(3)	1.436(3)	1.433(4)	1.430(2)
	B(2)-O(1)		1.673(3)	1.664(4)	1.686(4)	1.693(5)	1.683(3)	1.672(5)	1.669(1)
	O_3^A O(2)-O(2)	+	2.389(2)	2.385(4)	2.387(4)	2.382(4)	2.389(2)	2.390(4)	2.384(2)
	O_3^B O(2)-O(2)		2.981(2)	2.919(4)	2.945(4)	3.032(4)	2.993(2)	2.940(4)	2.931(2)
MO_4	M-O(2)		2.056(2)	1.991(3)	1.987(3)	2.023(3)	2.055(2)	2.025(3)	2.021(2)
	ε		0.238(1)	0.213(1)	0.221(2)	0.259(2)	0.241(1)	0.220(2)	0.218(1)
	X-O(2)^A		3.459(2)	3.410(3)	3.403(3)	3.417(3)	3.458(2)	3.442(3)	3.435(2)
	X-O(2)^B		3.853(2)	3.765(3)	3.772(3)	3.848(3)	3.858(2)	3.806(3)	3.798(2)
	M-X		3.030(1)	2.989(1)	2.993(1)	3.025(1)	3.033(1)	3.011(1)	3.004(2)
	Cell dimension		12.119(3)	11.955(3)	11.970(4)	12.099(1)	12.132(3)	12.049(3)	12.016(10)

In Co-I the O(2)-O(2) distances are found to be equal (within error) and the BO_4 group is not significantly distorted from cubic symmetry. This is not the case in Cu-Br where the constraints 1 and 2, that all the O(2)-O(2) distances are equal and that the BO_4 group is regular, are strongly rejected. These constraints are also strongly rejected in Cu-Cl (Thornley et al, 1976), Cr-Cl and Ni-I (Nelmes and Thornley, 1974, 1976) showing that at present the results for these constraints in Co-I seem to be unusual.

Although Kriz and Bray (1971) expressed doubts that the OBO_3 configuration in boracites was correct, it can be seen that there is little variation in the dimensions of the OBO_3 group given in Table 7.10 for the various boracites. It must be concluded that the unique OBO_3 configuration is an established feature of the structure of cubic halogen boracites.

The value of ξ and also that of the O(2)-O(2) distance in the O_3^B group decrease as M = Mg→Cr→Co→Cu, Ni.

An interesting feature in the cubic boracites Cr-Cl, Cu-Cl, Cu-Br, Co-I and Ni-I is that the justification for considering the thermal motion of the B(2) as being anisotropic, i.e. the value of S, increases as X = I→Br→Cl. A comparison of the thermal anisotropy of the B(2) ion in the cubic boracites studied to date is given in Table 7.11. It can be seen that the anisotropy of the thermal motion of the B(2) ion gets larger as X = I→Br→Cl, and that it is larger in Cu-Cl than in Cr-Cl.

Table 7.11

Anisotropy of B(2) thermal motion in cubic boracites

Boracite	Mean Square Amplitude of Thermal Motion ($Å^2$)		Ratio $\frac{\text{Along Triad}}{\text{Perpendicular to Triad}}$	S
	Along Triad	Perpendicular to Triad		
Mg-Cl (673°K) Sueno et al (1973)	0.029(3)	0.007 (2)	4 (1)	
Cr-Cl (293°K) Nelmes and Thornley (1974)	0.021(1)	0.003 (1)	7 (2)	14
Cu-Cl (390°K) Thornley et al (1976)	0.020(1)	0.002 (1)	10 (5)	15
Cu-Br (291°K) Present Work	0.012(1)	0.0044(8)	3.0(5)	4.5
Co-I (291°K) Present Work	0.013(1)	0.007 (1)	1.8(3)	2.2
Ni-I (291°K) Nelmes and Thornley (1976)	0.011(2)	0.005 (1)	2.2(6)	0.7

Raman scattering and X-ray diffuse scattering find increasing anharmonic effects as X = I→Br→Cl. From previous boracite structural studies it would seem that the third cumulant of the halogen may be taken as an index of the anharmonicity. The third-cumulant parameter for the halogen is more significant in Cu-Cl than in Cr-Cl and is very small in Ni-I. Thornley et al (1976) also find that the thermal motion of the Cl ion in orthorhombic Cu-Cl at T_c-70°K (room temperature) is harmonic, in agreement with the range for disappearance of the Raman wing and the X-ray diffuse sharp streaks in Cu-Cl (Lockwood et al, 1977; Felix, 1973). However, the third cumulant for the Br ion in Cu-Br is not at all significant while the third cumulant for the I ion in Co-I is significant at the 0.1 level - the same as for the Cl ion in Cr-Cl. It may be, therefore, that the halogen anharmonicity is not simply correlated to X and that the B(2) ion in its unique OBO_3 environment is a more sensitive probe of the anharmonicity of the system.

The introduction of higher cumulants to describe the thermal motion, particularly of the halogen ion, allowed a fuller investigation of the possibility that the halogen ions were disordered over four sites (Schmid, 1970). The 123 third cumulant for both the bromine and iodine ions in Cu-Br and Co-I was not significant, indicating that any distortion from an isotropic harmonic potential is small. In testing the disordered model directly by displacing the halogen an amount δ along the triad and regarding δ as a variable parameter in the least-squares refinement, it was found that δ is non-significant and of magnitude $\delta = -0.03(1)$Å in Cu-Br and of magnitude

δ = 0.12(1)Å in Co-I. In both cases δ was strongly correlated to the temperature factor B(X). It must be concluded from these results and the results of the previous boracite studies of Cr-Cl, Ni-I and Cu-Cl (Nelmes and Thornley, 1974, 1976; Thornley et al, 1976) that there is no evidence for the gross disorder previously suggested for the halogen. This does not mean that there is no disorder, only that if the halogen is disordered then δ is less than the r.m.s. thermal amplitude of the halogen. In fact, in orthorhombic Cu-Cl (at T_c-70°K), Thornley et al (1976) found that the thermal motion of the Cl ion was no longer anharmonic indicating that the Cl ion may be ordered (in this sense) in the orthorhombic phase.

The suggestion that the metal ion is disordered in cubic boracites, with two minima along the $\bar{4}$ axis, was first made by Ascher (1970). The inclusion of fourth cumulants for the metal is significant at the 0.005 level for both copper and cobalt. Though the 3333 fourth cumulant in both cases has a small value and low significance, it does indicate a slight sharpening of the potential along the $\bar{4}$ axis. This is the opposite effect to that expected with two minima along the tetrad. Further evidence against the disorder of the metal ion is found in the structural study of orthorhombic Cu-Cl (Thornley et al, 1976). They find that the thermal motion of the Cu ion retains the anharmonicity found in the cubic phase.

Therefore, in summary, it can be stated that there is no evidence of any kind of disorder of the metal ions and no evidence of any gross disorder of the halogen ions in the cubic phase of boracites.

This does not necessarily mean that there is no disorder, particularly in the case of the halogen where δ may be less than the r.m.s. thermal amplitude, only that it is not necessary to use a disordered model to explain the experimental results.

Appendix A

An isotropic extinction parameter was used in the refinement of data for the single-crystal experiments. The form of the extinction factor was that used by Cooper, Rouse and Willis (1968), based on the theory of Zachariasen (1967) for secondary extinction, i.e. for each reflection

$$F_c = y^{\frac{1}{2}} F_k$$

with $$y = (1 + x^{*2})^{\frac{1}{2}} - X^*$$

and $$X^* = \frac{cF_o^2}{\sin 2\theta}$$

where F_k is the calculated kinematic structure factor, F_c the 'extinguished' structure factor, θ the Bragg angle and c the extinction parameter to be determined. Path-length variation is neglected.

Appendix B

The expansion of the probability density function (P.D.F.) describing the time-averaged vibrational displacement of each atom in terms of higher cumulant tensors allows contributions from anharmonic thermal motion to be considered (Johnson, 1969, 1970). The usual crystallographic structure-factor equation has 3 positional parameters (first-cumulant tensor) and six anisotropic thermal parameters (second-cumulant tensor). The third and fourth cumulants describe anharmonic contributions to the P.D.F. for thermal motion which are respectively antisymmetric and symmetric about the mean position $\underline{X}_r$.

The modified structure factor expression may be written as

$$F(\underline{H}) = \sum_r f_r \quad \exp\,(i a_r(\underline{H}) \quad \exp\,(\beta_r(\underline{H}))$$

where the r^{th} atom at $\underline{X}_r$ $(= X_r^1, X_r^2, X_r^3)$ has scattering factor f_r and

$$a_r(\underline{H}) = 2\pi X_r^j \quad H_j - C_r^{jkl} \quad H_j H_k H_l$$

$$\beta_r(\underline{H}) = -2\pi^2 \quad b_r^{jk} \quad H_j \quad H_k + d_r^{jklm} \quad H_j H_k H_l H_m$$

$$j, k, l, m = 1, 2, 3$$

The Hj are components of the reciprocal lattice vector $\underline{H}$ and the b_r^{jk} coefficients describe the harmonic thermal motion of the r^{th} atom.

In general there are ten independent third-cumulant coefficients and fifteen independent fourth-cumulant coefficients for each ion but the site symmetry at $\underline{X}_r$ reduces the number of independent parameters.

Appendix C

The observed structure amplitudes and errors, and the calculated structure factors for $Cs(D_xH_{1-x})_2AsO_4$ at room temperature.

H	K	L	Y(OBS)	Y(CALC)	SIG(O)	H	K	L	Y(OBS)	Y(CALC)	SIG(O)
8.	7.	1.	2.20	2.22	0.12	9.	4.	3.	1.44	1.39	0.22
1.	8.	1.	3.08	3.00	0.06	6.	5.	3.	1.50	1.50	0.15
3.	8.	1.	3.25	3.28	0.09	8.	5.	3.	1.33	1.38	0.09
5.	8.	1.	1.62	1.56	0.19	10.	5.	3.	1.13	1.10	0.27
0.	9.	1.	0.85	0.59	0.22	7.	6.	3.	4.45	4.54	0.08
2.	9.	1.	3.53	3.54	0.13	9.	6.	3.	1.90	1.98	0.14
4.	9.	1.	2.29	2.24	0.18	8.	7.	3.	2.65	2.76	0.19
6.	9.	1.	2.71	2.74	0.04	2.	0.	4.	6.99	7.43	0.22
1.	10.	1.	2.81	2.64	0.14	6.	0.	4.	6.78	6.75	0.13
3.	10.	1.	2.34	2.19	0.30	8.	0.	4.	2.36	2.32	0.04
5.	10.	1.	1.07	1.02	0.17	10.	0.	4.	3.94	4.03	0.08
0.	11.	1.	2.20	2.30	0.15	3.	1.	4.	2.35	2.22	0.08
2.	11.	1.	0.81	0.70	0.42	5.	1.	4.	5.66	5.68	0.09
2.	0.	2.	3.81	3.91	0.12	7.	1.	4.	3.01	3.15	0.06
4.	0.	2.	4.06	3.81	0.08	9.	1.	4.	5.15	5.04	0.10
6.	0.	2.	9.75	9.53	0.30	2.	2.	4.	7.26	7.55	0.14
8.	0.	2.	3.49	3.60	0.06	4.	2.	4.	6.52	6.54	0.15
10.	0.	2.	6.82	6.59	0.13	6.	2.	4.	3.63	3.59	0.11
5.	1.	2.	7.28	7.29	0.23	8.	2.	4.	4.21	4.22	0.10
7.	1.	2.	6.48	6.43	0.11	10.	2.	4.	4.68	4.70	0.05
9.	1.	2.	4.22	4.25	0.07	5.	3.	4.	5.15	5.23	0.10
11.	1.	2.	3.46	3.41	0.05	7.	3.	4.	1.87	1.87	0.23
4.	2.	2.	2.51	2.39	0.05	9.	3.	4.	3.84	3.78	0.09
6.	2.	2.	0.90	0.63	0.11	4.	4.	4.	2.05	1.61	0.12
8.	2.	2.	0.91	0.76	0.31	6.	4.	4.	3.09	3.03	0.06
10.	2.	2.	0.92	0.70	0.16	8.	4.	4.	4.40	4.32	0.14
3.	3.	2.	8.17	8.02	0.16	10.	4.	4.	3.77	3.84	0.18
5.	3.	2.	7.21	7.17	0.18	7.	5.	4.	3.31	3.32	0.06
7.	3.	2.	5.15	5.16	0.07	9.	5.	4.	1.65	1.54	0.09
9.	3.	2.	4.15	4.07	0.09	6.	6.	4.	8.83	8.80	0.09
11.	3.	2.	3.32	3.33	0.05	8.	6.	4.	5.08	5.16	0.10
6.	4.	2.	6.56	6.61	0.09	1.	0.	5.	4.41	4.63	0.09
8.	4.	2.	1.21	1.21	0.14	3.	0.	5.	6.85	7.11	0.13
10.	4.	2.	3.87	3.89	0.08	5.	0.	5.	2.16	1.92	0.14
5.	5.	2.	6.00	6.11	0.12	7.	0.	5.	4.68	4.69	0.09
7.	5.	2.	5.42	5.40	0.08	9.	0.	5.	0.80	0.75	0.19
9.	5.	2.	5.69	5.70	0.08	2.	1.	5.	3.77	3.90	0.15
8.	6.	2.	2.09	2.10	0.12	4.	1.	5.	2.88	2.68	0.18
7.	7.	2.	4.10	4.13	0.08	6.	1.	5.	3.56	3.50	0.07
9.	7.	2.	3.81	3.91	0.10	8.	1.	5.	3.11	3.06	0.06
1.	0.	3.	4.36	4.90	0.14	10.	1.	5.	1.03	0.74	0.44
3.	0.	3.	7.20	7.18	0.25	3.	2.	5.	4.83	4.92	0.10
5.	0.	3.	1.82	1.72	0.12	0.	4.	6.	3.07	2.84	0.06
7.	0.	3.	5.22	5.19	0.08	2.	4.	6.	1.79	1.69	0.07
9.	0.	3.	2.65	2.58	0.07	6.	4.	6.	4.69	4.75	0.07
11.	0.	3.	3.23	3.24	0.05	8.	4.	6.	1.17	1.02	0.22
2.	1.	3.	5.52	5.52	0.12	1.	5.	6.	5.07	5.01	0.09
4.	1.	3.	3.45	3.52	0.08	3.	5.	6.	5.38	5.32	0.12
6.	1.	3.	5.71	5.62	0.11	5.	5.	6.	6.20	6.31	0.12
8.	1.	3.	2.36	2.37	0.07	7.	5.	6.	4.52	4.64	0.09
10.	1.	3.	2.00	1.91	0.23	0.	6.	6.	7.18	7.20	0.15
3.	2.	3.	5.47	5.35	0.11	2.	6.	6.	0.93	0.87	0.44
5.	2.	3.	2.14	2.09	0.05	1.	7.	6.	4.74	4.74	0.10
7.	2.	3.	3.18	3.15	0.05	3.	7.	6.	4.66	4.58	0.06
9.	2.	3.	3.40	3.44	0.08	0.	8.	6.	2.96	2.74	0.10
11.	2.	3.	0.83	0.89	0.52	2.	8.	6.	1.45	1.27	0.38
4.	3.	3.	3.63	3.71	0.07	1.	9.	6.	3.86	3.83	0.10
6.	3.	3.	5.26	5.32	0.08	3.	9.	6.	3.91	3.95	0.21
8.	3.	3.	3.05	3.03	0.13	1.	0.	7.	3.53	3.58	0.09
10.	3.	3.	3.37	3.40	0.09	3.	0.	7.	3.82	4.02	0.08
5.	4.	3.	0.80	0.78	0.35	5.	0.	7.	0.71	0.35	0.21
7.	4.	3.	3.55	3.53	0.04	7.	0.	7.	4.28	4.17	0.10

H	K	L	Y(OBS)	Y(CALC)	SIG(O)	H	K	L	Y(OBS)	Y(CALC)	SIG(O)
9.	0.	7.	1.21	1.36	0.46	4.	2.	0.	6.83	6.81	0.26
2.	1.	7.	4.18	4.21	0.10	6.	2.	0.	8.11	8.14	0.15
4.	1.	7.	1.88	1.89	0.17	8.	2.	0.	5.28	5.33	0.05
6.	1.	7.	3.75	3.71	0.15	10.	2.	0.	2.29	2.29	0.13
8.	1.	7.	1.45	1.50	0.31	5.	3.	0.	6.00	6.12	0.11
3.	2.	7.	3.37	3.17	0.12	7.	3.	0.	2.24	2.20	0.04
5.	2.	7.	0.99	0.88	0.36	9.	3.	0.	4.26	4.27	0.04
7.	2.	7.	1.95	1.70	0.17	11.	3.	0.	1.54	1.45	0.16
4.	3.	7.	2.74	2.83	0.13	6.	4.	0.	7.73	7.89	0.18
6.	3.	7.	4.41	4.36	0.07	8.	4.	0.	4.38	4.50	0.08
8.	3.	7.	2.18	2.19	0.13	10.	4.	0.	2.70	2.71	0.08
7.	4.	7.	1.89	2.01	0.11	7.	5.	0.	4.02	4.01	0.11
6.	5.	7.	1.81	1.80	0.31	9.	5.	0.	1.65	1.65	0.10
2.	0.	8.	4.99	4.89	0.09	6.	6.	0.	1.47	1.20	0.36
4.	0.	8.	1.21	0.96	0.17	8.	6.	0.	2.32	2.07	0.22
6.	0.	8.	3.23	3.35	0.06	10.	6.	0.	6.94	6.84	0.07
8.	0.	8.	4.70	4.64	0.15	9.	7.	0.	1.83	1.95	0.15
3.	1.	8.	1.38	1.18	0.15	8.	8.	0.	2.05	2.08	0.07
5.	1.	8.	3.58	3.54	0.08	3.	0.	1.	7.36	7.19	0.34
7.	1.	8.	1.86	1.72	0.10	5.	0.	1.	1.02	0.96	0.11
2.	2.	8.	4.51	4.62	0.09	7.	0.	1.	6.99	6.83	0.19
4.	2.	8.	4.48	4.61	0.19	2.	1.	1.	5.53	5.38	0.17
6.	2.	8.	5.08	5.09	0.05	4.	1.	1.	3.01	2.98	0.07
8.	2.	8.	3.40	3.38	0.09	6.	1.	1.	4.41	4.44	0.09
5.	3.	8.	3.23	3.13	0.07	3.	2.	1.	5.78	5.73	0.06
7.	3.	8.	1.22	1.16	0.15	5.	2.	1.	2.60	2.68	0.07
4.	4.	8.	6.89	6.62	0.14	7.	2.	1.	4.77	4.70	0.08
6.	4.	8.	5.12	4.97	0.10	4.	3.	1.	4.93	4.77	0.10
1.	0.	9.	2.83	2.99	0.09	6.	3.	1.	6.30	6.38	0.08
3.	0.	9.	3.92	3.83	0.09	5.	4.	1.	1.20	0.96	0.21
5.	0.	9.	0.92	0.72	0.26	7.	4.	1.	2.73	2.66	0.24
7.	0.	9.	3.24	3.24	0.07	6.	5.	1.	2.20	2.31	0.15
2.	1.	9.	2.12	1.88	0.12	7.	6.	1.	4.05	4.11	0.14
4.	1.	9.	0.97	1.01	0.92	9.	4.	7.	1.58	1.72	0.13
6.	1.	9.	1.72	1.29	0.13	4.	5.	7.	0.97	0.74	0.31
3.	2.	9.	2.85	2.66	0.42	9.	2.	5.	2.93	2.96	0.06
5.	2.	9.	1.75	1.71	0.14	7.	2.	5.	4.12	4.13	0.06
7.	2.	9.	2.57	2.75	0.10	5.	2.	5.	2.68	2.47	0.25
4.	3.	9.	1.79	2.04	0.14	10.	3.	5.	2.48	2.48	0.09
6.	3.	9.	2.61	2.50	0.16	8.	3.	5.	2.53	2.40	0.10
5.	4.	9.	0.74	0.60	0.29	6.	3.	5.	3.95	4.01	0.11
2.	0.	10.	1.63	1.25	0.37	4.	3.	5.	2.98	3.00	0.12
4.	0.	10.	1.65	1.51	0.36	9.	4.	5.	1.36	1.50	0.27
1.	1.	10.	4.84	5.09	0.10	7.	4.	5.	2.76	2.78	0.06
3.	1.	10.	4.09	3.91	0.08	5.	4.	5.	0.96	0.90	0.15
5.	1.	10.	4.13	4.03	0.07	6.	5.	5.	1.84	1.75	0.21
4.	2.	10.	0.97	0.82	0.29	7.	6.	5.	4.26	4.37	0.08
3.	3.	10.	4.68	4.67	0.09	2.	0.	6.	2.63	2.74	0.06
5.	3.	10.	3.58	3.65	0.07	3.	1.	6.	7.91	8.01	0.19
1.	0.	11.	1.60	1.31	0.60	1.	1.	6.	7.73	8.57	0.24
3.	0.	11.	2.00	1.85	0.17	3.	3.	6.	5.50	5.37	0.11
2.	1.	11.	2.07	2.01	0.36	12.	0.	0.	3.96	3.87	0.08
4.	0.	0.	4.05	3.95	0.11	12.	2.	0.	2.43	2.54	0.08
6.	0.	0.	5.10	5.03	0.15	5.	11.	0.	0.44	0.36	0.37
8.	0.	0.	7.73	7.58	0.15	12.	1.	1.	2.13	2.39	0.22
10.	0.	0.	3.43	3.42	0.04	11.	4.	1.	1.38	1.47	0.13
3.	1.	0.	2.78	2.71	0.11	12.	0.	2.	1.41	1.71	0.48
5.	1.	0.	6.53	6.50	0.22	11.	4.	3.	0.78	0.69	0.58
7.	1.	0.	3.84	3.83	0.09	11.	1.	4.	1.27	1.34	0.40
9.	1.	0.	5.74	5.70	0.10	11.	3.	4.	1.26	1.29	0.17
11.	1.	0.	1.64	1.56	0.35	11.	0.	5.	2.84	2.92	0.14
2.	2.	0.	6.57	6.49	0.13	9.	6.	5.	1.45	1.89	0.25

H	K	L	Y(OBS)	Y(CALC)	SIG(O)
8.	7.	5.	1.03	1.32	0.46
10.	0.	6.	4.89	4.90	0.11
10.	2.	6.	1.47	1.45	0.61
9.	5.	6.	3.32	3.61	0.10
8.	6.	6.	0.85	1.44	0.43
7.	7.	6.	2.82	2.99	0.20
9.	2.	7.	2.59	2.30	0.24
7.	6.	7.	1.95	2.15	0.23
5.	8.	7.	0.81	1.17	0.71
9.	1.	8.	3.07	3.40	0.36
8.	4.	8.	1.95	2.79	0.92
7.	5.	8.	1.51	1.88	0.92
8.	1.	9.	1.80	1.76	0.51
7.	4.	9.	1.16	0.97	0.43
6.	5.	9.	1.16	1.03	0.92
2.	3.	11.	0.91	1.43	0.85
1.	4.	11.	1.17	1.03	0.69

Appendix D

The observed structure amplitudes and errors and the calculated structure factors for $Cs(D_xH_{1-x})_2AsO_4$ at T_c+5^oK (213^oK).

H	K	L	Y(OBS)	Y(CALC)	SIG(I)
5.	1.	0.	6.47	6.56	0.13
7.	1.	0.	4.20	3.95	0.14
9.	1.	0.	6.49	6.54	0.21
11.	1.	0.	2.31	1.98	0.45
2.	1.	1.	5.40	5.25	0.16
4.	1.	1.	2.96	2.98	0.06
6.	1.	1.	4.66	4.69	0.13
8.	1.	1.	3.30	3.24	0.13
10.	1.	1.	3.28	3.25	0.09
3.	1.	2.	8.86	8.73	0.18
5.	1.	2.	7.17	7.37	0.14
7.	1.	2.	6.79	6.82	0.29
1.	0.	11.	2.15	2.03	0.61
4.	0.	4.	13.47	13.12	0.26
2.	0.	10.	1.61	1.67	0.34
4.	0.	10.	2.20	2.00	0.24
1.	0.	9.	3.34	3.60	0.41
3.	0.	9.	4.62	4.76	0.17
5.	0.	9.	0.93	0.98	0.56
0.	0.	8.	13.76	13.97	0.26
2.	0.	8.	5.28	5.15	0.48
4.	0.	8.	1.71	1.41	0.51
6.	0.	8.	3.65	3.71	0.49
1.	0.	7.	3.99	3.86	0.11
3.	0.	7.	4.62	4.90	0.23
5.	0.	7.	1.05	0.65	0.20
7.	0.	7.	4.95	5.50	0.17
2.	0.	6.	3.37	2.96	0.54
4.	0.	6.	3.24	3.09	0.07
6.	0.	6.	7.75	8.20	0.16
8.	0.	6.	5.32	5.31	0.08
1.	0.	5.	4.73	4.87	0.13
3.	0.	5.	7.27	7.17	0.13
5.	0.	5.	2.29	1.90	0.21
7.	0.	5.	4.97	5.14	0.16
9.	0.	5.	0.74	1.14	0.25
0.	0.	4.	8.20	8.46	0.16
2.	0.	4.	7.39	7.26	0.41
6.	0.	4.	6.94	7.16	0.13
8.	0.	4.	2.93	2.55	0.34
10.	0.	4.	4.78	4.73	0.11
1.	0.	3.	4.92	4.76	0.95
3.	0.	3.	7.15	7.39	0.14
5.	0.	3.	2.11	1.79	0.82
7.	0.	3.	5.78	5.86	0.17
9.	0.	3.	2.97	2.78	0.41
2.	0.	2.	3.69	3.84	0.11
4.	0.	2.	4.01	3.77	0.11
6.	0.	2.	9.97	9.95	0.20
8.	0.	2.	3.85	3.97	0.11
10.	0.	2.	8.03	7.94	0.16
3.	0.	1.	6.82	7.15	0.13
5.	0.	1.	1.17	0.95	0.24
7.	0.	1.	7.20	7.17	0.14
9.	0.	1.	1.48	0.82	0.31
11.	0.	1.	2.93	2.91	0.07
2.	0.	0.	6.47	6.54	0.12
4.	0.	0.	4.07	3.92	0.11
6.	0.	0.	4.95	5.21	0.14
8.	0.	0.	8.04	8.26	0.16
10.	0.	0.	4.20	4.14	0.11
2.	1.	11.	2.82	2.83	0.10

H	K	L	Y(OBS)	Y(CALC)	SIG(I)
1.	1.	10.	5.75	6.16	0.17
3.	1.	10.	4.79	4.79	0.14
5.	1.	10.	4.82	4.76	0.13
2.	1.	9.	2.62	2.45	0.20
4.	1.	9.	2.08	1.53	0.24
6.	1.	9.	2.42	2.14	0.13
3.	1.	8.	1.39	1.44	0.49
5.	1.	8.	4.33	4.25	0.31
7.	1.	8.	2.22	2.17	0.17
2.	1.	7.	4.61	4.59	0.21
4.	1.	7.	2.31	2.10	0.34
6.	1.	7.	4.25	4.22	0.11
8.	1.	7.	1.67	1.72	0.52
1.	1.	6.	8.84	8.67	0.13
3.	1.	6.	8.41	8.31	0.11
5.	1.	6.	5.47	5.47	0.14
7.	1.	6.	5.43	5.49	0.14
9.	1.	6.	4.54	4.59	0.23
2.	1.	5.	4.02	4.15	0.11
4.	1.	5.	3.14	2.94	0.08
6.	1.	5.	3.98	4.12	0.20
8.	1.	5.	3.87	3.39	0.20
3.	1.	4.	2.29	2.29	0.17
5.	1.	4.	5.87	5.96	0.23
7.	1.	4.	3.38	3.43	0.11
9.	1.	4.	6.13	5.97	0.15
2.	1.	3.	5.53	5.42	0.10
4.	1.	3.	3.42	3.46	0.07
6.	1.	3.	5.59	5.79	0.16
8.	1.	3.	2.38	2.62	0.54
10.	1.	3.	2.25	2.37	0.08
9.	1.	2.	4.71	4.85	0.17
11.	1.	2.	5.69	4.17	0.17
3.	1.	0.	3.10	2.62	0.16
10.	1.	5.	1.14	1.24	0.25
4.	2.	10.	1.28	1.15	0.25
6.	2.	0.	8.79	8.54	0.17
3.	2.	9.	3.31	3.32	0.03
5.	2.	9.	1.76	2.05	0.16
2.	2.	8.	5.14	4.76	0.51
4.	2.	8.	4.96	5.03	0.11
6.	2.	8.	5.84	6.01	0.16
3.	2.	7.	3.82	3.76	0.07
5.	2.	7.	2.03	1.86	0.63
7.	2.	7.	2.59	2.24	0.38
4.	2.	6.	2.26	1.86	0.38
6.	2.	6.	0.53	0.55	0.49
8.	2.	6.	0.91	1.40	0.25
3.	2.	5.	5.35	5.14	0.20
5.	2.	5.	2.77	2.58	0.08
7.	2.	5.	4.85	4.61	0.16
9.	2.	5.	3.77	3.72	0.31
2.	2.	4.	7.68	7.58	0.10
4.	2.	4.	6.62	6.66	0.12
6.	2.	4.	3.91	3.59	0.51
8.	2.	4.	4.58	4.65	0.11
10.	2.	4.	5.92	5.88	0.17
5.	2.	3.	5.43	5.49	0.30
7.	2.	3.	3.55	3.65	0.20
9.	2.	3.	4.11	4.08	0.14
4.	2.	2.	2.41	2.35	0.10
10.	2.	2.	0.62	0.64	0.52
3.	2.	1.	5.47	5.73	0.15

H	K	L	Y(OBS)	Y(CALC)	SIG(Y)
5.	2.	1.	2.59	2.68	0.07
7.	2.	1.	4.98	5.07	0.14
9.	2.	1.	3.96	4.13	0.25
11.	2.	1.	1.84	1.83	0.31
2.	2.	0.	6.51	6.24	0.12
4.	2.	0.	6.92	6.78	0.14
8.	2.	0.	6.04	5.97	0.12
10.	2.	0.	2.48	2.52	0.13
3.	3.	10.	5.60	5.30	0.23
6.	3.	1.	6.79	6.71	0.20
4.	3.	9.	2.34	2.52	0.21
6.	3.	9.	3.30	3.27	0.14
5.	3.	8.	3.62	3.91	0.17
7.	3.	8.	1.58	1.77	0.36
4.	3.	7.	3.74	3.28	0.17
6.	3.	7.	5.82	5.86	0.13
8.	3.	7.	2.36	2.89	0.20
3.	3.	6.	5.92	5.38	0.21
5.	3.	6.	6.17	6.10	0.18
7.	3.	6.	5.12	4.89	0.21
9.	3.	6.	4.66	4.68	0.20
4.	3.	5.	3.59	3.40	0.14
6.	3.	5.	4.79	4.86	0.20
8.	3.	5.	2.72	3.35	0.21
5.	3.	4.	5.63	5.58	0.23
9.	3.	4.	4.55	4.54	0.20
6.	3.	3.	5.62	5.72	0.28
8.	3.	3.	3.91	3.62	0.17
10.	3.	3.	4.06	4.23	0.23
7.	3.	2.	5.42	5.78	0.21
9.	3.	2.	4.66	4.89	0.20
8.	3.	1.	4.36	3.87	0.20
10.	3.	1.	3.25	2.80	0.34
5.	3.	0.	5.14	6.24	0.18
7.	3.	0.	2.32	2.68	0.14
9.	3.	0.	5.05	4.96	0.21
4.	3.	1.	4.67	4.90	0.20
3.	3.	2.	7.94	7.96	0.24

Appendix E

The observed structure amplitudes and the calculated structure factors for $Cs(D_xH_{1-x})_2AsO_4$ at 77^oK.

H	K	L	Y(OBS)	Y(CALC)
4.	0.	0.	86.62	84.38
8.	0.	0.	155.66	160.42
12.	0.	0.	46.48	49.89
6.	2.	0.	72.17	71.16
8.	2.	0.	65.09	63.27
10.	2.	0.	117.85	117.11
14.	2.	0.	53.33	49.11
16.	2.	0.	42.34	43.26
2.	4.	0.	39.04	32.36
12.	4.	0.	59.07	57.76
4.	6.	0.	70.38	73.22
10.	6.	0.	70.15	74.90
12.	6.	0.	82.46	78.36
2.	8.	0.	89.79	88.70
4.	8.	0.	115.41	110.29
10.	8.	0.	89.82	92.49
2.	10.	0.	111.16	109.65
4.	10.	0.	62.08	57.09
6.	10.	0.	89.85	91.54
8.	10.	0.	105.42	103.56
2.	12.	0.	63.55	63.24
6.	12.	0.	72.56	65.18
3.	1.	1.	61.23	66.33
5.	1.	1.	65.66	70.30
7.	1.	1.	48.32	44.70
9.	1.	1.	31.54	27.38
15.	1.	1.	46.74	54.16
1.	3.	1.	65.70	56.72
15.	3.	1.	54.27	54.80
11.	5.	1.	53.92	51.53
1.	7.	1.	71.37	65.89
11.	7.	1.	64.50	65.71
13.	7.	1.	45.89	45.63
3.	9.	1.	73.66	77.41
7.	9.	1.	48.88	43.93
5.	11.	1.	55.51	62.19
7.	11.	1.	54.01	60.69
1.	13.	1.	75.10	63.14
7.	13.	1.	58.55	55.93
10.	0.	2.	106.41	100.16
6.	0.	2.	98.39	99.77
14.	0.	2.	75.43	79.33
16.	2.	2.	86.86	80.69
2.	4.	2.	127.06	119.90
2.	6.	2.	37.04	33.37
4.	6.	2.	88.92	92.79
12.	6.	2.	86.52	80.90
14.	6.	2.	85.24	87.98
2.	8.	2.	92.62	96.90
6.	8.	2.	98.20	93.35
2.	10.	2.	106.37	111.96
4.	10.	2.	72.37	77.97
8.	10.	2.	76.34	74.27
12.	10.	2.	73.29	74.55
2.	12.	2.	79.72	86.43
6.	12.	2.	84.96	80.42
10.	12.	2.	75.52	78.93
4.	14.	2.	103.53	109.97
3.	1.	3.	63.16	60.86
7.	1.	3.	50.51	45.43
11.	1.	3.	20.98	20.86
13.	7.	3.	69.77	67.22
5.	9.	3.	54.24	52.32
7.	11.	3.	60.89	59.13
12.	2.	0.	48.10	46.36
2.	2.	0.	76.64	76.12
8.	4.	0.	123.94	120.87
6.	4.	0.	90.31	93.00
0.	14.	0.	66.20	68.06
4.	12.	0.	72.21	72.68
0.	8.	0.	142.58	139.41
8.	8.	0.	109.37	115.06
2.	6.	0.	102.46	96.36
6.	6.	0.	62.15	69.61
8.	6.	0.	69.83	61.40
0.	4.	0.	57.54	60.82
7.	7.	1.	94.59	87.77
9.	7.	1.	53.10	51.74
3.	3.	1.	92.02	96.86
5.	3.	1.	49.85	45.56
9.	3.	1.	89.69	88.24
1.	1.	1.	66.83	63.43
0.	14.	2.	80.44	76.84
0.	10.	2.	99.31	98.53
10.	10.	2.	135.79	139.69
8.	8.	2.	53.61	50.21
10.	8.	2.	77.61	79.98
0.	6.	2.	83.76	83.06
6.	6.	2.	144.33	149.39
6.	4.	2.	87.02	85.67
10.	4.	2.	73.25	81.31
4.	2.	2.	115.74	116.58
1.	13.	3.	91.83	88.95
5.	13.	3.	59.57	62.56
1.	7.	3.	47.59	55.97
5.	7.	3.	81.36	80.01
9.	7.	3.	49.35	42.90
7.	5.	3.	76.53	68.92
11.	5.	3.	51.70	52.21
3.	3.	3.	90.46	98.25
5.	3.	3.	56.33	56.79
11.	3.	3.	51.53	55.93
15.	3.	3.	58.17	53.74
18.	2.	0.	98.61	100.52
16.	4.	0.	161.93	171.30
18.	4.	0.	48.33	45.26
14.	10.	0.	62.35	61.11
10.	14.	0.	66.68	67.32
17.	1.	1.	52.23	52.27
17.	3.	1.	60.42	57.99
15.	9.	1.	74.29	70.17
11.	13.	1.	59.67	56.85
1.	17.	1.	57.69	56.67
18.	0.	2.	113.60	117.84
16.	6.	2.	74.32	75.26
2.	16.	2.	99.60	97.39
0.	16.	2.	72.59	69.25
15.	9.	3.	71.11	71.82
8.	14.	2.	98.94	94.12
0.	16.	0.	76.21	76.63

Appendix F

The observed structure amplitudes and errors and the calculated structure factors for $Co_3B_7O_{13}I$ at room temperature.

H	K	L	Y(OBS)	Y(CALC)	SIG(O)	H	K	L	Y(OBS)	Y(CALC)	SIG(O)
0.	2.	2.	113.48	117.51	4.74	0.	18.	6.	89.64	88.21	3.60
0.	2.	8.	340.01	330.84	10.27	0.	18.	12.	125.18	126.78	4.09
0.	4.	8.	455.55	451.32	16.19	0.	20.	0.	169.84	169.95	2.59
0.	6.	2.	167.89	160.89	7.30	0.	22.	4.	92.40	91.83	3.69
0.	6.	8.	216.69	211.05	5.53	0.	24.	0.	112.18	110.07	2.89
0.	8.	8.	387.36	388.37	13.52	1.	3.	13.	25.97	24.56	7.72
0.	10.	4.	251.02	243.10	5.84	1.	3.	19.	43.28	41.77	3.92
1.	3.	9.	78.30	75.21	1.86	1.	5.	15.	17.32	14.63	2.31
1.	5.	3.	195.13	186.57	9.59	1.	5.	21.	28.14	26.73	3.49
1.	5.	9.	57.07	57.15	1.25	1.	7.	15.	42.13	42.53	7.98
1.	7.	5.	77.51	75.10	1.90	1.	7.	21.	22.42	19.89	6.10
1.	9.	7.	52.38	54.35	1.56	1.	9.	15.	26.17	26.39	3.55
2.	2.	6.	201.24	193.39	8.03	1.	9.	21.	26.30	28.50	5.58
2.	4.	6.	176.84	177.11	7.56	1.	11.	5.	57.31	59.08	4.56
2.	6.	6.	99.91	101.94	7.71	1.	11.	17.	30.22	27.55	1.42
2.	8.	2.	53.13	53.94	2.09	1.	13.	7.	38.20	38.18	3.35
2.	8.	8.	213.32	222.57	15.84	1.	13.	19.	18.23	13.93	9.58
2.	10.	4.	102.05	101.99	2.38	1.	15.	11.	16.61	12.92	4.11
3.	1.	11.	30.30	28.70	1.39	1.	15.	17.	28.41	28.14	4.36
3.	5.	7.	46.05	44.16	2.12	1.	17.	5.	42.30	40.50	2.71
4.	2.	4.	242.92	255.26	25.49	1.	19.	11.	30.15	30.15	4.90
4.	4.	10.	263.76	267.60	6.59	1.	21.	3.	23.93	27.10	8.98
4.	6.	4.	296.69	317.06	18.57	1.	23.	3.	10.61	2.95	5.97
4.	8.	6.	201.83	208.96	4.64	2.	0.	22.	81.11	80.04	2.31
5.	9.	3.	40.31	39.40	1.77	2.	2.	12.	93.23	90.75	4.52
6.	2.	8.	151.36	156.36	4.32	2.	2.	18.	35.60	38.36	1.69
6.	6.	0.	114.61	110.18	22.62	2.	4.	14.	105.05	102.73	4.47
6.	6.	6.	106.31	114.91	2.94	2.	4.	20.	92.80	92.24	3.99
6.	10.	0.	151.45	150.44	5.53	2.	6.	10.	60.36	57.21	1.62
7.	3.	1.	91.06	85.13	4.17	2.	6.	16.	19.14	14.21	5.16
8.	4.	4.	445.66	477.45	22.01	2.	6.	22.	15.66	8.88	4.90
10.	2.	2.	25.48	24.64	2.09	2.	8.	14.	74.31	73.56	3.10
0.	0.	10.	147.84	141.45	4.35	2.	8.	20.	81.90	81.46	6.02
0.	2.	10.	158.55	153.65	3.33	2.	10.	8.	49.75	47.86	2.84
0.	6.	4.	341.16	327.01	10.21	2.	10.	14.	27.76	25.39	1.89
2.	2.	2.	149.61	165.83	5.60	2.	10.	20.	13.34	15.25	3.84
2.	4.	2.	191.73	194.89	1.64	2.	12.	4.	212.64	206.36	13.36
2.	4.	8.	236.95	233.79	5.79	2.	12.	10.	76.23	76.03	3.15
4.	6.	6.	46.74	47.05	1.67	2.	12.	16.	84.32	81.85	4.48
6.	6.	8.	91.56	94.30	3.24	2.	14.	0.	72.32	71.72	3.30
0.	0.	6.	299.65	289.67	7.62	2.	14.	6.	26.11	24.21	12.82
0.	0.	16.	260.15	259.22	2.33	2.	14.	12.	57.58	57.82	4.20
0.	0.	22.	90.52	88.29	2.52	2.	14.	18.	20.45	18.39	6.62
0.	2.	12.	159.82	153.36	6.33	2.	16.	4.	122.41	117.23	4.55
0.	2.	18.	66.33	62.86	3.49	2.	16.	10.	68.47	66.38	4.48
0.	2.	24.	53.84	54.81	5.83	2.	16.	16.	87.31	88.05	3.36
0.	4.	12.	372.65	361.59	10.43	2.	18.	4.	70.84	69.91	4.39
0.	4.	18.	128.28	128.40	4.99	2.	18.	10.	19.75	15.87	8.34
0.	6.	14.	47.13	47.72	1.61	2.	20.	0.	100.82	103.37	2.03
0.	6.	20.	41.91	40.23	3.93	2.	20.	6.	29.52	28.59	5.82
0.	8.	12.	310.35	306.58	10.58	2.	20.	12.	62.08	59.84	2.74
0.	8.	18.	107.81	107.08	3.24	2.	22.	4.	31.84	31.18	3.75
0.	10.	12.	125.84	122.35	4.27	3.	5.	15.	46.52	44.66	5.31
0.	10.	18.	45.83	45.03	2.51	3.	7.	13.	17.63	17.41	3.34
0.	12.	14.	131.77	132.22	6.41	3.	9.	15.	16.14	14.58	4.95
0.	12.	20.	128.49	128.14	4.62	3.	9.	21.	15.19	11.39	4.35
0.	14.	4.	215.65	212.57	2.63	3.	11.	5.	71.14	74.64	2.42
0.	14.	10.	44.60	43.83	2.81	3.	11.	17.	22.27	21.79	8.92
0.	14.	16.	80.80	79.47	3.36	3.	13.	10.	20.02	13.31	8.01
0.	16.	2.	118.04	115.77	3.45	3.	15.	11.	21.00	17.48	5.90
0.	16.	8.	264.54	263.92	6.63	3.	15.	17.	18.98	19.90	8.85
0.	18.	0.	195.37	197.73	3.51	3.	17.	5.	21.29	21.93	5.20

H	K	L	Y(OBS)	Y(CALC)	SIG(O)	H	K	L	Y(OBS)	Y(CALC)	SIG(O)
3.	19.	7.	9.80	10.09	5.45	7.	11.	15.	22.06	19.72	8.13
3.	21.	5.	14.76	12.90	5.86	7.	15.	17.	19.18	13.18	16.36
3.	21.	11.	25.16	21.96	5.85	7.	17.	11.	21.94	20.64	6.73
3.	23.	5.	19.35	9.03	4.76	7.	19.	13.	10.00	11.04	5.85
4.	4.	16.	252.65	246.26	10.00	7.	23.	1.	23.40	11.57	20.50
4.	4.	22.	134.70	138.07	5.20	8.	0.	14.	187.52	185.56	7.52
4.	6.	10.	112.92	112.36	4.44	8.	0.	20.	130.69	182.01	4.12
4.	6.	16.	147.37	145.71	7.74	8.	2.	12.	171.44	174.69	6.83
4.	6.	22.	43.11	42.51	3.95	8.	2.	18.	68.98	67.75	1.25
4.	8.	10.	206.81	215.29	9.08	8.	4.	12.	297.99	304.23	13.12
4.	8.	16.	242.69	239.88	6.47	8.	4.	18.	132.86	133.75	3.21
4.	8.	22.	112.91	114.55	2.46	8.	8.	8.	310.09	318.65	12.40
4.	10.	10.	93.53	97.29	3.14	8.	8.	14.	116.55	114.88	2.08
4.	10.	16.	99.99	101.05	2.99	8.	8.	20.	136.30	136.07	5.35
4.	12.	6.	165.70	166.55	9.55	8.	10.	10.	68.69	70.21	3.42
4.	12.	12.	244.85	247.66	9.51	8.	10.	16.	79.37	80.11	3.40
4.	12.	18.	89.68	89.75	5.43	8.	12.	12.	210.46	215.18	8.40
4.	14.	8.	133.50	136.26	4.36	8.	12.	18.	80.06	81.24	3.05
4.	14.	14.	70.79	74.95	2.83	8.	14.	10.	59.64	58.81	2.30
4.	16.	0.	275.22	270.33	9.68	8.	14.	16.	78.86	80.27	2.88
4.	16.	12.	192.55	195.39	4.80	8.	16.	16.	113.34	117.30	2.15
4.	18.	6.	66.00	65.36	1.76	8.	18.	10.	61.40	61.91	2.41
4.	20.	8.	156.64	155.06	5.03	8.	22.	2.	45.56	43.02	4.52
5.	1.	23.	26.63	28.82	3.16	9.	3.	11.	33.20	34.56	3.75
5.	7.	13.	43.67	44.29	6.65	9.	3.	17.	20.73	21.40	9.54
5.	9.	15.	26.63	23.62	3.42	9.	7.	3.	58.08	60.73	3.21
5.	9.	21.	17.25	14.97	8.50	9.	7.	15.	31.02	30.44	7.02
5.	11.	17.	38.36	37.71	4.07	9.	11.	15.	13.84	14.03	7.27
5.	13.	3.	25.40	26.49	3.15	9.	13.	1.	17.80	16.03	3.63
5.	13.	9.	25.83	24.19	5.86	9.	15.	13.	30.44	30.13	5.90
5.	13.	15.	14.78	12.21	5.26	9.	19.	1.	15.65	17.30	4.32
5.	15.	7.	22.10	16.84	9.27	9.	19.	7.	16.72	9.84	6.50
5.	17.	7.	14.30	6.95	4.22	10.	0.	10.	140.06	137.97	9.90
5.	17.	13.	25.68	26.43	5.05	10.	0.	16.	118.02	117.17	4.17
5.	19.	3.	19.36	15.22	4.46	10.	4.	14.	72.34	71.20	3.51
5.	21.	7.	9.31	4.44	5.73	10.	4.	20.	68.85	68.93	4.02
6.	0.	16.	150.95	151.71	4.60	10.	6.	10.	48.25	48.98	1.32
6.	0.	22.	64.59	65.53	3.22	10.	6.	16.	32.86	32.39	4.37
6.	2.	12.	54.98	55.19	3.87	10.	8.	0.	225.68	224.10	6.50
6.	2.	18.	17.97	15.46	8.09	10.	8.	12.	126.68	128.55	3.91
6.	6.	10.	55.97	54.40	3.27	10.	10.	2.	36.24	38.91	4.60
6.	6.	16.	16.05	3.29	8.35	10.	10.	14.	13.23	7.45	3.45
6.	6.	22.	20.11	25.13	2.86	10.	12.	12.	86.42	86.90	4.12
6.	8.	10.	88.25	88.20	4.06	10.	12.	18.	30.45	29.73	5.26
6.	8.	16.	109.02	108.49	1.82	10.	14.	16.	39.34	39.09	2.11
6.	10.	12.	58.91	59.14	6.85	10.	16.	10.	49.23	46.80	4.50
6.	10.	18.	15.90	8.96	3.95	11.	1.	7.	47.84	48.48	3.27
6.	12.	8.	132.19	134.30	5.00	11.	1.	13.	15.34	9.22	5.49
6.	12.	14.	31.28	26.74	6.06	11.	9.	1.	29.82	29.80	4.10
6.	12.	20.	41.50	41.01	3.87	11.	9.	13.	24.63	11.31	15.13
6.	14.	4.	115.58	115.30	4.60	11.	9.	19.	24.68	25.88	5.14
6.	14.	16.	39.59	38.30	3.09	11.	13.	5.	13.84	8.69	3.76
6.	18.	8.	45.81	46.05	5.31	11.	13.	17.	17.60	18.06	6.87
6.	18.	14.	17.36	13.24	4.00	11.	15.	5.	16.74	13.73	7.15
6.	20.	4.	51.04	50.51	2.48	11.	21.	1.	17.39	15.14	5.19
6.	20.	10.	23.88	18.81	9.46	12.	8.	16.	177.35	176.43	3.18
7.	1.	19.	19.89	17.63	5.40	12.	10.	14.	43.02	42.16	2.83
7.	3.	11.	28.37	28.85	2.21	12.	12.	0.	307.04	296.08	14.18
7.	3.	17.	16.45	12.38	3.20	12.	12.	6.	122.66	123.77	5.03
7.	5.	9.	34.97	27.06	13.76	12.	12.	12.	225.50	221.78	9.00
7.	9.	13.	59.66	60.61	2.65	12.	14.	12.	81.19	81.54	4.40
7.	11.	9.	50.66	49.47	3.43	12.	18.	6.	52.09	53.13	3.31

H	K	L	Y(OBS)	Y(CALC)	SIG(O)	H	K	L	Y(OBS)	Y(CALC)	SIG(O)
13.	1.	5.	27.18	24.11	3.57	2.	2.	20.	19.91	14.69	6.35
13.	1.	17.	17.13	17.91	2.94	2.	8.	16.	85.20	84.33	3.84
13.	3.	9.	38.92	39.61	1.85	2.	12.	12.	103.91	105.36	4.40
13.	3.	15.	24.74	25.90	8.40	2.	12.	18.	37.02	38.50	2.16
13.	5.	19.	20.86	21.93	6.22	2.	14.	14.	44.02	46.02	1.88
13.	7.	11.	32.21	32.42	3.24	3.	7.	21.	21.91	20.03	3.70
13.	7.	17.	20.47	16.57	5.04	3.	11.	19.	27.00	28.10	5.90
13.	11.	3.	22.57	20.38	2.05	3.	19.	9.	26.53	24.24	4.62
13.	15.	11.	14.16	7.72	7.47	4.	4.	12.	336.07	338.07	6.55
13.	17.	3.	21.02	18.53	6.93	4.	4.	18.	148.94	145.41	3.51
13.	17.	9.	23.54	25.81	3.94	4.	10.	12.	143.56	146.56	2.86
14.	0.	0.	270.96	262.88	6.78	4.	10.	18.	71.65	69.92	3.51
14.	0.	18.	58.88	60.91	4.00	4.	12.	20.	153.53	153.64	3.76
14.	2.	16.	34.94	34.26	6.61	4.	14.	4.	155.11	153.45	12.06
14.	6.	6.	53.48	54.76	3.55	4.	20.	4.	197.85	196.72	3.18
14.	12.	4.	140.20	143.32	6.16	5.	1.	19.	18.96	18.95	4.29
14.	14.	0.	109.17	109.29	6.14	5.	9.	11.	49.87	47.85	2.28
14.	14.	6.	19.36	18.52	2.99	5.	11.	7.	31.64	29.92	3.65
14.	14.	12.	51.16	54.09	6.90	6.	0.	12.	195.48	190.80	9.96
14.	16.	4.	86.07	87.16	7.25	6.	6.	12.	85.32	88.13	2.06
14.	18.	4.	57.13	57.04	2.58	6.	6.	18.	27.42	24.23	4.55
15.	1.	3.	30.11	26.39	6.05	6.	10.	14.	15.71	11.89	6.93
15.	7.	3.	37.81	36.06	5.27	7.	9.	21.	8.20	9.84	6.38
15.	13.	7.	50.50	51.26	2.43	8.	4.	8.	377.04	402.58	18.12
15.	17.	5.	23.48	20.15	6.12	8.	6.	8.	190.09	191.82	6.76
16.	6.	12.	80.54	79.27	1.35	8.	6.	14.	88.29	87.33	2.75
16.	10.	12.	82.08	80.54	3.25	8.	6.	20.	84.18	83.98	2.63
16.	16.	0.	141.07	140.53	5.89	8.	8.	10.	180.01	184.45	5.19
16.	16.	6.	56.13	55.46	4.74	8.	8.	16.	225.42	228.93	2.40
17.	1.	7.	22.08	23.59	3.82	8.	12.	8.	264.92	271.81	6.09
17.	3.	1.	39.85	38.38	2.35	8.	12.	14.	123.15	121.86	4.23
17.	5.	9.	13.75	11.43	10.02	9.	11.	17.	19.90	19.51	4.48
17.	9.	1.	18.86	13.53	2.97	10.	10.	10.	24.29	23.29	5.45
17.	9.	7.	16.06	2.26	4.42	11.	5.	19.	20.03	8.82	12.24
18.	0.	16.	73.11	74.68	1.68	12.	10.	10.	69.64	68.75	3.70
19.	11.	7.	14.18	13.17	8.72	14.	14.	8.	51.47	53.56	1.35
20.	6.	6.	53.69	53.04	4.35	16.	2.	2.	86.86	86.25	1.11
20.	8.	10.	58.20	60.38	1.97	18.	10.	10.	33.76	34.85	5.66
22.	0.	8.	82.47	82.88	1.66	19.	5.	7.	16.78	6.97	5.43
0.	0.	12.	458.24	453.04	19.01	2.	22.	2.	16.49	15.44	3.74
0.	4.	20.	220.97	222.20	4.10	4.	16.	16.	140.32	142.13	3.76
0.	10.	20.	97.80	100.08	3.53	8.	8.	18.	122.35	122.89	3.36
0.	12.	16.	190.12	139.02	4.74	9.	19.	5.	11.49	10.39	10.75
1.	15.	13.	14.55	7.31	4.11	10.	14.	14.	38.99	35.54	3.54
2.	2.	14.	75.10	74.43	3.04	12.	12.	16.	138.57	138.59	1.22

Appendix G

The observed structure amplitudes and errors and the calculated structure factors for $Cu_3B_7O_{13}Br$ at room temperature.

H	K	L	Y(OBS)	Y(CALC)	SIG(O)	H	K	L	Y(OBS)	Y(CALC)	SIG(O)
0.	6.	2.	56.23	51.21	4.26	0.	6.	18.	55.00	57.61	8.04
0.	6.	8.	134.67	133.70	6.85	0.	8.	14.	138.12	143.73	15.82
0.	10.	0.	74.46	72.55	6.18	0.	12.	8.	228.00	237.28	16.59
1.	3.	7.	74.53	69.73	9.11	0.	12.	14.	89.74	94.95	4.38
1.	5.	7.	69.70	65.45	5.35	0.	14.	4.	153.69	162.35	10.83
1.	7.	9.	51.27	52.86	2.44	0.	14.	10.	14.58	8.57	7.31
1.	9.	5.	51.72	52.99	2.58	0.	16.	2.	69.27	73.03	3.58
1.	11.	3.	25.21	25.11	1.76	0.	16.	8.	199.39	209.99	16.32
2.	0.	10.	73.40	70.47	4.93	1.	3.	15.	33.09	30.95	5.34
2.	2.	4.	111.35	96.23	9.80	1.	5.	15.	16.15	17.71	4.44
2.	2.	10.	112.23	110.70	8.77	1.	7.	15.	38.27	40.69	2.86
2.	4.	4.	153.08	148.74	3.26	1.	9.	15.	24.02	22.63	4.48
2.	4.	10.	50.54	53.06	3.61	1.	11.	9.	28.65	25.87	3.76
2.	6.	4.	78.51	72.18	5.18	1.	11.	15.	17.93	12.52	7.63
2.	8.	6.	69.83	69.96	2.82	1.	13.	11.	9.69	3.13	6.89
3.	1.	9.	69.65	70.39	4.89	1.	17.	3.	35.99	36.25	5.65
3.	9.	5.	49.75	48.93	2.21	1.	17.	9.	22.80	17.08	3.40
4.	2.	8.	155.45	153.23	10.01	2.	2.	18.	68.21	71.79	5.11
4.	6.	8.	137.58	134.81	4.09	2.	4.	18.	26.36	25.92	5.36
5.	1.	3.	163.63	147.22	11.08	2.	6.	18.	68.88	71.30	4.01
5.	7.	3.	46.18	41.26	3.58	2.	8.	14.	25.39	26.02	1.76
6.	6.	6.	40.57	33.12	3.58	2.	10.	14.	53.54	54.74	5.71
8.	2.	2.	58.19	56.79	5.76	2.	12.	8.	111.86	114.81	6.02
8.	2.	8.	158.37	159.18	3.67	2.	12.	14.	37.28	37.64	2.88
10.	4.	0.	170.21	170.32	12.05	2.	14.	4.	53.00	53.03	4.25
2.	2.	0.	14.65	18.14	3.32	2.	16.	2.	40.03	42.38	4.19
2.	6.	6.	175.17	173.76	8.51	2.	16.	8.	57.37	60.17	3.01
4.	4.	10.	187.68	190.41	15.19	3.	5.	15.	40.78	41.60	6.32
6.	4.	6.	89.98	79.97	4.00	3.	7.	13.	17.21	13.89	6.59
0.	6.	6.	30.95	28.75	4.55	3.	9.	13.	35.96	36.41	5.33
0.	2.	14.	13.01	13.62	3.26	3.	11.	9.	39.32	36.76	4.37
0.	6.	12.	133.12	139.05	11.23	3.	11.	15.	24.98	22.54	2.80
0.	10.	8.	150.19	158.27	5.40	3.	13.	5.	30.47	28.42	6.77
0.	12.	2.	99.52	98.90	6.73	3.	15.	9.	15.72	11.03	7.76
1.	3.	13.	22.04	20.76	3.74	3.	19.	1.	43.03	46.71	2.67
1.	7.	11.	47.26	48.45	3.78	4.	4.	18.	102.73	111.14	10.94
1.	13.	5.	30.44	30.41	2.83	4.	6.	16.	100.76	104.29	10.24
2.	2.	12.	61.59	59.75	5.04	4.	8.	16.	181.88	195.93	22.70
2.	6.	12.	34.57	33.99	2.00	4.	10.	10.	38.83	37.74	3.81
2.	10.	8.	24.80	20.89	3.63	4.	10.	16.	66.65	68.47	3.73
2.	12.	4.	132.37	140.55	8.71	4.	12.	10.	108.47	108.13	6.59
3.	5.	11.	66.73	69.43	4.54	4.	14.	6.	58.76	62.04	4.16
3.	9.	7.	52.68	52.35	3.85	4.	14.	12.	103.00	105.70	6.18
4.	4.	12.	239.08	255.66	25.47	4.	16.	4.	185.67	196.16	18.97
4.	10.	8.	148.77	151.18	3.92	5.	7.	15.	20.19	16.73	3.16
5.	7.	9.	20.47	16.99	5.62	5.	9.	15.	26.42	25.82	3.81
6.	0.	10.	75.75	79.29	4.21	5.	13.	7.	43.46	41.75	7.15
6.	6.	8.	39.95	39.55	3.29	6.	0.	16.	97.39	102.33	9.57
6.	8.	8.	132.15	132.76	3.97	6.	2.	16.	33.89	33.89	2.15
6.	10.	2.	127.30	130.83	7.82	6.	6.	12.	20.39	20.49	4.30
6.	10.	8.	36.64	35.24	2.13	6.	8.	12.	87.82	86.57	2.00
6.	12.	4.	113.06	116.85	5.67	6.	10.	12.	15.94	8.16	3.13
7.	3.	11.	20.09	22.47	3.02	6.	14.	0.	14.65	15.84	1.95
10.	6.	4.	48.67	46.85	2.58	6.	14.	6.	98.71	98.53	4.24
0.	10.	10.	85.66	86.41	3.03	6.	16.	6.	57.01	55.93	4.94
1.	5.	11.	49.57	50.27	3.94	7.	1.	17.	19.74	21.08	8.96
5.	7.	11.	37.31	36.58	4.39	7.	3.	15.	35.66	37.20	11.67
6.	6.	10.	124.05	123.90	2.52	7.	9.	13.	59.62	57.63	5.57
8.	8.	8.	229.66	230.04	4.00	7.	11.	9.	53.53	51.40	2.89
0.	0.	16.	208.24	210.09	24.50	7.	13.	1.	38.21	37.11	5.70
0.	2.	18.	22.69	23.01	8.58	7.	17.	3.	18.56	13.77	3.11
0.	4.	18.	90.79	90.77	5.92	8.	6.	16.	69.69	71.29	4.61

H	K	L	Y(OBS)	Y(CALC)	SIG(O)	H	K	L	Y(OBS)	Y(CALC)	SIG(O)
2.	22.	2.	61.29	65.32	6.17	8.	8.	10.	136.61	136.42	4.29
4.	4.	22.	109.48	117.12	4.52	8.	10.	12.	90.45	89.52	8.48
4.	6.	22.	12.47	11.50	8.67	8.	12.	8.	212.97	212.51	4.06
4.	8.	22.	81.56	86.53	3.53	8.	14.	6.	40.21	40.75	4.86
4.	12.	16.	154.19	157.28	6.91	9.	7.	15.	24.07	21.55	11.99
4.	14.	14.	47.05	47.83	4.24	10.	4.	14.	38.78	38.18	4.14
4.	18.	6.	37.78	37.90	3.24	10.	6.	14.	48.44	47.81	5.20
4.	18.	12.	62.64	60.73	2.14	10.	8.	10.	21.05	23.57	3.40
4.	20.	8.	122.80	130.47	2.38	10.	10.	6.	106.61	106.23	6.88
4.	22.	0.	72.54	72.50	1.49	10.	10.	12.	38.64	38.14	3.83
6.	6.	18.	58.40	58.66	2.69	10.	16.	0.	73.25	77.60	2.96
6.	8.	18.	33.82	34.19	3.09	11.	7.	13.	29.13	29.01	6.52
6.	10.	18.	57.03	58.44	2.71	11.	9.	5.	51.89	50.05	5.96
6.	12.	16.	53.97	51.93	4.15	11.	15.	5.	8.81	7.15	4.95
6.	14.	14.	63.18	66.06	3.53	12.	0.	10.	75.06	75.29	2.92
6.	16.	10.	24.41	18.89	6.05	12.	2.	12.	73.19	76.04	5.89
6.	16.	16.	33.31	35.68	16.45	12.	4.	8.	230.30	236.49	5.19
6.	18.	14.	48.21	49.32	17.25	12.	12.	0.	225.40	234.99	4.03
6.	20.	4.	22.49	16.79	2.78	12.	12.	6.	86.69	85.89	6.05
6.	20.	10.	26.86	21.34	2.30	13.	1.	9.	17.21	17.17	7.80
8.	2.	20.	51.14	54.12	6.78	13.	5.	11.	17.53	10.03	7.50
8.	6.	20.	52.23	54.36	4.23	13.	11.	3.	18.93	14.82	4.16
8.	8.	20.	105.27	112.61	4.54	13.	11.	9.	18.52	14.52	12.75
8.	10.	20.	38.22	38.74	12.35	14.	2.	2.	122.23	124.47	5.25
8.	12.	18.	60.60	61.67	2.96	14.	8.	4.	91.05	91.04	1.58
8.	14.	16.	51.06	52.43	3.82	14.	8.	10.	36.15	32.80	4.13
8.	16.	12.	142.40	145.18	18.46	16.	4.	0.	206.98	213.22	5.84
8.	18.	8.	98.62	99.59	2.91	17.	5.	1.	39.43	40.19	4.87
8.	22.	0.	57.39	57.37	5.09	17.	7.	5.	13.32	2.75	2.83
10.	0.	18.	19.60	16.28	15.16	0.	0.	18.	138.12	139.65	2.43
10.	8.	16.	51.77	49.40	19.46	0.	14.	0.	197.83	195.24	3.55
10.	10.	14.	38.01	37.45	7.46	2.	6.	14.	81.58	82.66	3.12
10.	12.	12.	50.09	49.45	3.39	2.	10.	10.	100.90	100.68	4.06
10.	14.	16.	14.17	11.71	4.78	2.	10.	16.	43.25	47.98	2.99
10.	16.	10.	37.23	36.50	2.29	2.	12.	10.	24.33	23.33	3.80
12.	2.	18.	23.45	26.09	4.20	2.	16.	4.	73.28	76.11	5.31
12.	10.	14.	19.36	14.22	2.38	3.	5.	17.	17.14	16.82	4.70
12.	12.	12.	188.02	190.92	13.16	4.	4.	14.	106.34	104.41	7.00
12.	14.	6.	25.98	23.26	13.53	4.	12.	12.	185.47	192.55	4.70
12.	14.	12.	55.47	55.10	3.14	5.	13.	9.	23.07	22.91	9.25
12.	18.	6.	24.90	25.43	5.04	8.	14.	8.	79.38	75.75	7.98
12.	20.	2.	30.49	30.79	7.69	12.	12.	8.	167.48	172.49	4.34
14.	0.	16.	58.30	58.50	1.70	10.	10.	10.	85.78	84.22	3.34
14.	4.	16.	61.65	59.68	9.88	0.	0.	20.	152.36	142.95	4.28
14.	8.	12.	89.14	88.90	6.29	0.	2.	22.	47.12	47.67	3.10
14.	14.	0.	69.05	70.05	10.61	0.	8.	20.	139.85	148.23	3.88
14.	14.	12.	25.08	21.98	6.21	0.	10.	20.	65.64	69.93	6.90
14.	18.	4.	34.00	32.00	5.61	0.	12.	20.	108.92	115.17	7.58
16.	8.	8.	185.58	189.14	6.80	0.	14.	18.	24.08	25.81	14.07
16.	12.	0.	150.58	155.62	5.30	0.	16.	16.	111.04	118.77	7.28
16.	12.	12.	115.29	116.61	6.97	0.	18.	12.	88.32	91.36	3.21
16.	16.	4.	116.02	124.22	3.80	0.	20.	2.	65.39	67.23	7.02
18.	4.	10.	38.14	38.92	2.90	0.	22.	0.	72.89	71.45	3.24
18.	8.	0.	81.98	81.62	6.00	0.	22.	6.	31.17	27.61	4.74
18.	10.	10.	54.31	55.11	7.14	2.	4.	20.	62.12	63.20	3.16
20.	0.	4.	176.63	183.52	7.25	2.	6.	22.	38.87	39.23	16.18
20.	2.	2.	58.77	60.90	4.13	2.	8.	22.	23.41	26.50	2.07
20.	4.	12.	125.02	133.07	3.04	2.	12.	16.	47.55	48.86	14.77
20.	10.	4.	42.64	43.35	7.97	2.	14.	14.	88.94	91.71	3.01
22.	6.	6.	53.16	57.44	5.65	2.	18.	8.	22.98	20.62	9.94
2.	4.	22.	16.30	10.70	7.35	2.	18.	14.	42.02	42.88	9.50
2.	10.	18.	56.66	58.45	7.11	2.	20.	10.	35.99	36.02	5.55

H	K	L	Y(OBS)	Y(CALC)	SIG(O)
2.	14.	16.	20.11	8.06	9.71
2.	20.	6.	23.13	16.51	12.13
4.	8.	18.	102.35	104.04	12.17
4.	20.	4.	155.48	164.57	12.78
6.	6.	20.	17.43	12.39	4.24
6.	20.	0.	21.14	14.21	3.78
8.	18.	10.	28.45	29.87	4.20
10.	16.	12.	54.87	53.97	3.57
14.	6.	16.	13.05	8.16	4.29
14.	8.	14.	26.40	26.59	3.96
16.	2.	16.	51.32	54.07	8.08
10.	14.	14.	67.09	64.97	4.46
0.	0.	24.	91.42	82.47	5.51
0.	6.	24.	55.67	57.58	2.63
0.	12.	22.	57.60	56.54	3.45
0.	16.	20.	116.98	118.41	4.40
0.	20.	14.	48.79	44.21	5.55
0.	24.	4.	122.83	119.89	5.46
2.	0.	24.	35.27	30.39	4.61
2.	6.	24.	50.57	49.33	4.42
2.	12.	22.	27.88	29.25	5.26
2.	16.	20.	29.20	30.44	6.74
2.	20.	14.	36.08	33.95	4.74
2.	24.	4.	25.73	24.25	6.34
4.	6.	24.	15.77	14.32	6.99
4.	12.	22.	58.05	57.07	3.18
4.	18.	16.	51.74	51.23	2.50
4.	22.	10.	32.86	31.75	4.44
4.	24.	8.	114.10	112.92	5.03
6.	10.	22.	49.49	46.92	3.57
6.	14.	20.	13.26	12.67	5.38
6.	20.	12.	17.21	10.59	4.14
8.	0.	24.	109.20	110.69	3.87
8.	6.	22.	18.35	10.39	4.72
8.	12.	20.	121.66	116.72	6.45
8.	16.	16.	108.15	101.84	6.51
8.	18.	16.	57.46	56.19	2.96
10.	0.	22.	34.62	33.29	5.16
10.	12.	20.	45.85	42.34	2.00
10.	18.	14.	48.52	48.34	3.56
12.	6.	22.	23.99	18.64	10.44
12.	12.	18.	63.77	61.22	3.82
12.	16.	14.	47.24	46.22	3.24
12.	18.	14.	20.98	19.15	5.24
14.	8.	18.	24.57	18.61	5.59
14.	14.	16.	8.55	4.08	6.80
16.	12.	16.	101.64	98.40	1.77
16.	18.	0.	53.40	51.61	3.65
18.	2.	16.	16.99	7.13	3.75
18.	4.	18.	38.21	37.67	2.00
18.	18.	0.	35.39	32.84	8.25
20.	10.	10.	30.55	34.69	7.91
20.	14.	8.	37.79	35.21	5.93
24.	2.	2.	20.22	20.55	11.46
24.	2.	8.	20.51	8.44	8.96
24.	4.	4.	129.98	127.23	4.88
4.	14.	20.	58.05	58.44	5.37
6.	6.	24.	16.74	13.43	4.83
6.	16.	18.	21.72	9.62	6.66
8.	8.	22.	67.13	61.94	5.01
10.	2.	22.	70.66	69.77	4.01
10.	8.	22.	28.60	28.98	4.91
16.	10.	16.	37.17	36.42	2.47
18.	2.	18.	51.20	50.21	2.08
14.	14.	14.	46.22	46.52	3.32

Appendix H

Published work.

Ferroelectrics
1976, Vol. 14, pp. 599–600

STRUCTURAL STUDIES OF CsD_2AsO_4 IN THE PARAELECTRIC PHASE AND THE FERROELECTRIC PHASE

W. J. HAY and R. J. NELMES

Department of Physics, University of Edinburgh, Mayfield Road, Edinburgh

(Received September 22, 1975)

Neutron single-crystal structural studies have been made of $Cs(D_xH_{1-x})_2AsO_4$, nominal $x = 0.95$, in its tetragonal phase at T_c + 5 K (208 K) and at 77 K in its orthorhombic ferroelectric phase.

$Cs(D_xH_{1-x})_2AsO_4$ (hereafter DCsDA) is assumed to be isomorphous with KH_2PO_4 (KDP). It has a similar transition from a tetragonal ($I\bar{4}2d$) paraelectric phase to an orthorhombic ($Fdd2$) ferroelectric phase on cooling, It has attracted growing attention (see Ref. 1, for example) as being at the "other end" of the KDP family from KDP itself–the potassium and phosphorus are both replaced–but no known study has been made of its structure. Preliminary results of detailed structural studies of the tetragonal and orthorhombic phase are presented here.

The specimens were cut from a single crystal supplied by Quantum Technology Ltd. Three-dimensional neutron data have been collected (i) in the tetragonal phase at T_c + 5 K (T_c = 203 K) and (ii) at 77 K in the ferroelectric phase. Only half the crystal changed phase at the transition temperature (203 K) appropriate to the nominal deuteration of $x = 0.95$; the remainder changed gradually over a large temperature range. Experiments on crystals of widely varying volume show this is not a surface hydrogenation effect[6] and the feature is as yet unexplained.

For the experiment at T_c + 5 K a cube-shaped crystal (side 2 mm) was mounted with its b-axis vertical in a variable temperature cryostat. The data were collected out to $\sin\theta/\lambda = 0.71$ Å^{-1} ($\lambda = 1.075$ Å) on a two-circle diffractometer with tilting counter at A.E.R.E., Harwell. The cell dimensions measured were $a = 7.99(1)$ Å, $c = 7.88(1)$ Å. Data were collected in the four layers (h, $k = 0 - 3$, l) yielding 170 independent reflections–most of the full three-dimensional data set because ($h\ k\ l$) and ($k\ h\ l$) are equivalent.

For the experiment in the ferroelectric phase a 2 x 2 x 4 mm^3 crystal was mounted with the c-axis vertical on the same machine and cooled to 77 K. The cell dimensions were measured as $a = 11.516(5)$ Å, $b = 11.103(4)$ Å, $c = 7.87(2)$ Å. Preliminary x-ray investigations showed the shear angle in the ferroelectric phase to be 2.0(1)°. This separates the four reciprocal lattices of the ferroelectric phase sufficiently to allow data collection from just one of the lattices without poling and constraining the crystal. The main limitation of this technique is that it can only be applied readily with the tetragonal c-axis vertical, and the tilting counter permitted measurement of just the four layers (h, k, l = 0-3). At this stage data reduction has been completed only for those 36 reflections in which the measured peak is completely separated from those of the other three reciprocal lattices.

1) The tetragonal phase at T_c + 5 K: least-squares refinement was started from the positional and thermal parameters of KDP[2] with the deuterium disordered over the two sites of a double minimum well (designated model I). The deuterium scattering length was refined to 0.22(2): this corresponds to a mean value of x of 0.57(1). The R index was 0.05.

The techniques of constrained refinement and significance testing[3,4] have been applied to investigate some important details of model I–particularly of the deuterium bond. This bond is illustrated in Figure 1. In the conventional setting with As at the origin, the diad shown in Figure 1 is at $Y = b/4$, $Z = c/8$.

Three models in which constraints are applied (less parameters than model I) have been refined and tested. These were (i) the ordered model with the deuterium constrained to lie on the diad ($Y = b/4$, $Z = c/8$. (ii) z of oxygen is $c/8$ (i.e. ϕ is zero) and (iii) the deuteriums lie on the O-O line (i.e. ψ is zero). The significance levels at which these constraints can be rejected are given in Table I. It is $100(1 - \alpha)\%$ probable that the unconstrained model gives a better fit to the data than a model constrained in the way considered. ζ is an "index of scepticism":

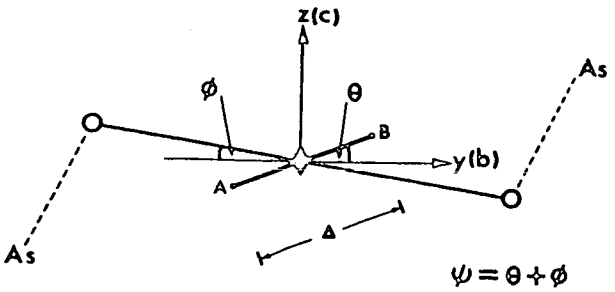

FIGURE 1 The deuterium bond in DCsDA. The bond is viewed down the X-axis and has a two-fold symmetry axis (diad) at its centre. The open circles denote the oxygen atoms. A and B are the sites of the two "half" deuterium atoms in the double minimum potential well (the disordered model). For the single minimum model (the ordered model) the deuterium atom lies on the diad. The approximate location of the arsenic to which each oxygen is attached is indicated: the arsenic are below the plane of the diagram.

a conservative inference is that when $\zeta < 2$ the significance may not indicate *physical* significance.[4] For comparison the results obtained in KDP at T_c + 5K are included.[5]

It is seen that (i) the separation of the deuterium onto two sites is significant at the 0.001 level, (ii) ϕ is nonzero at the 0.001 level, and (iii) the inclination of the D-D line to the O-O line is non-zero at the 0.005 level. In all three cases the physical significance is, on a conservative interpretation, marginal ($\zeta < 2$).

The final positional parameters of the unconstrained disorder model (model I) are given in Table II.

In Table III some dimensions calculated from these parameters are compared with the corresponding results for KDP[5] at T_c + 5 K. Note that ϕ in DCsDA is negative.

2) The orthorhombic phase at 77 K: least-squares refinement was started from the positional parameters of the tetragonal phase at T_c + 5 K (Table II) transformed to the *Fdd*2 cell. Because of the small data set available (see above) only twelve parameters were refined: a scale factor, the ten positional parameters

TABLE I

Significance levels for constraints in DCsDA compared with KDP[5] at T_c + 5 K

Constraint	DCsDA α	DCsDA ζ	KDP α	KDP ζ
Ordered D(H)	0.001	1.5	< 0.001	27
$\phi = 0$	0.001	1.7	< 0.001	36
$\psi = 0$	0.005	1.7	0.001	1.7

TABLE II

Positional parameters in DCsDA at T_c + 5 K: in Å units

	x	y	z
Cs	0	0	3.945
As	0	0	0
O	1.164(3)	0.732(2)	0.974(2)
D	1.105(16)	1.754(8)	0.924(17)

TABLE III

The deuterium (hydrogen) bonds in DCsDA and KDP[5] compared at T_c + 5 K

	DCsDA	KDP
O-O in Å	2.531(4)	2.477(1)
O-D in Å	1.03(2)	1.066(1)
D-D in Å	0.50(2)	0.349(2)
θ	14(4)°	8(2)°
ϕ	−0.5(1)°	0.60(15)°

and an overall thermal parameter. The R index was 0.088.

The deuteriums are ordered on to one site consistent with the expected order/disorder transition for KDP-type ferroelectrics. The calculated O-O and O-D distances are 2.56(3) Å and 1.10(2) Å respectively.

Full three-dimensional x-ray and neutron data have been collected from DCsDA at room temperature. The analyses of these experiments and the completion of the analysis of the 77 K data are in hand.

ACKNOWLEDGEMENTS

We should like to acknowledge the kind assistance of our colleagues Mr. N. S. J. Kennedy and Dr. F. R. Thornley, and of the technical support staff at A.E.R.E. Harwell. We are grateful for the support of a Harwell E.M.R. Contract (W.J.H.) and a Science Research Council Research Fellowship (R.J.N.).

REFERENCES

1. R. P. Lowndes, N. E. Tornberg and R. C. Leung, *Phys. Rev. B* 10, 911 (1974).
2. V. R. Eiriksson, Ph.D. Thesis, University of Edinburgh (1974)
3. W. C. Hamilton, *Acta Cryst.* 18, 502 (1965).
4. G. S. Pawley, In *Advances in Structure Research by Diffraction Methods*, Vol. 4, edited by W. Hoppe and R. Mason (Oxford, Pergamon, 1971).
5. N. S. J. Kennedy, R. J. Nelmes, F. R. Thornley and K. D. Rouse, *Ferroelectrics*, 12, 591 (1976).
6. G. M. Meyer, O. W. Dietrich, R. J. Nelmes, W. J. Hay and R. A. Cowley, *J. Phys. C.* 9, L83 (1976).

J. Phys. C: Solid State Phys., Vol. 9, 1976. Printed in Great Britain.

LETTER TO THE EDITOR

The structure of ferroelectric DCsDA

G M Meyer†‡, O W Dietrich†, R J Nelmes‡, W J Hay‡ and R A Cowley‡

† Physics Department, Danish Atomic Energy Commission, Research Establishment Risø, Denmark

‡ Department of Physics, Edinburgh University, Mayfield Road, Edinburgh, Scotland

Received 14 November 1975

Abstract. In further neutron scattering experiments on the (orthorhombic) ferroelectric phase of DCsDA and CsDA, a study has been made of the scattering arising at wavevectors along the a^* direction at positions away from Bragg reflections. It is shown that this most probably arises from Bragg scattering in which two different ferroelectric domains are involved.

Below T_c each Bragg reflection can split into four separate spots corresponding to the different domain types. Surprisingly in DCsDA a central Bragg spot from the (tetragonal) paraelectric phase persists with decreasing intensity over a 60 K temperature range. This effect has been observed with both neutron and x-ray scattering techniques and is independent of crystal size.

1. Satellites in CsDA

Dietrich *et al* (1974) reported observing a satellite structure in the ferroelectric phase of DCsDA (CsD_2AsO_4). Peaks in the scattering were observed around a number of Bragg points in the $(h0l)$ zone. These peaks appeared at reduced wavevectors 0·1 and 0·2 along the $[\eta 00]$ direction at (004) and (303), at 0, 0·034 and 0·067 for (002) and at combinations of these reduced wavevectors around other Bragg points. The indexing of the tetragonal phase is used throughout this paper.

The experiments have been repeated in greater detail on a 1 cm^3 crystal of the corresponding hydrogenous compound, CsDA (CsH_2AsO_4), obtained from Quantum Technology§. The crystal was mounted with the *ac* plane horizontal and maintained at a temperature of 115 K in a cryostat on a double-axis spectrometer at the DR3 reactor, Risø. Elastic neutron scattering scans of the type $(h + \eta, \xi, l)$ were made using neutrons of wavevector $k = 2{\cdot}65\ \text{Å}^{-1}$. η was varied under the control of a PDP 8 computer and at the end of each scan ξ was incremented manually by tilting the counter vertically. Contour maps of the intensities observed at the systematic absence (002) and at (004) are shown in figure 1. These are similar to those observed in DCsDA, but in the present study the vertical resolution has been improved.

The ferroelectric cell can be described as a distortion of the paraelectric cell by a spontaneous shear x_y (Jona and Shirane 1962). The shear angle is about 1·8° and decreases to 70% of this value close to the transition temperature (Meyer and Dietrich 1975). When

§ Quantum Technology, 60 Nugget Avenue, Unit 5 Agincourt (Toronto), Ontario, Canada.

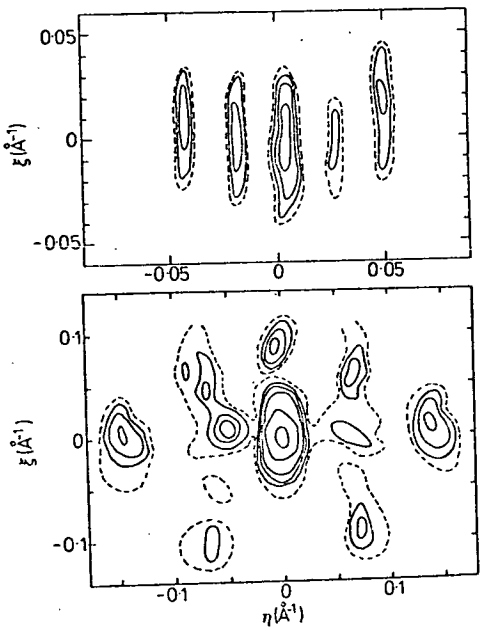

Figure 1. The intensities observed in the ferroelectric phase of CsDA at 115 K. Maps of (002) and (004) with contours at 10, 30, 100, 300, 1000 and 3000 above background.

a single crystal of CsDA is taken through the transition it is expected in general to shear four different ways. There are thus four types of ferroelectric domain distinguished by their mutual orientation. The proportion of the crystal forming each type of domain can

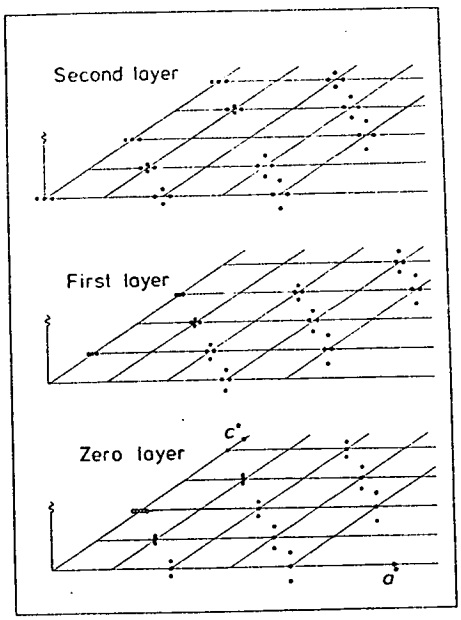

Figure 2. The domain splitting for Bragg points in ($h0l$) and parallel planes. The points are split only in the a^*b^* plane. In addition the satellite positions at (002) are shown as open circles.

vary but the process is otherwise reversible. The effect of the domain splitting on Bragg peaks is shown schematically in figure 2. At the position of each Bragg peak of the paraelectric phase there appear in general four separate peaks, lying in the a^*b^* plane: for $a^* = 0$ or $b^* = 0$, two superpose so that only three peaks are distinguished.

In a single crystal, multiple Bragg scattering affects only the intensities at reciprocal lattice vectors. But when the crystal consists of domains with a number of different orientations, multiple scattering can give rise to scattering at points other than those permitted by a single scattering process—as we shall now demonstrate. The problem is equivalent to determining whether reciprocal lattice points from two parallel co-ordinate systems, with origins at either end of the scattering vector, simultaneously lie on the Ewald sphere. Thus intensity seen at $(h + \eta, k + \xi, l)$ can result as scattering from a Bragg point (h', k', l') in one domain type followed by scattering from a Bragg point $(h' - h, k' - k, l' - l)$ in a different domain type. For brevity we shall refer to this scattering as multiple scattering from $((h', k', l'))$.

A translation of the co-ordinate system along the c-axis by a reciprocal lattice vector like (002) leaves the splitting of the Bragg peaks unchanged. Peaks from the two co-ordinate systems will completely overlap (systematic absences in either system excepting). If a scan in the $[\eta 00]$ direction is made at (002), points in the two co-ordinate systems will 'pass through' each other. For example, a reciprocal lattice point such as (011), which splits into three collinear Bragg peaks with spacing d, will have peaks from the two systems overlapping at five equispaced positions in the scan, namely at $(-2d, 0, 2)$, $(-d, 0, 2)$, $(0, 0, 2)$, $(d, 0, 2)$ and $(2d, 0, 2)$ where

$$d = \tan x_y \simeq 0{\cdot}03.$$

These positions are the same as those at which the satellites were observed around (002). They are marked as open circles on figure 2. The above, however, only provides a necessary condition for multiple scattering—to make the condition sufficient, we must ensure that pairs of points, designated by $((0, 1, 1))$, simultaneously lie on the Ewald sphere.

A computer simulation was set up to investigate all the possible ways that multiple scattering from two different domain types can produce satellites. This shows that only the first four points on the $(\eta 02)$ scan listed above have contributions from $((0, 1, 1))$ multiple scattering. The first point has a further contribution from $((3, 1, 4))$. Normal multiple scattering (i.e. in a *single* domain type)—at $((5, 2, 3))$ and at $((5, 2, -1))$—also meets the necessary conditions for the centre point at $(0, 0, 2)$. The correct condition for the last point is only met by multiple scattering from $((3, 1, -2))$. There is no first-order reflection at (002), but a slight second-order contamination of the neutron beam reflected at (004) contributes to the intensity observed at $(0, 0, 2)$.

It can similarly be shown that multiple scattering from $((4, 3, 3))$, $((4, 3, 1))$, $((1, 3, 2))$ and $((0, 2, 2))$ contribute towards the intensities observed round (004). The slight up–down asymmetry in the contour map, figure 1, is probably caused by incorrect alignment of the crystal, since multiple Bragg scattering is particularly sensitive to correct alignment.

There are two ways of checking whether an effect observed in a neutron scattering experiment is due to multiple scattering. Firstly the wavelength of the monochromatic beam can be altered. Thereby the radius of the Ewald sphere in the crystal, monochromator or analyser changes and so do the conditions for the multiple scattering. Unfortunately with the present experimental set-up it was difficult to change the wavelength of the incident beam.

Alternatively, rotation of the crystal about the scattering vector also changes the conditions for multiple scattering. When the crystal was rotated about (002) and (004) a large variation in the intensity of the satellites was observed. This supports our conclusion that the appearance of satellites is caused by multiple Bragg scattering.

2. Tetragonal Bragg peak in ferroelectric DCsDA

Deuteration changes a number of properties of CsDA. The shear angle, when measured away from the transition temperature, increases from 1·75° to 2·0°. The transition temperature increases from 146 K in CsDA to 227 K at a deuteration level of ~85% (Loiacono *et al* 1976).

We have now found that in our samples of DCsDA, obtained from Quantum Technology, only part of the crystal transforms at the nominal transition temperature with the remainder transforming over a 60 K temperature range. In figure 3 we show the neutron

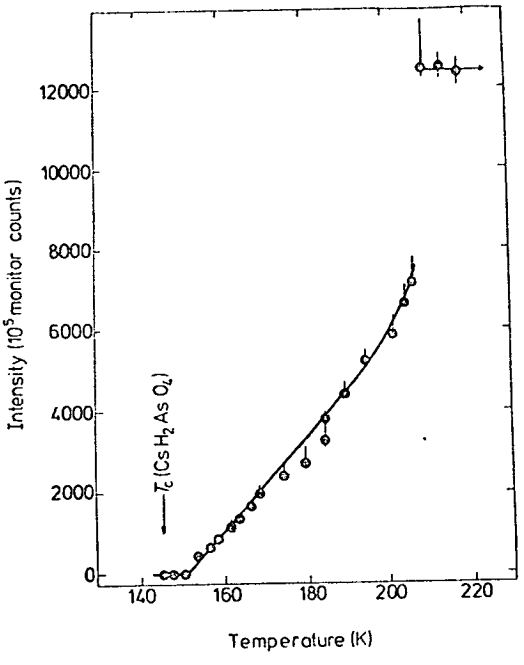

Figure 3. The temperature dependence of the central Bragg peak intensity at (220). T_c (CsDA) was measured as 145·9 ± 0·2 K.

intensity scattered in a 1 cm^3 sample at the (220) tetragonal reciprocal lattice point, plotted against temperature. Obviously, only 40% of the intensity in the tetragonal high-temperature phase disappears at 205 K; the lost intensity is distributed over the four peaks of the orthorhombic low-temperature phase. The remaining tetragonal peak intensity transfers to the orthorhombic peaks gradually, over a range extending nearly to the transition temperature of the hydrogenous compound.

Two smaller crystals (8 mm^3 and 16 mm^3) were investigated on a four-circle neutron diffractometer and showed quantitatively similar behaviour. Structure refinements (Hay

and Nelmes 1976) indicate that the average deuteration of the 8 mm^3 sample is 57%. Such a high hydrogen content is consistent with the unexpectedly intense incoherent neutron scattering found in the experiment on the 1 cm^3 sample. (*hk*0) photographs of a 0·01 mm^3 crystal taken with a Weissenberg x-ray camera again showed similar effects and confirmed that all reflections were affected.

The fact that crystals of such diverse sizes exhibit quantitatively similar behaviour makes surface rehydrogenation an unlikely explaination. We conclude rather that the observations suggest an inhomogeneity of the hydrogen–deuterium concentration over regions small in comparison with our smallest sample (0·2 mm). This could be consistent with peculiar growth behaviour observed in DCsDA (G M Loiacono, private communication) and could be a characteristic common to all solution-grown samples.

The transition temperature of 227 K given by Loiacono *et al* (1976) for a deuteration level ~85% suggests that the deuteration levels for DCsDA samples quoted in the literature have been grossly overestimated. If, in addition, the pronounced inhomogeneity of our specimens is a common characteristic, some further doubt must attach to the interpretation of the results of most previous experiments in DCsDA.

We are making further studies of the nature and reproducibility of the observed inhomogeneity.

Acknowledgments

G M Meyer would like to thank the Danish AEK for their hospitality during a four month stay, and the Science Research Council for finance during that period. R J Nelmes acknowledges the support of a Science Research Council Research Fellowship.

References

Dietrich O W, Cowley R A and Shapiro S M 1974 *J. Phys. C: Solid St. Phys.* **7** L239

Hay W J and Nelmes R J 1976 *3rd European Meeting on Ferroelectricity, Zurich 1975* (to be published in *Ferroelectrics*)

Jona F and Shirane G 1962 *Ferroelectric Crystals* (Oxford: Pergamon)

Loiacono G M, Ladell J and Osborne W N 1976 *3rd European Meeting on Ferroelectricity, Zurich 1975* (to be published in *Ferroelectrics*)

Meyer G M and Dietrich O W 1976 *3rd European Meeting on Ferroelectricity, Zurich 1975* (to be published in *Ferroelectrics*)

REFERENCES

Arndt, U W and Willis, B T M, 1966, Single Crystal Diffractometry, Cambridge : University Press.

Ascher, E, 1970, J. Phys. Soc. Japan 28, suppl. 7.

Ascher, E, Rieder, H, Schmid, H and Stossel, H, 1966, J. Appl. Phys. 37, 1404.

Ascher, E, Schmid, H and Tar, D, 1964, Sol. State. Commun. 2, 45.

Baberschke, K, Reich, S and Dormann, E, 1970, Phys. Stat. Solidi 39, 139.

Bacon, G E, 1972, Acta. Cryst. A 28, 357.

Bacon, G E, and Pease, R S, 1953, Proc. Royal Soc. A 220, 397.

Bacon, G E, and Pease, R S, 1955, Proc. Royal Soc. A 230, 359.

Baddur, A, Strukov, B A, Velichko, I A and Setkina, V N, 1973, Sov. Phys. Cryst. 17, 943.

Barker, W and Tinkham, M, 1963, J. Chem. Phys. 38, 2257.

Bastie, P, Bornarel, J, Lajzeroweiz, J, Vallade, M and Schnieder, J R, 1975 Phys. Rev. B12, 5112.

Becker, W J, and Will, G, 1970, Z. Kristallogr. 131, 139.

Bither, T A and Young, H S, 1974, J. Sol. State Chem. 10, 302.

Blinc, R, 1960, J. Phys. Chem. Solids 13, 204.

Blinc, R, Burgar, M and Levstick, A, 1973, Sol. State Commun. 12, 573.

Blinc, R, Dimic, V, Kolar, V, Lahajnar, G, Stepisnik, I, Zumer, S and Vene, N, 1968, J. Chem. Phys. 49, 4996.

Blinc, R, O'Reilly, D E, Peterson, E M and Williams, J M, 1969, J. Chem. Phys. 50, 5408.

Busch, G and Scherrer, P, 1935, Natur. Wissenschaften 23, 737.

Cochran, W, 1959, Phys. Rev. Lett. 3, 412.

Cochran, W, 1960, Advances in Physics. 9, 387.

Cochran, W, 1961, Advances in Physics. 10, 401.

Cochran, W, 1969, Advances in Physics. 18, No. 72, 157.

Cowley, R A, 1962, Phys. Rev. Lett. 9, 159.

Cromer, D T, 1965, Acta Crystallogr. 18, 17.

de Gennes, P G, 1963, Sol. State Commun. 1, 132.

Dietrich, O W, Cowley, R A and Shapiro, S M, 1974, J. Phys. C : Solid St. Phys. 7, L239.

Devonshire, A F, 1949, Phil. Mag. 40, 1040.

Devonshire, A F, 1951, Phil. Mag. 42, 1065.

Devonshire, A F, 1954, Phil. Mag. Suppl. 3, 85.

Dowty, E and Clark, J R, 1972, Sol. State Commun. 10, 543.

Doyle, P A and Turner, P S, 1968, Acta Crystallogr. A24, 390.

Drozhdin, S N, Bochkov, B G, Gavrilova, N D, Popova, T V, Kopstik, V A and Novik, V K, 1975, Sov. Phys. Cryst. 20, 256.

Dvorak, V and Petzelt, J, 1971, Czech. J. Phys. B21, 1141.

Eiriksson, V R, 1974, Thesis, University of Edinburgh.

Eiriksson, V R, Rouse, K D and Nelmes, R J, 1974 Ferroelectrics 8, 485.

Felix, P, 1973, Thèsis L'Université de Paris-Sud.

Felix, P, Lambert, M, Comès, R, and Schmid, M, 1974, Proc. 3rd. Int. Meeting on Ferroelectriciy, Edin., 1973.

Fouassier, C, Levasseur, A, Joubert, J C and Hagenmuller, P, 1970, Z. Anorg. All Chem. 375, 202.

Fraser, B C and Pepinsky, R, 1953, Acta Cryst. 6, 273.

Friedel, C and Curie, J, 1883, Bull. Soc. Miner 3, 90.

Gould, R and Nelmes, R J, 1977, private communcation.

Grunberg, J, Levin, S, Pelan, I and Weiner, E, 1967, Sol. State Commun. 5, 863.

Hewat, A W, 1973, J. Appl. Cryst. 6, 42.

Isherwood, B J, 1976, private communication.

Ito, T, Morimoto, N and Sadanga, R, 1951, Acta Cryst. 4, 310.

Itoh, K, Matsubayashi, T, Nakamura, E and Motegi, H, 1975, J. Phys. Soc. Japan 39, 843.

Johnson, C K, 1969, Acta Cryst., A25, 187.

Johnson, C K, 1970, Thermal Neutron Diffraction. ed. Willis, B T M, London : Oxford University Press.

Jona, F, 1959, J. Phys. Chem. 63, 1750.

Joubert, J C, Muller, A, Pernet, M and Ferrand, B, 1972, Bull. Soc. Fr. Miner. Cryst. 95, 68.

Kaminow, I P, 1965, Phys. Rev. 138, 1539.

Kaminow, I P and Damen, T C, 1968, Phys. Rev. Lett. 20, 1105.

Katiyar, R S, Ryan, J F and Scott, J F, 1971, Phys. Rev. B4, 2685.

Kelling, R O and Pepinsky, R, 1955, Z. Kristallogr. 106, 286.

Kennedy, N S J, 1977, Thesis, University of Edinburgh.

Kennedy, N S J, Nelmes, R J, Thornley, F R and Rouse, K D, 1976, Ferroelectrics 14, 591.

Kobayashi, J, Sato, N and Schmid, H, 1972, Phys. Stat. Solid. (a) 10, 259.

Kobayashi, J, Schmid, H and Ascher, E, 1968, Phys. Stat. Solid. 26, 277.

Kobayashi, K K, 1968, J. Phys. Soc. Japan, 24, 497.

Kriz, H M and Bray, P J, J. Phys. Chem. Solids. 32, 303.

Landau, L D, 1937, Physik. A. Sowjetunion 11, 26.

Lang, A R, 1959, Acta Cryst., 12, 249.

Lang, A R, 1963, J. Appl. Phys. 14, 904.

Le Corre, Y, 1957, J. Phys. Radium, Paris 18, 629.

Levasseur, A, 1973, Thésis L'Université de Bordeaux No. 409.

Levasseur, A, Fouassier, C and Hagenmuller, R, 1971, Mater. Res. Bull. 6, 15.

Levasseur, A, Rouby, B and Fouassier, C, 1973a, Acad. Sci., Paris 227, 421.

Levy, H A, Peterson, S W and Simonsen, S H, 1954, Phys. Rev. 93, 1120.

Lipson, H and Cochran, W, 1968, The Determination of Crystal Structures 3rd Edn. London : Bell.

Lockwood, D J, 1975, Light Scattering in Solids, ed. Balkanski, M and Leite, R C C, Paris : Flammarion.

Lockwood, D J, 1977, private communication.

Lockwood, D J, and Syme, R W G, 1977, Ferroelectrics to be published.

Loiacono, G M, 1976, private communication.

Loiacono, G M, Ladell, J, Osborne, W N and Nicholosi, J, 1976. Unpublished. Abstract in Ferroelectrics 14, 725

Lowndes, R P, Tornberg, N E and Leung, R C, 1974. Phys. Rev. B10, 911.

Lyddane, R H, Sachs, R G and Teller, E, 1941, Phys. Rev. 59, 673.

Mellor, J W, 1924, A Comprehensive Treatise on Inorganic and Theoretical Chemistry, vol V, (New York : Longmans) p137.

Meuller, H, 1940, Phys. Rev. 58, 565, 805.

Meuller, H, 1940, Phys. Rev. 57, 829.

Meyer, G M and Deitrich, O W, 1976, Ferroelectrics 14, 595.

Meyer, G M, Deitrich, O W, Nelmes, R J, Hay, W J and Cowley, R A, 1976, J. Phys. C : Solid State Phys. 9, L83.

Muller, J, 1970, Thesis L'Université de Grenoble.

Murray, A F and Lockwood, D J, 1977, private communication.

Nakamo, J and Shiozaki, Y, 1973, J. Phys. Soc. Japan, 34, 1423.

Nakamo, J, Shiozaki, Y and Nakamura, E, 1974, Ferroelectrics. 8, 483.

Nelmes, R J, 1972, Phys. Stat., Solid. (b) 52, K 89.

Nelmes, R J, 1974, J. Phys. Chem. 7, 3840.

Nelmes, R J, 1975, Acta Cryst. A31, 273.

Nelmes, R J, 1978, private communication.

Nelmes, R J, Eiriksson, V R and Rouse, K D, 1974, Sol. Stat. Commun. 11, 1261.

Nelmes, R J and Rouse, K D, 1974, Ferroelectrics 8, 487.

Nelmes, R J and Thornley, F R, 1974. J. Phys. Chem. 7, 3855

Nelmes, R J and Thornley, F R, 1976. J. Phys. Chem. 9, 665.

* Pawley, G.S., 1971, In Advances in Structure Research by Diffraction Methods, Vol. 4, ed. W Hoppe and R. Mason, (Oxford, Pergamon).

Paphowov, V I, Rez, I A and Silnitskaya, G B, 1972. Sov. Phys. Solid State 13, 2690.

Paul, G L, Cochran, W, Buyers, W J L and Cowley, R A, 1970. Phys. Rev. B11, No. 2, 4603.

*→ Peercy, P S and Samara, G A, 1973. Phys. Rev. B8, 2623.

Pereverseva, L P, Pagosskaya, N Z, Poplavko, Vu M, Pakhomov, V I, Rez, I A and Silnitskaya, G B, 1972, Sov. Phys. Solid State 13, 2690.

Peterson, S W, Levy, H A and Simonsen, S H, 1954, Phys. Rev. 21, 2084.

Pippard, A B, 1964, The Elements of Crystal Thermodynamics, Cambridge University Press.

Plesser, T H and Stiller, H, 1969, Sol. State Commun. 7, 323.

Pirenne, J, 1949, Physica 15, 1019.

Pirenne, J, 1955, Physica 21, 219.

de Quervain, M, 1944, Helv. Phys. Acta. 17, 509.

Rivera, J P, Bill, H, Weber, J, Lacroix, R, Hochstrasser, G and Schmid H, 1974, Sol. State Commun. 14, 21.

Rivera, J P, Bill, H and Lacroix, R, 1976, Ferroelectrics 13, 361.

Rivera, J P, Bill, H and Lacroix, R, 1976a, Ferroelectrics 13, 363.

Rivera, J P, Bill, H and Lacroix, 1976b, Phys. Stat. Sol. (a) 35, K105.

Rollet, J S, 1965, ed. Computing Methods in Crystallography, (article by D W S Cruickshank) Pergamon Press : Oxford.

Scott, J F and Wilson, C M, 1972, Sol. State Commun. 10, 597.

Schmid, H, 1965. J. Phys. Chem. Sol. 26, 973.

Schmid, H, 1969, Growth of Crystals, 7, 25. (New York, Consultants Bureau).

Schmid, H, 1970, Phys. State Sol. (a) 9, K109.

Schmid, H, 1974, private communication.

She, C Y, Broberg, T W, Wall, L S and Edwards, D F, 1972, Phys. Rev. B6, 184.

She, C Y and Pan, C L, 1975, Sol. State Commun. 17, 529.

Skalyo, J, Fraser, B C and Shirane, G, 1970, Phys. Rev. B1, 278.

Slater, J C, 1941, J. Chem. Phys. 9, 16.

Smutny, F, 1972, Phys. State Sol. (a). 9, K109.

Smutny, F and Fousek, J, 1970, Phys. State Sol. 40, K13.

Stewart, J M, 1972, XRAY 72 System of Computer Programs. University of Maryland.

Strukov, B A, Badder, A, Zimenko, V I, Mikhailov, V K and Kopstik, V A, 1973, Sov. Phys. Sol. State. 15, 541.

Strukov, B A, Vaks, A, Badder, A, Zimenko, V I and Kopstik, V A, 1974, Sov. Phys. Sol. State 15, 1347.

Takagi, Y, 1948, J. Phys. Soc. Japan. 3, 273.

Thomas, A, Benoit, J L, Herpin, P and Mercier, D, 1974, Compt. Rend. Acad. Sci. (Paris) B278, 779.

Thornley, F R, Nelmes, R J and Rouse, K D, 1975, Chem. Phys. Lett. 34, 175.

Thornley, F R, Nelmes, R J and Kennedy, N S J, 1976, Ferroelectrics 13, 357.

Thornley, F R, Kennedy N S J and Nelmes, R J, 1976a, J. Phys. C : Solid State Phys. 9, 681.

Tokunaga, M, 1966, Prog. Theor. Phys. 36, 857.

Tokunaga, M and Matsubara, T, 1966, Prog. Theor. Phys. 35, 581.

Trooster, J M, 1969. Phys. State Sol. 32, 179.

Ubbelohde, A R and Woodward, I, 1939, Nature (Lond.) 144, 632.

Ubbelohde, A R and Woodward, I, 1947, Proc. Roy. Soc. A 188, 358.

von Wartberg, W, 1973, E.I.R., Bericht 235, Wurenlingen.

von Wartberg, W, 1974, Phys. State, Sol. 21, 557.

Wallace, E A, Cochran, W and Stringfellow, M, 1972, Suppl. J. de Physique 33, C2-59.

Waugh, J L T, 1968, Structural Chemistry and Molecular Biology, ed. A Rich and N Davidson (San Francisco : Freeman) p731.

Wilson, C M, 1970, Thesis, the John Hopkins University, Baltimore.

Wilson, C M and Cummings, H Z, 1969, Light Scattering Spectra of Solids, ed. Wright, G B, Springer, New York.

Zachariasen, W H, 1967, Acta. Cryst. 23, 558.

Zheludev, I S, Perekalina, T M, Pyl'nev, V G, Smirnovskaya, E M, Belov, V F, Kostov, M M, Yarmukhamedov, Yu N, 1975, Insv. Acad. Nauk. Serv. Fiz. 39, 4. 72.

Zimmerman, A, Bollman, W and Schmid, H, 1970, Phys. State Sol. (a) 3, 707.